The role of Glutaredoxin-2 in the modulation of fat metabolism and ROS production in skeletal muscle mitochondria

Adrian Young

A Thesis submitted to the School of Graduate Studies in partial fulfilment of the requirements for the degree of

Master of Science

Department of Biochemistry, Faculty of science

Memorial University of Newfoundland

August 2019

St. Johns Newfoundland and Labrador

ABSTRACT

Protein S-glutathionylation (PGLU) reactions in mitochondria, catalyzed by glutaredoxin-2 (Grx2), have been shown to regulate carbon catabolism, oxidative phosphorylation and reactive oxygen species (ROS) production in response to changes in redox balance. In addition, deletion of the *Grx2* gene increases phosphorylating respiration and proton leaks in muscle tissue which correlates with decreased fat mass and body weight. However, whether or not manipulation of Grx2 levels protects from diet-induced obesity (DIO) has never been investigated. Our objective was to examine the potential anti-obesity effect associated with the absence of the *Grx2* gene in C57BL/6N mice. Here, we demonstrate that *Grx2*$^{+/-}$ mice were protected from diet-induced weight gain and obesity-related disorders associated with increases in mitochondrial respiration attributed, in part, to increased leaks through uncoupling protein-3. Collectively, our results demonstrate that S-glutathionylation reactions are integral for regulating muscle metabolism and fat combustion and reveal that manipulation of Grx2 signaling may serve as an exercise mimetic that can be employed to treat/prevent DIO.

ACKNOWLEDGMENTS

I would foremost like to thank my supervisor, Dr. Ryan Mailloux. His patience, guidance, and expertise enabled the timely completion of my project and successful analysis of the results enclosed. I would also like to thank my supervisory committee, Dr. Sukhinder Cheema and Dr. Margaret Brosnan, for their help and supervision of my progress in this project. Their kind suggestions enabled better understanding and presentation of my project. I would like to thank Danielle Gardiner, who provided hands on aid with mouse care and other laboratory procedures during her time with our lab.

Lastly, I would also like to thank the student members of the Mailloux lab group in addition to my family and friends whose aid and input were invaluable for the completion of this project. Thank you to Julia Chalker, Marisa O'Brien, Robert Gill, Nidhi Kuksal, Catherine Oldford, Ibrahim Dogar, and Sarah Mallay.

TABLE OF CONTENTS

LIST OF FIGURES

LIST OF TABLES

LIST OF EQUATIONS

ABBREVIATIONS

ADP	Adenosine diphosphate
ANOVA	analysis of variance
ANT	Adenine nucleotide translocase
APS	ammonium persulfate solution
ATP	Adenosine triphosphate
AUR	Amplex UltraRed
BCOADH	Branch chained 2-oxoapidic acid dehydrogenase complex
BM	Basic medium
BSA	Bovine serum albumin
CACT	Acyl-carnitine/carnitine transporter
cAMP	Cyclic-AMP
CD	Control diet
CO2	Carbon dioxide
CoASH	Coenzyme A
CPT1	Carnitine palmitoyltransferase 1
CPT2	Carnitine palmitoyltransferase 2
Cys	Cysteine
Cyt c	Cytochrome c
cyt c1	Cytochrome c1
DHODH	Dihydroorotate dehydrogenase
DIO	Diet induced obesity
DMSO	Dimethyl sulfoxide
ΔpH_m	proton concentration gradient
DTNB	5,5'-dithiobis (2-nitrobenzoic acid)
ΔY_m	Membrane potential
EGTA	ethylene glycol-bis (β-aminoethyl ether)-N,N,N',N'-tetraacetic acid
ETC	Electron transport chain
ETF	Electron transfer protein
ETFQO	Electron transferring flavoprotein:ubiquinone oxidoreductase
FA	Fatty acid
FAD	Flavin adenine dinucleotide
Fe-S	Iron-sulfur
FMN	Flavin mononucleotide
FUM	Fumarase
GAPDH	Glyceraldehyde 3-phosphate dehydrogenase
GDP	Guanosine Diphosphate
GPx1	Glutathione peroxidase 1

Grx2	Glutharedoxin-2
Grx2	Glutharedoxin -2 (gene)
GSH	Glutathione
GSSG	Glutathione disulfide
GTP	Guanosine triphosphate
H&E	Hematoxylin and eosin
H^+	proton
H_2O_2	Hydrogen peroxide
HEPES	(4-(2-hydroxyethyl)-1-piperazineethanesulfonic acid)
HFD	High-fat diet
HM	Homogenization medium
HMMPS	N-(3-isopropyl)-3methoxy-5-methylaniline
HRP	Horseradish peroxidase
IDH	Isocitrate dehydrogenase
IMS	Inter membrane space
KCL	Potassium chloride
KH_2PO_4	Monobasic potassium phosphate
K_{mix}	Equilibrium constant
KMV	α-Keto-β-methyl-n-valeric acid
MDH	Malate dehydrogenase
$MgCl_2$	Magnesium chloride
MIM	Mitochondrial inner membrane
MPC-1	Mitochondrial pyruvate carrier-1
MTF	Mitofusin
MPTP	Mitochondrial permeability transition pore
NAD^+	Nicotinamide adenine dinucleotide
O_2	Molecular oxygen
$O_2^{\cdot-}$	Superoxide
OADH	2-oxoapidic acid dehydrogenase complex
OAP1	Autosomal dominant optic atrophy protein 1
OGDH	Oxoglutarate dehydrogenase
$OH^\bullet$	Hydroxyl radical
$ONOO^-$	peroxynitrite
OXPHOS	Oxidative phosphorylation
PCR	Polymerase chain reaction
PDH	Pyruvate dehydrogenase
PGLU	Protein S-glutathionylation
P_i	Inorganic phosphate
PMF	Proton motive force

PRX	Peroxiredoxin
PSSG	Protein glutathione-mixed disulfides
Pt	Platinum
PVDF	O_2-permeant polyvinylidene difluoride
QC	Quality control
RB	Respiration medium
ROS	Reactive oxygen species
SCS	Succinyl-CoA synthase
SDH	Succinate dehydrogenase
SEM	Standard error of the mean
SO_2H	Sulfinic acid
SO_3H	Sulfonic acid
SOD	Superoxide dismutase
SOH	Sulphenic acid
TAG	Triacylglycerol
TBE	Tris Borate-EDTA
TBS	Tris-buffered saline
TEMED	N,N,N',N'-tetramethylethane-1,2-diamine
TNB	5-thio-2-nitrobenzoic acid
TR2	Thioredoxin reductase-2
TRX	Thioredoxin reductase
UCP	Uncoupling protein
UQ	Ubiquinone
$UQ^{\bullet-}$	semiquinone radical
UQH_2	Ubiquinol
VLDL	Very low-density lipoproteins
WT	Wild-type

Chapter 1: Introduction

1.1 Energy Metabolism

Mitochondria are referred to as the powerhouses of mammalian cells for good reason. Indeed, these double-membrane organelles are required to satisfy most of the cell's energy demands, which is achieved by oxidizing fuel (*e.g.* carbon) to make ATP (1)(1). The evolution of multicellular organisms was driven, in part, by the capacity of mitochondria to conserve and produce large amounts of energy. The upshot of this feature was the genesis of complex lifeforms like mammals. ATP is required to drive most physiological functions ranging from heartbeat and locomotion to immune cell function and xenobiotic detoxification (2). This also includes mediating cell signals emanating from extracellular hormones through the phosphorylation of proteins or production of cyclic-AMP (cAMP). At its core, mitochondrial ATP production relies on the production of a protonmotive force (PMF) across the mitochondrial inner membrane (MIM). This process begins when different forms of carbon (*e.g.* sugars, fats, and amino acids) are converted to Krebs cycle intermediates. The electrons released by metabolizing intermediates in the Krebs cycle are transported to the electron transport chain (ETC) and used to reduce the terminal acceptor molecular oxygen (O_2) to H_2O. Movement of these electrons through the chain is coupled to the pumping of protons into the intermembrane space (IMS), creating a PMF that is then used to make ATP. However, it is not the ETC and carbon oxidizing enzymes that imbued mitochondria with the capacity to generate large quantities of ATP. Rather, it is the highly folded MIM, which greatly increased the energy transducing surface area of mitochondria (2).

1.1.1 Glycolysis

The aerobic oxidation of monosaccharides begins with glycolysis, a 10-step process that transforms and breaks down glucose molecules to generate two pyruvate and two ATP molecules. The process is outlined in (Figure 1.1). Pyruvate then enters the Krebs cycle where it undergoes

further oxidation. The glycolytic breakdown of monosaccharides can be subdivided into two different steps. The first step is called the "*preparatory phase*", where 2 ATP molecules are used to prime the hexose ring for electron extraction and degradation. The first step of the preparatory phase is initiated by hexokinase, which, in the presence of Mg^{2+}, expends ATP to phosphorylate glucose on the C6 position, yielding glucose-6-phosphate. Notably, there are four different hexokinase isozymes including glucokinase, which is found in hepatocytes and pancreatic β-cells and is required for the maintenance of blood glucose levels. Myocytes contain hexokinase isoforms I and II, which are both allosterically inhibited by glucose-6-phosphate. Phosphohexose isomerase then mediates conversion of glucose-6-phosphate to fructose-6-phosphate in the presence of Mg^{2+}. This product is then phosphorylated a second time by phosphofructokinase-1, generating fructose 1,6-bisphosphate at the expense of 1 molecule of ATP (3). Aldolase then splits fructose 1,6-bisphosphate into two 3-carbon molecules, 1 glyceraldehyde 3-phosphate, and dihydroxyacetone phosphate. In the final step of the preparatory phase, the dihydroxyacetone phosphate molecule is converted to glyceraldehyde 3-phosphate by the action of trisphosphate isomerase (3).

Next, the two glyceraldehyde-3-phosphate molecules are used to drive the substrate-level phosphorylation of ADP, forming ATP, via the second part of glycolysis. First, glyceraldehyde 3-phosphate is oxidized and phosphorylated to 1,3 bisphosphoglycerate by the glyceraldehyde-3-phosphate dehydrogenase complex (GADPH) (4). Electrons released by this process are transferred to nicotinamide adenine dinucleotide (NAD^+) generating an NADH. After its production, the hydride from NADH can be transferred to oxaloacetate in the cytosol forming malate, which is then taken up by mitochondria through the malate-aspartate shuttle.

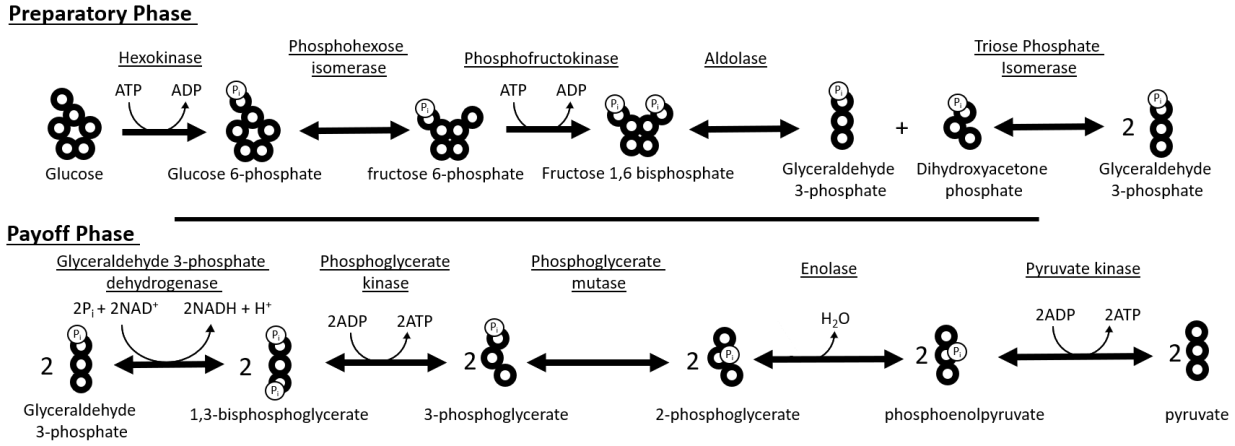

Figure 1.1: Glycolysis

Carbon is denoted by black rings.

Alternatively, the NADH formed in the cytosol by glycolysis can be used to reduce pyruvate to lactate by lactate dehydrogenase when cells are deprived of O_2. 1,3-bisphosphoglycerate is a mixed acid-anhydride which encourages nucleophilic attack of the terminal phosphate by ADP molecule, resulting in the formation of ATP and 3-phosphoglycerate, a reaction catalyzed by phosphoglycerate kinase (1). Steps 8 and 9 comprise an intramolecular rearrangement of the phosphate bond, and a dehydration reaction catalyzed by phosphoglycerate mutase and enolase, respectively, generating the high energy molecule, phosphoenolpyruvate. The final step occurs in 2 parts. Pyruvate kinase catalyzes the transfer of the phosphate group from phosphoenolpyruvate to ADP generating another molecule of ATP, as well as an enolate form of pyruvate, which is further reduced to the keto form through the electrophilic addition of a proton (H^+). Once formed, pyruvate is either converted to lactate or taken up by mitochondria where it undergoes further oxidation. The net reaction for glycolysis is as follows:

Equation 1.1: Glycolysis

$$\text{Glucose} + 2\ NAD^+ + 2\ ADP + 2\ Pi \rightarrow 2\ \text{pyruvate} + 2\ ATP + 2\ NADH + 2\ H^+$$

1.1.2 Krebs Cycle

The Krebs cycle acts as a central point where carbons from multiple sources converge for the extraction and transfer of electrons to the ETC (5). For instance, pyruvate yielded from glycolysis is oxidized further by the concerted action of Krebs cycle enzymes. This begins when pyruvate carrier translocates pyruvate into the matrix of mitochondria (Figure 1.2). This is driven by the Gibbs free energy stored in the PMF, which couples the energetically unfavorable transport of pyruvate into the matrix. Pyruvate is then converted to acetyl CoA by the action of the pyruvate dehydrogenase complex (PDH). PDH is a 3-subunit enzyme complex that carries out the oxidative decarboxylation of pyruvate generating acetyl-CoA, NADH, and CO_2. The E1 subunit of PDH,

pyruvate decarboxylase, decarboxylates pyruvate, transferring the acetyl group to thiamine pyrophosphate. The acetyl group is then transferred to lipoic acid of the E2 subunit, dihydrolipoyl transacetylase. The prosthetic lipoic acid arm of the E2 subunit is covalently attached but swings freely allowing the acetyl group to be transferred to coenzyme A (CoASH) generating acetyl-CoA. This reduction-oxidation reaction leaves the lipoic acid group in a reduced, inactive state. The E3 subunit, dihydrolipoyl dehydrogenase, restores the active lipoic acid prosthetic group by transferring its electrons to FAD. Finally, the FAD prosthetic group is restored by transferring electrons to NAD^+ generating NADH (6). It is important to point out that acetyl-CoA sits at a metabolic intersection for oxidative metabolism. Indeed, the oxidation of fatty acids (FA) by mitochondria also generates acetyl-CoA. Various amino acids including alanine, cysteine, glycine, and tryptophan also yield acetyl-CoA (1). With this in mind, disparate sources of carbon that are catabolized for mitochondrial ATP production in mitochondria are first converted to common intermediates that can then undergo further oxidation by the Krebs cycle.

Pyruvate is also required to prime the Krebs cycle through the production of oxaloacetate. This is achieved by pyruvate carboxylase, which carboxylates pyruvate using ATP and bicarbonate in the presence of biotin. Next, acetyl-CoA enters the Krebs cycle through condensation with oxaloacetate, a reaction mediated by citrate synthase, which generates citrate. There is a large negative free energy associated with this condensation reaction that is essential for the progress of the cycle (1). In the next step, citrate is isomerized to isocitrate through a cis-aconitate intermediate by the enzyme aconitase (1). Isocitrate is then oxidized by isocitrate dehydrogenase (IDH), generating 2-oxoglutarate and CO_2. The evolution of CO_2 following isocitrate oxidation is coupled with the production of NADH. It is important to note that mitochondria contain two IDH isozymes. IDH1 is required to generate NADH during fuel combustion by the Krebs cycle (7).

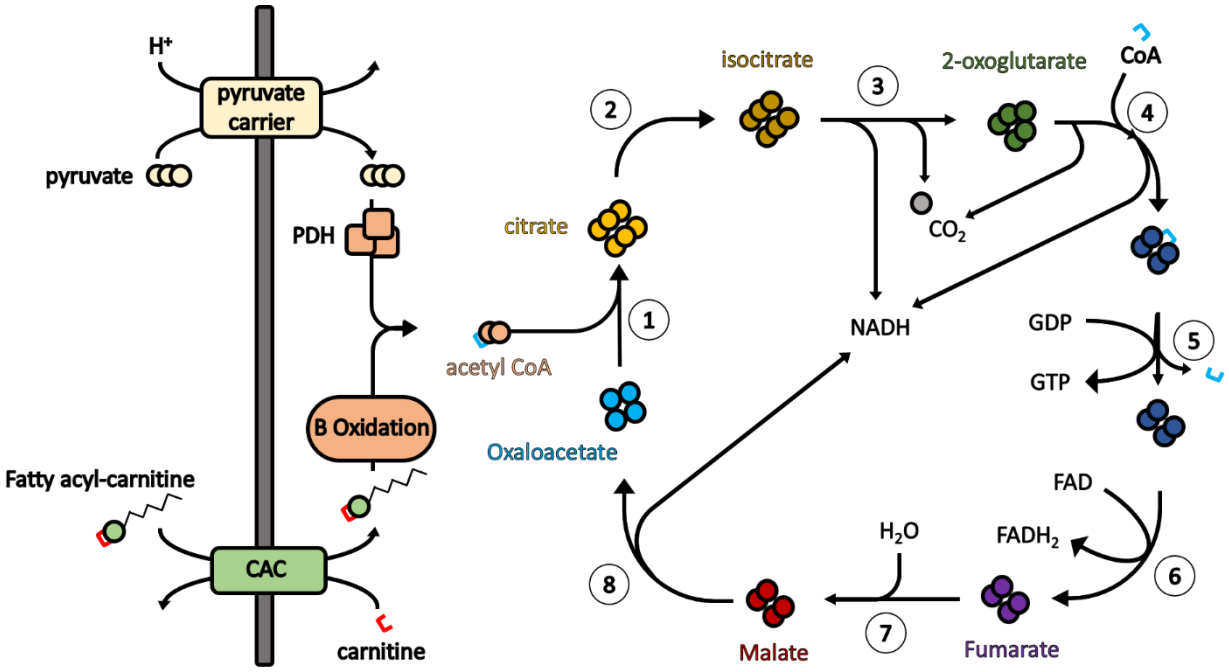

Figure 1.2: The Krebs cycle

The enzymes involved in carbon conversion are as follows: 1- citrate synthase, 2- aconitase, 3- isocitrate dehydrogenase, 4- 2-oxoglutarate dehydrogenase, 5- succinyl CoA synthase, 6- succinate dehydrogenase, 7- fumarase, 8- malate dehydrogenase.

IDH2, on the other hand, couples isocitrate oxidation to the genesis of NADPH, a critical factor required for antioxidant defenses. The next step is catalyzed by the 2-oxoglutarate dehydrogenase complex (OGDH), a structural analog to the PDH complex discussed earlier. OGDH uses E3 and E2 subunits that are highly homologous to the PDH equivalents (8). The difference between OGDH and PDH lies in the E1 and E2 subunits, which are named 2-oxoglutarate decarboxylase (E1) and dihydrolipoamide:succinyl-CoA transferase (E2), respectively. Decarboxylation of 2-oxoglutarate generates succinyl-CoA, CO_2 and NADH. Various amino acids can also enter into the Krebs cycle at the level of 2-oxoglutarate. Indeed, the oxidation of all amino acids by the Krebs cycle relies on aminotransferases, which produce 2-oxoglutarate from reversible deamination reactions. Hydrolysis of succinyl-CoA is mediated by succinyl-CoA synthase (SCS) generating succinate and GTP/ATP (note that production of either GTP or ATP depends on the SCS isoform) (9). The next step is catalyzed by the succinate dehydrogenase (SDH), also known as complex II. SDH is embedded in the inner leaflet of the MIM and therefore, electrons released from the oxidation of succinate to fumarate are transferred directly to the UQ pool. Since UQ serves as an electron carrier in the respiratory chain, SDH directly links the Krebs cycle and the ETC. The hydration of fumarate by fumarase (FUM) generates malate which is finally oxidized by malate dehydrogenase (MDH) for the generation of oxaloacetate which re-enters the cycle (2). This final stage also produces the electron carrier NADH (1).

1.1.3 Lipid metabolism and the β oxidation of fatty acids

Fatty acids used for the production of ATP can either be derived from dietary lipids or lipids formed by *de novo* lipogenesis. Absorption of dietary lipids begins when they are emulsified by bile acids in the small intestine. This generates micelles that contain a variety of lipids, including triacylglycerol (TAG), cholesterol, and phospholipids, that are imported into enterocytes (10).

These lipids are then processed further inside enterocytes and packaged into chylomicrons along with apolipoproteins, which are then secreted into the lymph (1, 11). *De novo* lipogenesis, on the other hand, primarily occurs in hepatocytes where amino acids, glucose and other monosaccharides are used for lipid biosynthesis (12). Triglycerides formed by lipogenesis are then packaged into very low-density lipoproteins (VLDL) for transport around the body as outlined in Figure 1.3.

Transport of chylomicrons or VLDL to energy-requiring cells, like myocytes in skeletal muscle. TAG in Chylomicrons and VLDL are degraded by lipoprotein lipases to give fatty acids which are then taken up by myocytes. Fatty acids are then taken up by mitochondria by β-oxidation (also called fatty acid oxidation). Palmitate (long chain fatty acid) is the most abundant fatty acid found in the human body (13) and is thus the main substrate for fatty acid oxidation. However, it is important to point out that mitochondria can also oxidize short and medium-chain fatty acids, which either originate from dietary sources or are produced by palmitate oxidation. Fatty acid oxidation is initiated by first modifying palmitate (or other fatty acyl molecules) with CoASH generating palmitoyl-CoA, a reaction catalyzed by acyl-CoA synthetase in the presence of ATP (14). Carnitine palmitoyltransferase 1 (CPT1) then catalyzes the removal of CoASH, replacing it with L-carnitine (15). This allows mitochondrial import of fatty acyl-carnitine by the action of the acyl-carnitine/carnitine transporter (CACT) (16). Note that CACT is an antiporter that couples the uptake of acyl-carnitine to the export of L-carnitine. Once delivered to the matrix of the mitochondria, fatty acyl-CoA is regenerated in a transfer reaction mediated by the MIM associated isozyme carnitine palmitoyltransferase 2 (CPT2) (15). The fatty acyl-CoA units are now primed for β oxidation.

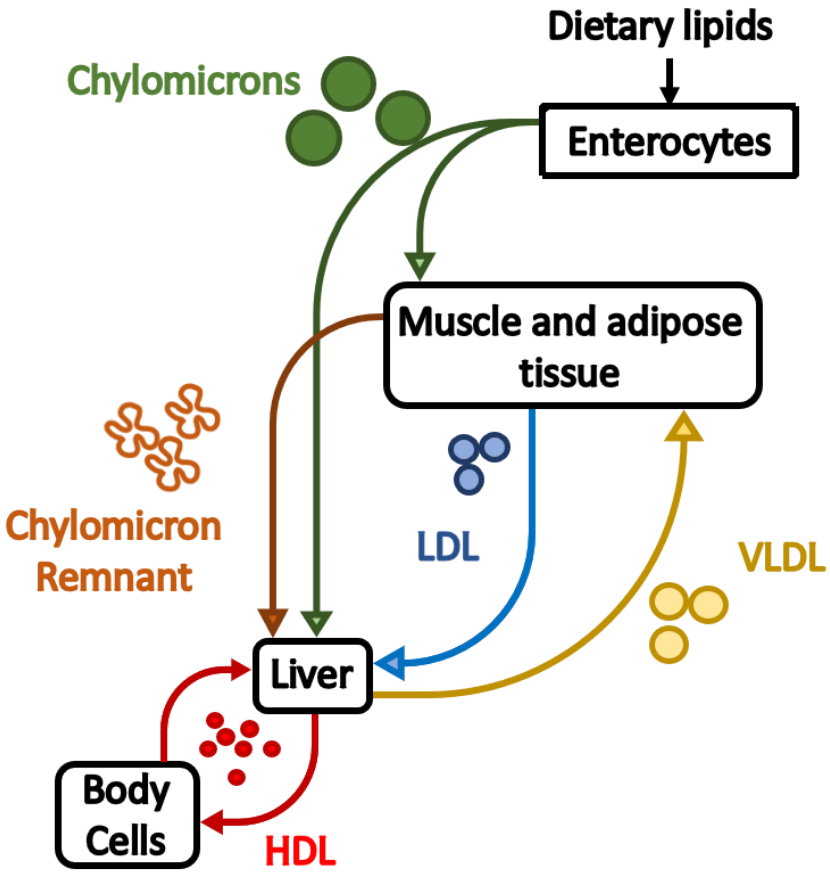

Figure 1.3: Lipid transport

Dietary lipids are converted to chylomicrons for fatty acid delivery to liver and adipose tissue for storage as well as muscle tissue to meet energy demands. The liver stores fatty acids as triglycerides, which are then packaged into VLDL for release into circulation.

Fatty acid oxidation in the matrix of mitochondria is initiated by acyl CoA dehydrogenase, which oxidizes palmitoyl-CoA (and other acyl-CoA molecules) introducing a double bond in a trans configuration between the α and β carbon of the fatty acid chain (17). The two electrons yielded from palmitoyl-CoA oxidation reduce a flavin adenine dinucleotide (FAD) prosthetic group to $FADH_2$. These electrons are then transferred to electron-transferring flavoprotein:ubiquinone oxidoreductase (ETF-QO), an FAD-containing enzyme that reduces UQ in the respiratory chain. The second reaction, mediated by enoyl hydratase, is a hydration reaction which adds H_2O across the newly forged double bond. Enoyl hydratase is incapable of acting on the naturally occurring cis double bonds present in unsaturated fatty acids. For this reason, auxiliary isomerase and reductase enzymes generate double bonds in the trans configuration to facilitate an unimpeded β oxidation cycle in mono and poly-unsaturated fatty acids (18). Beta-hydroxy palmitoyl-CoA is then oxidized by β-hydroxyacyl-CoA dehydrogenase, generating β-keto palmitoyl-CoA and NADH. Finally, acyl-CoA acetyltransferase catalyzes the transfer of the 2 carboxyl terminal carbons of the recently generated β-ketoacyl-CoA to a free CoA generating acetyl CoA and a new acyl-CoA that will re-enter the cycle. This process produces 1 $FADH_2$, 1 NADH, and 1 Acetyl CoA per 2 carbons of the fatty acid chain. Electrons transferred to FAD immediately enter the ETC by subsequent reductions of electron transfer protein (ETF) followed by ETF-QO and finally the Ubiquinone (UQ) pool (2). Electrons transferred to NADH enter the ETC at the level of complex I, and acetyl CoA enters the Krebs cycle, discussed later.

1.1.4 Oxidative phosphorylation

Oxidative phosphorylation represents the final stage of energy extraction from common carbon intermediates for the genesis of ATP. This process is outlined in Figure 1.4. Electrons can enter the ETC at either complex I through the oxidation of NADH or can be fed directly into the

chain via the reduction of UQ to ubiquinol (UQH_2) (*e.g.* during succinate oxidation). NADH acts as an efficient electron carrier, shuttling electrons donated from crucial enzymes of the glycolytic pathway, β oxidation, the Krebs cycle, and other metabolic sources. These electrons enter the ETC at NADH-UQ oxidoreductase (complex I). Complex I is the largest of the 4 complexes of the ETC with 14 core proteins and 31-32 accessory proteins (2). The subunits of complex I form a distinctive L-shape that consists of 3 major modules; N, Q and P modules. The N module consists of 7 of the 14 core proteins; NDUFV1, NDUFV2, NDUFS1, NDUFS2, NDUFS3, NDUFS7, and NDUFS8 (2). This module protrudes into the matrix of the mitochondria and contains a flavin mononucleotide (FMN) prosthetic group and 7 Fe-S clusters (2). The FMN of the N module is the site for NADH oxidation. Electrons extracted from NADH are transferred to the FMN prosthetic group and then through the 7 Fe-S clusters, reducing UQ to UQH_2 in the Q module, which sits at the junction between the N and P modules. The P module contains the core proteins ND1, ND2, ND3, ND4, ND4L, ND5 and ND6. It is a hydrophobic domain embedded in the MIM and is responsible for pumping 4 protons across the MIM for each NADH oxidized (2 electrons transferred) (2).

As previously discussed, complex II also feeds electrons into the ETC from succinate (2). Electron transfer in this complex is mediated by FAD and 3 Iron-sulfur (Fe-S) clusters. Electrons pass from succinate to FAD, and subsequently through the 3 Fe-S clusters to reduce UQ to UQH_2 in the UQ binding site in the MIM. Complex II is incapable of transferring electrons across the MIM; since the potential for the succinate/fumarate and UQH2/UQ pairs are very close, the Gibbs free energy change for e- transfer is almost 0. This contrasts with the other complexes where electron flow through their prosthetic groups is energetically favorable and thus coupled to the pumping of protons into the IMS. Similarly, electrons are transferred to the UQ pool by the

enzymes ETF-QO, and GAPDH discussed earlier, as well as dihydroorotate dehydrogenase (DHODH) (19–22). These three enzymes associate with the outer leaflet of the MIM in contrast to complex II.

The next step is catalyzed by the activity of ubiquinone: cytochrome *c* oxidoreductase (complex III). Complex III catalyzes the transfer of electrons from the UQ pool to cytochrome *c* through a process first proposed by Peter D. Mitchell known as the Q-cycle (23). Complex III contains 2 UQ binding sites, Q_P and Q_N and 2 B-type haeme, B_L and B_H. Q_P and B_L are located near the cytosolic side of the MIM while Q_N and B_H are located on the matrix side of the MIM (24). Also, associated with the outer leaflet of the MIM is the Rieske protein which contains an Fe-S cluster and interacts with cytochrome c_1 (cyt c_1) (24). Electron transfer and proton translocation across the MIM by the Q-cycle occur in multiple steps. First UQH_2 binds the Q_P site. Two single-electron transfer reactions occur. One electron is passed to cyt c_1 through the Fe-S cluster of the Rieske protein. This generates a semiquinone radical ($UQ^{\bullet-}$) in the Q_P site and releases 2 protons to the cytosolic side of the MIM (23). The second electron is passed to the adjacent B_L generating UQ. In the next step, the electron bound to B_L is transferred to B_H on the matrix side of the MIM. Free UQ binds to the adjacent Q_N site and is reduced to $UQ^{\bullet-}$. This $UQ^{\bullet-}$ radical is stabilized by the B_H haem while a second UQH_2 enters the Q_P site near the cytosolic side of the MIM. A second round of electrons then transfers 2 more protons to the cytosol, one more electron to cyt c_1 and finally a second electron to the $UQ^{\bullet-}$ radical bound to the Q_N site. Two protons are taken up from the matrix to reduce $UQ^{\bullet-}$ to UQH_2 and the cycle can begin again (23).

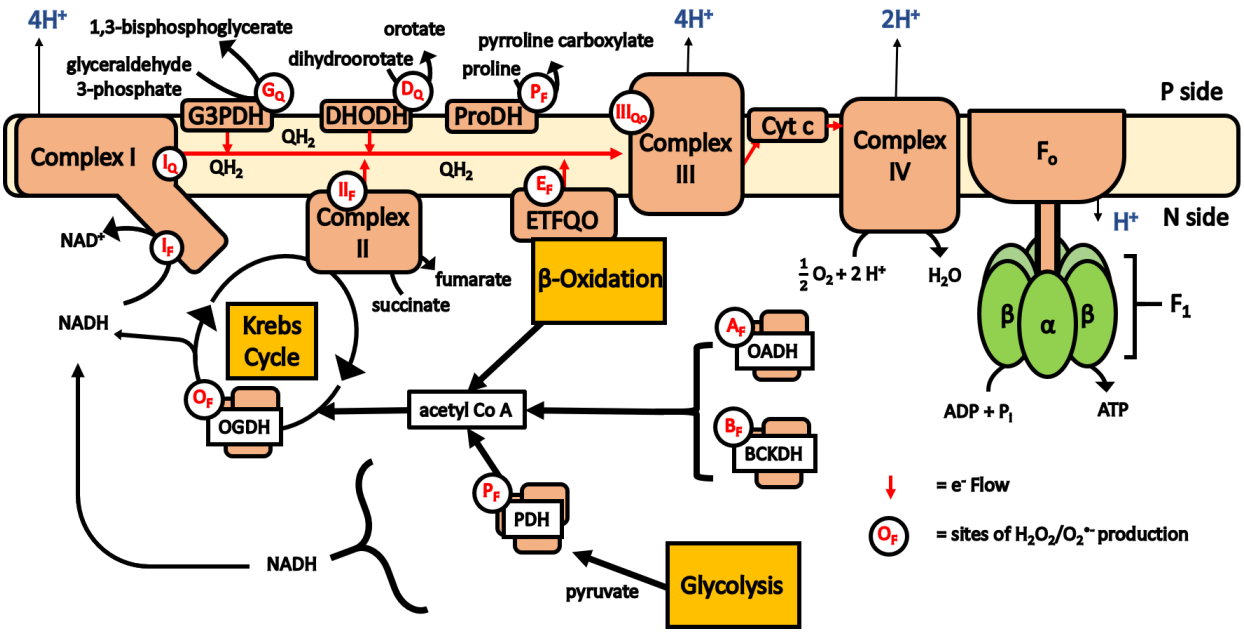

Figure 1.4: Nutrient oxidation.

Electrons from multiple carbon intermediates are transported to the ETC where the movement of these electrons in an energetically favorable fashion is coupled to the pumping of protons across the mitochondrial inner membrane. The PMF is then utilized by complex V for the generation of ATP. The 12 known sites of ROS production are indicated in red text. Enzymes contributing to acetyl CoA production include pyruvate dehydrogenase (PDH), branched chain keto acid dehydrogenase (BCKDH), oxoadipic acid dehydrogenase (OADH) and acetyl-CoA acyltransferase of β oxidation. Enzymes contributing electrons to the QH pool include, complex I, complex II, glycerate 3-phosphate dehydrogenase (G3PDH), dihydroorotate dehydrogenase (DHODH), proline dehydrogenase (ProDH), electron transfer flavoprotein:ubiquinone oxidoreductase (ETFQO). Electron flow from complex III to Complex IV is mediated by cytochrome c (Cyt c) and proton return to the matrix is coupled to ATP generation by the F_1F_o ATP synthase.

Electrons are transferred from cyt c_1 to cytochrome *c* (cyt *c*), which binds to cytochrome c_1 via electrostatic interactions on the outer leaflet of the MIM. Once it accepts an electron, it quickly diffuses to cytochrome *c* oxidase (complex IV) (25). Electrons are transferred from cyt *c* to Cu_A, a copper sulfur center in a subunit of complex IV that extends lightly into the cytosol. Electrons then flow through 2 haem groups haem *a* and a_3. O_2 is bound at haem a_3 and reduced to 2 molecules of H_2O after accepting four electrons. This process pumps 4 protons across the MIM for every H_2O molecule produced (26).

For every 2 electrons traveling through the ETC, 4 protons are pumped by complex I, 2 protons by complex III and 4 by complex IV. NADH oxidation drives the translocation of ~10 protons into the intermembrane space. By contrast, electron donors that by-pass complex I, donating electrons directly to the UQ pool (e.g. oxidation of succinate by complex II) pump only 6 protons across the MIM (27). The movement of protons into the intermembrane space establishes a transmembrane electrochemical gradient called the PMF. The PMF is comprised of a membrane potential ($\Delta\Psi_m$), the electric component, and a proton concentration gradient (ΔpH_m), the chemical component, with the latter making a smaller contribution to the PMF since the potential energy for $\Delta\Psi_m$ is much larger than ΔpH_m (28). The PMF acts as the driving force utilized by complex V for the generation of ATP and generally ranges between 180 - 220 mV (29). The PMF, however, is not exhaustively consumed by ATP production since cells have found utility in this imbalance for transport and antioxidant defense. For instance, various transport proteins embedded in the MIM, collectively referred to as the solute anion carrier superfamily, couple the selective uptake of charged or hydrophilic molecules to the proton gradient. Pyruvate delivery to the matrix of the mitochondria is not energetically favorable due to the similar charges of pyruvate and the matrix. As a result, the mitochondrial pyruvate carrier is a proton-pyruvate symporter which uses the

proton gradient to supply energy for active transport (30). For antioxidant defenses, the PMF is used by nicotinamide nucleotide transhydrogenase to drive the transfer of a proton from NADH to $NADP^+$ generating NADPH for reduction of antioxidant defense systems, discussed later (31). The PMF can also be siphoned by what are known as uncoupling proteins, discussed later in greater detail. These proteins are so called because they allow an alternative path for protons across the MIM bypassing complex V, "uncoupling" ATP generation from the pumping of protons across the MIM (32). All organisms on our planet rely on the genesis of electrochemical gradients, which is why it is now thought that the PMF (and other gradients), rather than ATP, is thought to be the universal energy currency (33).

Complex V consists of two subcomplexes arranged in the MIM as demonstrated in Figure 1.5. The hydrophobic F_o subcomplex consists of an a subunit, two b subunits and 8-14 c subunits. The number of c subunits is a debated topic and differs between mitochondria, thylakoids, and prokaryotes (34). The c subunits are arranged in a ring embedded in the MIM and provide the means for proton translocation. At the interface between the a subunit and the c-ring, are two half channels that are opened to the n and p sides of the MIM, denoted the entrance and exit channels, respectively (35). Alternate protonation, deprotonation of Arg61 of the c subunits result in movement of the c-ring encouraging interaction with the entrance and exit channels. This movement allows proton return through the MIM (35, 36). The a subunit remains stationary and is bound to the F_1 complex by the b subunits. The water-soluble F_1 complex consists of 3 α and 3 β subunits arranged in an alternating ring pattern surrounding a γ subunit (37). The γ subunit associates with b subunits of the F_o complex via a δ subunit and associates with the center of the F_o c-ring. When isolated the F_1 complex maintains ATPase activity but not ATP synthesizing activity (38).

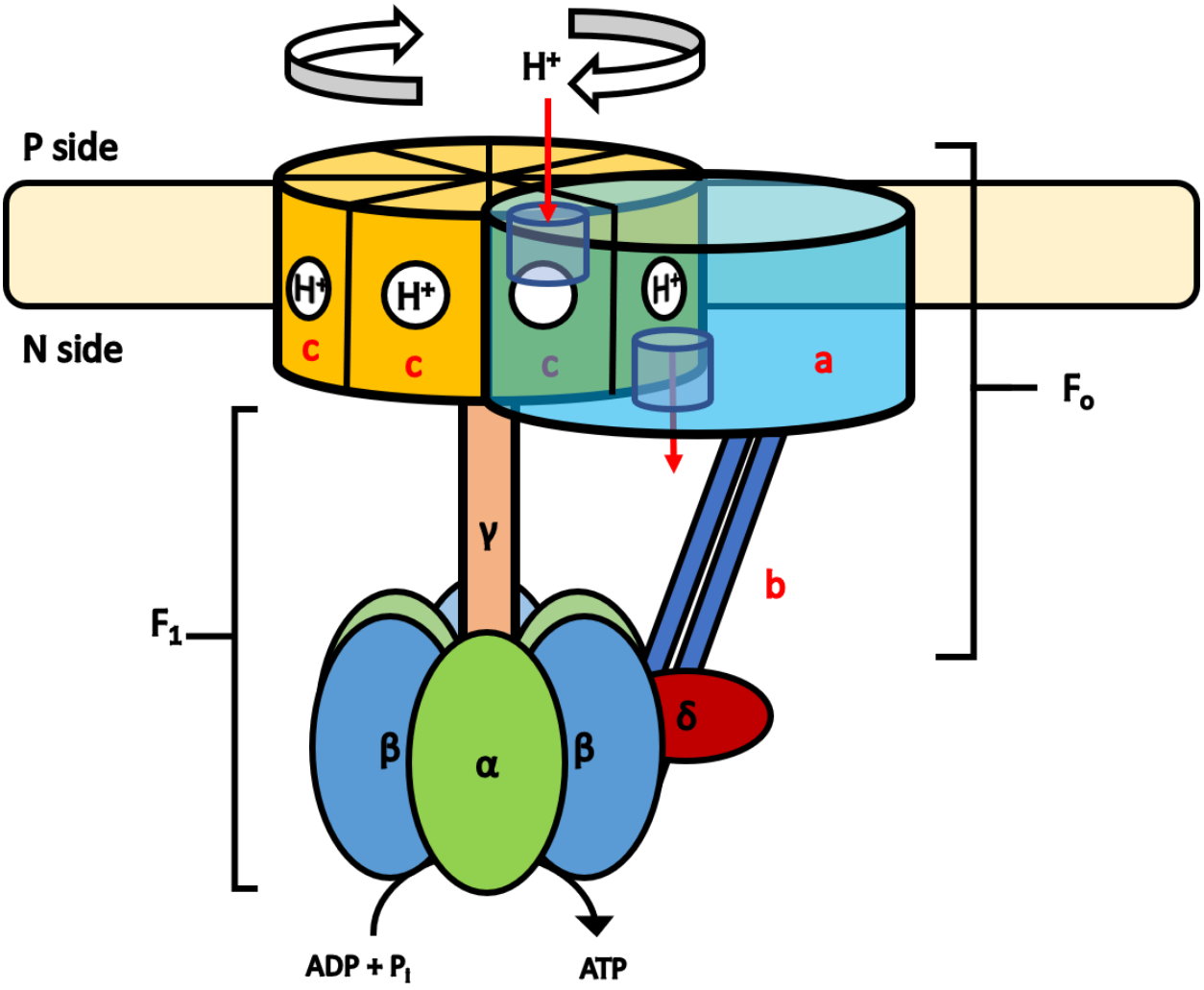

Figure 1.5: The F_oF_1 ATP Synthase

Proton return through channels in subunit a drives rotation of the c subunits resulting in rotation of the γ subunit within the α and β subunits that are anchored in place by attachment to the b subunits. This drives conformational changes that catalyze the phosphorylation of ADP generating ATP.

The PMF driven rotation of the c-ring drives the rotation of the γ subunit which rotates within the stationary αβ ring resulting in conformational changes in the α and β subunits. Each rotation of the αβ ring results in 3 ATP molecules produced. This process is known as rotational catalysis and drives ATP synthesis through changes in affinity of the α and β subunits for ATP, ADP and inorganic phosphate (P_i) (39). The H^+/ATP ratio of the mammalian complex V is 8/3 since a single rotation of the c-ring results in one single rotation of the αβ ring (2).

Electrons extracted from multiple dietary sources enter the ETC at a highly negative redox state through the oxidation of NADH or the direct reduction of the UQ pool. The movement of these electrons through the ETC is energetically favorable and is often perceived as moving in a "downhill fashion", from a negative redox potential to a more positive one. The redox potential of the NADH/NAD^+ pool is approximately -320 mV, while the redox potential of the H_2O/O_2 pair, the terminal electron acceptor, is approximately +820 mV (2). This process is coupled to the pumping of protons across the MIM generating a PMF utilized by the F_oF_1 ATP synthase (complex V) for the production of ATP.

1.2 Reactive Oxygen Species

Fuel combustion and the reduction of O_2 by complex IV is not perfectly coupled to the genesis of ATP. At various points in the Krebs cycle and the respiratory chain, in addition to other nutrient-oxidizing enzymes, electrons can "spin-off" and prematurely react with O_2 and form oxyradicals called reactive oxygen species (ROS). Mitochondria are the most important source of ROS in mammalian cells, a property attributed to the fact that their functions rely on fuel metabolism and redox reactions. Molecular oxygen contains two lone electrons with parallel spins in its outer most anti-bonding orbital (note that this feature also classifies O_2 as a reactive oxygen

species). Therefore, O_2 can only accept one electron at a time, resulting in the formation of several reactive intermediates such as superoxide ($O_2^{\bullet-}$), hydrogen peroxide (H_2O_2), and hydroxyl radical ($OH^{\bullet}$) before its full reduction to H_2O. Superoxide is often considered the proximal ROS formed by mitochondria due to the fact that its production only requires the monovalent reduction of O_2. However, it has now become clear that sites of production in mitochondria can produce a mixture of $O_2^{\bullet-}$ and H_2O_2 (40). Most sites for ROS release in mitochondria are flavoproteins and the capacity of these sites to generate $O_2^{\bullet-}$ and H_2O_2 is highly dependent on flavin chemistry and how it reacts with O_2. Furthermore, recent estimates have found that H_2O_2, not $O_2^{\bullet-}$, is the dominant ROS formed by sites of production. However, $O_2^{\bullet-}$ is formed by mitochondria nonetheless, which needs to be rapidly removed since it can disassemble Fe-S clusters at a rate of $k = 10^7\ M^{-1}\ s^{-1}$ (41, 42). This is especially important for mitochondria since several Krebs cycle enzymes and respiratory chain complexes are dependent on Fe-S clusters for nutrient oxidation and electron transport. For this reason, mitochondria contain high amounts of superoxide dismutase (SOD), which quickly dismutates $O_2^{\bullet-}$ to H_2O_2 at a rate of $k = 1.8 \times 10^9\ M^{-1}s^{-1}$. Mitochondria also contain two different SOD isoforms, SOD1 (copper and zinc-dependent) in the IMS, and SOD2 (manganese-dependent) in the matrix, meaning that $O_2^{\bullet-}$ formed on either side of the MIM can be rapidly removed (42). H_2O_2 concentrations range from $10^{-7} – 10^{-9}$ M, while $O_2^{\bullet-}$ concentrations are much lower at around $10^{-10} – 10^{-12}$ (43, 44). As a result, H_2O_2 is the most abundant form of ROS produced. Hydrogen peroxide can irreversibly oxidize protein cysteine thiols and is considered a strong oxidant. However, due to high activation energy restraints, it reacts with few protein cysteine thiols and only becomes a danger to cells when its concentration is in the low millimolar range (45, 46).

As noted above, H_2O_2 weakly reacts with most cysteine thiols and $O_2^{\bullet-}$ is a weak oxidant despite the fact it can react rapidly with Fe-S clusters. Superoxide and hydrogen peroxide become extremely dangerous to living systems in the presence of free Fe, which, through one electron transfer and homolytic cleavage reactions, can generate $OH^{\bullet}$. Hydroxyl radical generation occurs through H_2O_2 interactions with Fe^{2+} known as Fenton reactions. Fe^{3+} can also catalyze $OH^{\bullet}$ generation by transferring an electron from $O_2^{\bullet-}$ to H_2O_2 through a Fe^{2+} intermediate. This is known as a Haber-Weiss reaction:

Equation 1.2: Haber-Weiss reaction

$$Fe^{3+} + O_2^{\bullet-} \rightarrow Fe^{2+} + O_2$$

$$\underline{Fe^{2+} + H_2O_2 \rightarrow OH^{\bullet} + OH^- + Fe^{3+}} \quad \text{(Fenton reaction)}$$

$$O_2^{\bullet-} + H_2O_2 \rightarrow O_2 + OH^{\bullet} + OH^- \quad \text{(in the presence of } Fe^{2+}/Fe^{3+})$$

The volatile reactivity of $OH^{\bullet}$ allows it to directly modify protein and nucleotides leading to protein oxidation and inactivation as well as dsDNA breaks and accelerated mutagenesis (46, 47). The generation of $OH^{\bullet}$ can also lead to lipid peroxide initiation and propagation. Lipid peroxides are associated with a wide range of cellular dysfunction. They alter membrane fluidity and permeability and subsequently lead to protein and DNA modification as a result of by-products of their degradation (48–51) An additional danger lies in the generation of reactive nitrogen species through the interactions of NO and ROS (52–54). Peroxynitrite, for example, can lead to the oxidation as well as nitration of protein and DNA promoting cell cycle arrest or mutagenesis. The ensuing consequence of excessive mitochondrial ROS is programmed cell death to minimize damage caused to other cells or its progression to a cancerous state (53, 55).

Our collective understanding of the role of ROS has changed in recent decades due to new research revealing the hormetic relationship between mitochondrial ROS and the cell. Indeed, while high levels of ROS can be detrimental, as previously discussed, ROS at physiologically relevant levels are essential for normal cellular function and induce what has recently been coined as oxidative eustress (56). This term was created to differentiate between mitochondrial ROS associated with cellular damage (also called oxidative distress) and ROS levels that coordinate cellular processes including cellular adaptive response, cellular proliferation and growth, insulin signaling pathways, and T-cell activation (45, 57, 58). In skeletal muscle, for example, low-level ROS production is required for normal muscle force production in skeletal muscle mitochondria. Increased ROS production during exercise initiates AMPK mediated upregulation of GLUT4 membrane translocation, inducing insulin-independent glucose import (59). Low-level ROS production in skeletal muscle also modulates IGF-1 expression and signaling through regulation of the PI3K/Akt pathway (60). Finally, ROS production during exercise is also required for muscle growth and adaptation, increasing stress resistance in myofibers. However, overproduction of ROS in muscle can be damaging, leading to diminished muscle force generation and development of sarcopenia (61). In pancreatic beta cells, transient increases in glucose availability led to increased ROS production which modulated calcium mobility. This process was essential for glucose-stimulated insulin secretion (62).

The 12 known locations of ROS production have been extensively studied and reviewed by Martin D. Brand (63). The sites are subcategorized into the $NADH/NAD^+$ and UQH_2/UQ isopotential groups that operate at -270 mV and +20 mV respectively (63) and have been identified in Figure 1.5. ROS producing enzymes within the $NADH/NAD^+$ isopotential group include complex I, PDH OGDH, 2-oxoapidic acid dehydrogenase complex (OADH), and the branched

chained 2-oxoadipic acid dehydrogenase complex (BCOADH). In complex I, there are 2 sites of ROS production. At site I_F, electron transfer from the 2-electron carrier $FMNH_2$ to the 1-electron Fe-S clusters within the complex provides an opportunity for electron escape. This is also true for electron transfer from the Fe-S clusters to the 2-electron carrier UQH_2 in the MIM site I_Q (64). ROS production by the 2-oxoacid dehydrogenase complexes occurs during electron transfer from the E2-bound dihydrolipoate to FAD and finally NAD^+. The UQH2/UQ isopotential group includes complex III, complex II, GAPDH, ETFQO, and DHODH. Electron transfer through the ETC must inevitably pass through complex III. As previously discussed, electron transfer through complex III involves the formation of a $UQ^{\bullet-}$ radical intermediate formed in the III_{Qo} site. This radical formation offers an avenue for premature electron escape to oxygen (65). ROS production by complex II requires an electron source in addition to oxygen access to the flavin site (63). Indeed, it has been demonstrated that complex II accounts for a significant amount of ROS in cardiac mitochondria challenged with ischemia-reperfusion injury (66). GAPDH, ETFQO, and DHODH each transfer electrons directly to the quinone pool. ROS production by these sites is minimal under physiological circumstances. GADPH has been shown to act as a significant source of ROS when the ETC is inhibited in the presence of high amounts of glycerol-3-phosphate (63). The rate of ROS produced by ETFQO was recorded through inhibition of ROS by complex I, II, and III with the addition of rotenone, malonate, and myxothiazol respectively with acylcarnitine supplementation (63).

Complexes I and III have long been considered the major producers of ROS in mitochondria due to the maximum ROS producing capacity of these sites overshadowing that of other sites. However, the rates of ROS production from the 12 sites differ as a function of the concentration of the ROS producing enzyme, nutrient type and concentration, and O_2 availability.

It has been demonstrated and recently confirmed by the Mailloux laboratory that OGDH and PDH have the capacity to produce approximately 4 and 8 X more ROS than complex I in skeletal muscle mitochondria (67–69). Furthermore, the stoichiometry of complexes of the ETC and Krebs cycle enzymes can differ between cell types. Our laboratory has found that the hierarchy for ROS production in liver mitochondria is complex III > OGDH >> PDH > complex I (69). On the other hand, complex I and complex II serve as the major locations of ROS production in cardiac mitochondria (66, 69, 70). Liver mitochondria are a more potent source for ROS overall and skeletal muscle mitochondria can adjust how much ROS is made and which sites generate it in response to rest or exercise (71). Currently, our laboratory has also looked at sexual dimorphisms in mitochondrial performance. Past research has demonstrated that mitochondria isolated from female mice demonstrate increased basal respiration and increased capacity to burn fatty acids (72). Unpublished data from our laboratory demonstrate decreases in ROS production in mitochondria isolated from female mice.

1.3 Antioxidant defense systems

The dichotomy of mitochondrial ROS in cellular systems discussed previously mandates that considerable restriction is enforced to control ROS levels. For this reason, antioxidant defense systems exist to prevent excessive accumulation of ROS and strike a balance that promotes coordination between mitochondrial and cellular function while preventing oxidative damage and deregulation of essential biological systems. These systems are outlined in Figure 1.6

The activity of the SOD enzymes has been discussed above. They catalyze the conversion of $O_2^{\bullet-}$ to O_2 and H_2O_2 in the following reaction:

Equation 1.3: SOD activity

$$2O_2^{\bullet-} + 2H^+ \rightarrow H_2O_2 + O_2$$

SOD (1/2)

As a result of the superb efficiency of the SOD enzymes, H_2O_2 has been acknowledged as the major ROS produced by mitochondria. H_2O_2 clearance can be mediated by catalase, which primarily operates within peroxisomes but can also be found to a lesser extent in the cytoplasmic and extracellular environment (73). Recent evidence has also demonstrated catalase occurs in liver and cardiac mitochondria (74, 75). This enzyme catalyzes the conversion of H_2O_2 to H_2O and O_2 in the following reaction:

Equation 1.4: Catalase activity

$$2H_2O_2 \rightarrow 2\ H_2O + O_2$$

Catalase

Catalase quenches H_2O_2 in the absence of NADPH. Additionally, catalase dismutates H_2O_2 only when it is high in concentration (high nM to low µM). However, it displays low affinity when H_2O_2 levels are maintained at physiological levels (76, 77). Maintenance of steady-state H_2O_2 levels in and outside of mitochondria is mediated by the NADPH-dependent antioxidant defenses, the thioredoxin (TRX) and the glutathione (GSH) systems. TRX works in unison with peroxiredoxin (PRX) for the clearance of H_2O_2 mediated by the PRX3 isozyme, as well as lipid hydroperoxides, mediated by the PRX5 isozyme (78). PRX is a homodimer with each monomer organized in a head-to-tail fashion. Each PRX monomer contains a catalytic peroxidatic cysteine (Cys_{per}) and resolving cysteine (Cys_{res}). Hydrogen peroxide clearance begins when Cys_{per} is oxidized by H_2O_2 forming a sulfenic acid (SOH) (79). The SOH group is then resolved by an adjacent Cys_{res} forming a disulfide bridge between the two monomers. The disulfide bridge is then

reduced through a thiol disulfide exchange reaction with TRX2, regenerating active PRX3 or 5. Oxidized TRX2 is then reduced by thioredoxin reductase-2 (TR2) and NADPH (79).

GSH is a tripeptide consisting of glycine, cysteine, and glutamate. The γ-carboxy group in glutamate is required to form the amide bond with cysteine, a unique feature that renders GSH resistant to degradation by peptidases. GSH synthesis occurs primarily in the cytosol of hepatocytes and must be transported into the mitochondria (80). Glutamate and cysteine are bound by γ-glutamylcysteine synthase followed by the addition of glycine by glutathione synthase (81). Biosynthesis is dependent on the availability of cysteine. GSH mediated degeneration of H_2O_2 is catalyzed by glutathione peroxidase 1 (GPx1) and results in dimerization and disulfide bond formation generating glutathione disulfide (GSSG). This is achieved using a selenocysteine residue localized in the active site of GPx which is oxidized to a selenic acid by H_2O_2. Glutathione then binds to GPx, forming a glutathionyl-selenic acid intermediate which is then resolved by a second GSH molecule producing GSSG. The GSH/GSSG ratio is a well-recognized indicator of the redox status of the cell and is maintained at a 100:1 ratio by the action of glutathione reductase, which utilizes the reductive potential of the NADPH pool in a similar manner to thioredoxin reduction to reduce GSSG, replenishing GSH. An isozyme of GPx, GPx4, associates with the inner leaflet of the MIM slowing lipid peroxide propagation (82).

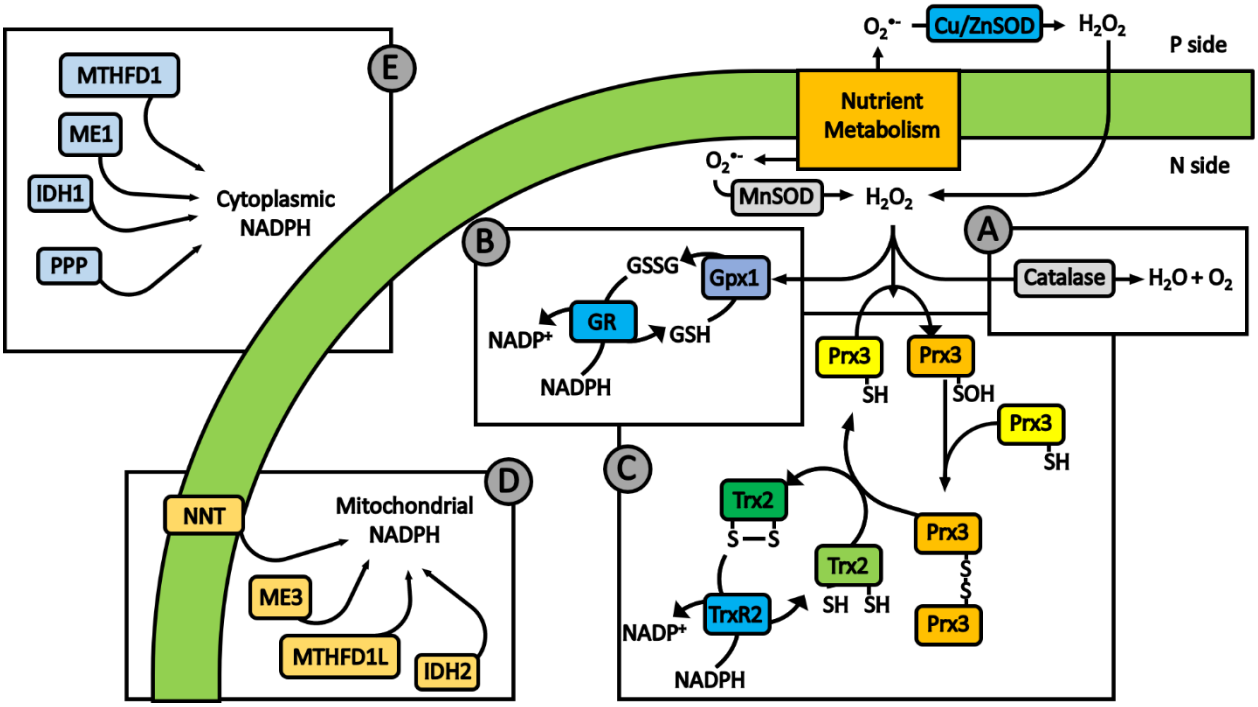

Figure 1.6: Mitochondrial antioxidant systems

A) Catalase found in the mitochondrial matrix mediates clearance of H_2O_2 B) GPX1 utilized GSH to clear H_2O_2. GSH is replenished by the action of GR. C) The thioredoxin system utilizes peroxiredoxin to clear H_2O_2. Dimerized PRX3 is reactivated through reduction by TRX2 which is in turn reactivated by thioredoxin reductase. D) and E) NADPH which provides the reductive power necessary to sustain the antioxidant systems is provided by the listed enzymes.

GSH is also capable of targeting by-products of oxidative damage and xenobiotic activity for removal from the mitochondrial matrix (82).The GSH/GSSG ratio is a well-recognized indicator of the redox status of the cell and is maintained at a 100:1 ratio by the action of glutathione reductase, which utilizes the reductive potential of the NADPH pool in a similar manner to thioredoxin reduction to reduce GSSG replenishing GSH. An isozyme of GPx, GPx4, associates with the inner leaflet of the MIM slowing lipid peroxide propagation (82). Mitochondrial concentrations of GSH are within 1-10 mM which allows it to act as an effective regulator of H_2O_2 levels while also carrying out additional functionality. GSH conjugation and protection of protein thiols, for example, is necessary to prevent excessive protein oxidation in a highly oxidized cellular environment. This process is known as protein S-glutathionylation and will be discussed in greater detail later. GSH is also capable of targeting by-products of oxidative damage and xenobiotic activity for removal from the mitochondrial matrix (82).

1.4 Control of ROS production

1.4.1 Proton leaks

Control of ROS levels in the mitochondria and the cell can be achieved on 2 fronts; degradation pathways, which was discussed in the prior section, and modulation of production. ROS production by the discussed sites is dependent on oxygen accessibility, and the redox status of the ROS generating site and the concentration of the electron donating site. Two particularly important aspects of the control of ROS production are proton leaks and redox signaling.

Proton leak occurs when protons are returned to the matrix, bypassing complex V. This can decrease the strength of the PMF, diminishing the amount of protonic back pressure on the respiratory chain. As a result, electrons flow more efficiently through the ETC limiting the over-

reduction of redox centers in the respiratory complexes which diminishes the number of electrons that can be used to produce ROS. This phenomenon has been demonstrated using protonophores which chemically uncouple the proton gradient, diminishing ROS production (83, 84). In addition, a non-Ohmic relationship exists between membrane potential strength and the rate of ROS production (84). Small increases in PMF can exponentially increase ROS production while increasing proton return by leaks can have the opposite effect. Mild leaks can be defined as either basal or inducible. Basal proton leak refers to the constant, unregulated movement of protons back into the matrix (85). This is thought to be mediated primarily by the adenine nucleotide translocase (ANT). The primary function of ANT is the exchange of free ADP for ATP across the inner mitochondrial membrane (85). This process is essential for continued and efficient ATP production (86). However, it was also shown that ANT can also basally leak protons and it was demonstrated that changes in proton conductance in mouse muscle and whole Drosophila mitochondria are proportional to changes in ANT expression (87). The basal leak of protons by ANT was also hypothesized to be associated with the opening of the mitochondrial permeability transition pore (MPTP) (88). In addition, recent evidence has suggested that leaks through ANT can be regulated by electrophiles such as 4-hydroxy-2-nonenal, a by-product of lipid peroxidation, and nitro-fatty acids (41).

Most inducible proton leaks in mammalian cells are thought to be carried out by the uncoupling proteins (UCP). There are five UCP isozymes found in mammals and the different isoforms display tissue-dependent expression. UCP1, also called thermogenin, was the first protein discovered that siphons protons from the IMS reducing the PMF and “uncoupling” electron transport and the generation of ATP. UCP1 makes up ~13% of the mitochondrial proteome in brown adipose tissue mitochondria and is only activated in response to cold exposure or over-

consumption of high-calorie foods (41). UCP1 activation involves induction of the sympathetic nervous system and the release of norepinephrine, which subsequently activates UCP1 using the cAMP-signaling pathway (89). The Gibbs free energy stored in the proton gradient is used to drive heat production through proton return to the matrix, instead of being coupled to the biosynthesis of ATP. Activation of UCP1 has also been found to control how ROS is release by brown fat mitochondria (41). Indeed, Echtay *et al* observed that ROS can regulate its own production by activating leaks through UCP1 (90). Another study made similar observations where it was found that 4-hydroxy-2-nonenal has the same effect (91). Finally, recent work by Chouchani *et al* found that UCP1 can be activated through the oxidation of cysteine residues located on the last matrix loop region of the protein (92). UCP2 and 3 were discovered in the late 1990s and share approximately 60% sequence identity with UCP1 and ~30% homology with one another (89). UCP2 is more ubiquitously expressed in the body and is found in stomach epithelia, the hypothalamus, macrophages, and pancreatic β cells. UCP3, on the other hand, is almost exclusively found in skeletal muscle. Notably, both proteins do not couple proton leaks to heat generation, which is attributed to the fact that both proteins only account for ~0.1% of total mitochondrial proteins (an exception is β-cells) (41). Like UCP1, leaks through UCP2 and UCP3 were also found to be regulated by ROS, specifically $O_2^{\bullet -}$, suggesting a possible mechanism for self-regulation of ROS production (90). This mechanism for regulation of UCP1-3 by ROS is still enthusiastically debated. Some have argued that activation by ROS is not physiologically relevant since it is abolished by physiological concentrations of GDP (2). However, despite the contentious nature associated with how ROS regulates leaks through UCP1-3, it is clear that UCP2 and UCP3 fulfill some important functions. First, there is an overwhelming amount of evidence demonstrating that both proteins protect cells from oxidative distress. Second, it has been found

that regulation of cellular ROS by UCP2 and UCP3 fulfills some vital physiological functions. In pancreatic islet cells, UCP2 regulates insulin and glucagon secretion through the regulation of ATP and ROS production (93, 94). UCP2 is also implicated in immune cell modulation of ROS production (95) and modulates satiety signaling in the hypothalamus. Its overexpression has also been associated with decreased apoptotic signaling in neuronal and cardiac mitochondria (96, 97).

UCP3 is expressed primarily in skeletal muscle with limited expression in cardiac and brown adipose tissue. The primary function of UCP3 like UCP2 is not currently known. UCP3 expression and activity, however, are dependent on fatty acid concentrations suggesting a strong case for a role in fatty acid metabolism (87). UCP3 is thought to protect against obesity as well as insulin resistance. Indeed, increased UCP3 expression is associated with decreased weight gain, and Grx2 deficiency induced a 60% increase in UCP3 expression associated with decreased fatty acid accumulation (98, 99). Additionally, down-regulation of UCP3 is associated with insulin resistance that can be rescued by exercise (89).

1.4.2 Redox switches

Post-translational modification is a well understood dynamic of cellular control of protein function. Phosphorylation, for example, is a vital element in the regulation of cellular pathways and embodies all required properties of a functional regulatory system. These characteristics are reversibility, specificity, speed and an ability to respond to physiological cues. Redox variability within the mitochondrial matrix, because of ROS generation, can result in post-translational protein modification, primarily at exposed cysteine residues. Pertinent protein modifications that result from changes in redox balance include sulfenylation, S-nitrosylation, and S-glutathionylation. Redox signaling is an influence of protein function as a result of changes in redox balance through post-translational protein modifications. Protein cysteine thiol oxidation,

however, is a slow nonspecific process that requires the formation of a thiolate anion (45) and, therefore, not all post-translational modifications fulfill the requirements for a physiologically relevant mitochondrial regulatory system.

S-nitrosylation is a promising candidate for modulation of protein function. The conjugation and removal of NO has been shown to alter cellular and mitochondrial processes (100–102). NO modification can inhibit complex IV activity, suggesting a possible role for S-nitrosylation in modifying respiration (103). Additionally, TRX of the antioxidant system discussed previously has been shown to mediate denitrosylation reactions (104). There are no known enzymes that mediate nitrosylation reactions. Additionally, the lack of specificity and the toxicity of high NO concentrations, particularly in mitochondria where NO and $O_2^{\bullet-}$ interaction leads to the development of peroxynitrite ($ONOO^-$), mark S-nitrosylation as unsuitable for mitochondrial regulation. In the presence of high H_2O_2 concentrations, the thiolate anion is oxidized to SOH. While this process can disable protein function, very few proteins are known to engage in sulfenylation. The process can be reversed by sulfiredoxin (105) unless sulfinic (SO_2H) and sulfonic acid (SO_3H) residues develop as a consequence of additional subsequent oxidation events. Sulfinic and sulfonic acid residues are irreversible and permanently disable protein function. Due to the nonspecific and slow rate of sulfenylation reactions, H_2O_2 has lost support as a useful regulator of mitochondrial function. Rather, it seems to elicit damage as a consequence of changes in redox balance that must be quickly and efficiently repaired by other antioxidant systems. Indeed, initial concepts of H_2O_2 mediated regulation have shifted in recent years to suggest that S-glutathionylation, rather, is the creditable regulatory agent. Of the three, S-glutathionylation is the only one that fulfills the requirements for a functional regulatory system.

As a result, it has gained much focus in recent decades as a primary regulatory tool for mitochondrial maintenance of homeostasis.

1.5 Protein S-glutathionylation

1.5.1 Spontaneous and enzymatically-driven reactions

Protein S-glutathionylation reactions involve the conjugation and removal of a glutathione moiety from a target protein. Proteins can either be modified by glutathione via spontaneous or enzyme-driven reactions. Spontaneous S-glutathionylation reactions usually proceed when the GSH/GSSG is ~1, which typically occurs during oxidative distress, as shown in Figure 1.7. Spontaneous protein S-glutathionylation reactions can proceed via three different pathways (Figure 1.8). The first involves a simple thiol-disulfide exchange reaction between cysteine and GSSG (42). This requires ionization of an available protein cysteine thiol, forming a highly nucleophilic thiolate anion which can attack the disulfide bridge in GSSG. The second reaction involves oxidation of protein cysteine thiolate anion by H_2O_2, forming SOH (42). Sulfenic acid is a good nucleophile which then attacks GSSG forming a protein-glutathione mixed disulfide. Finally, the third spontaneous reaction involves the formation of a thiyl radical on a protein cysteine residue resulting in its interaction with glutathione and the S-glutathionylation of a protein (42).

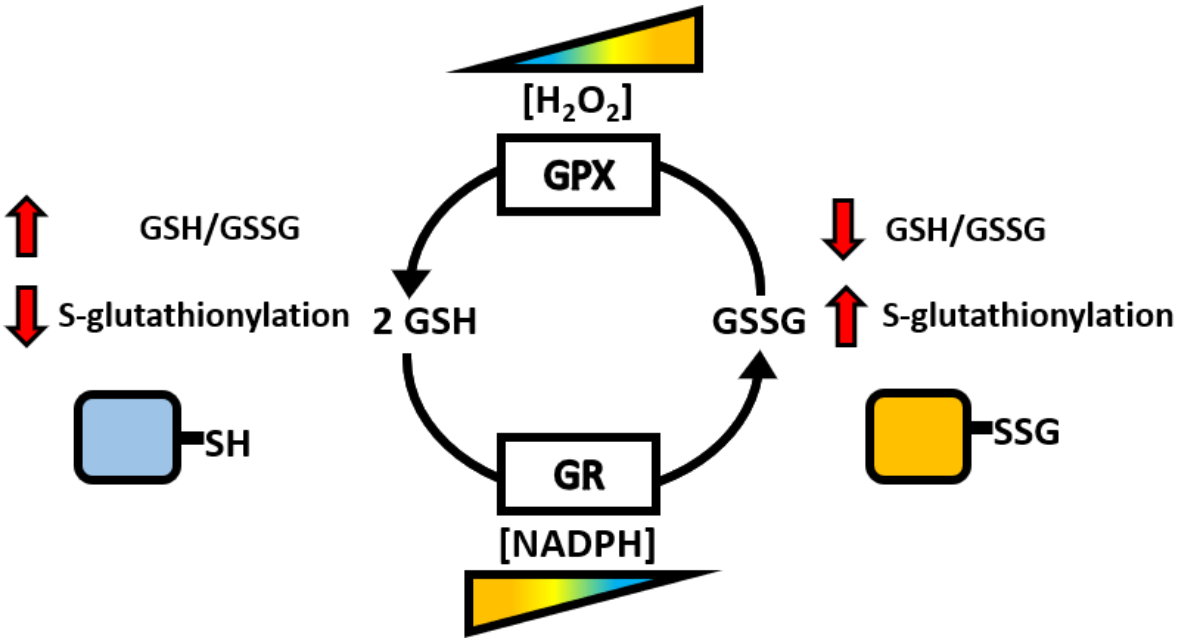

Figure 1.7: S-glutathionylation reactions

Reversible S-glutathionylation occurs as a function of redox balance and GSH availability. Oxidation and reduction of the glutathione pool is catalyzed by glutathione peroxidases (GPX) and glutathione reductases (GR).

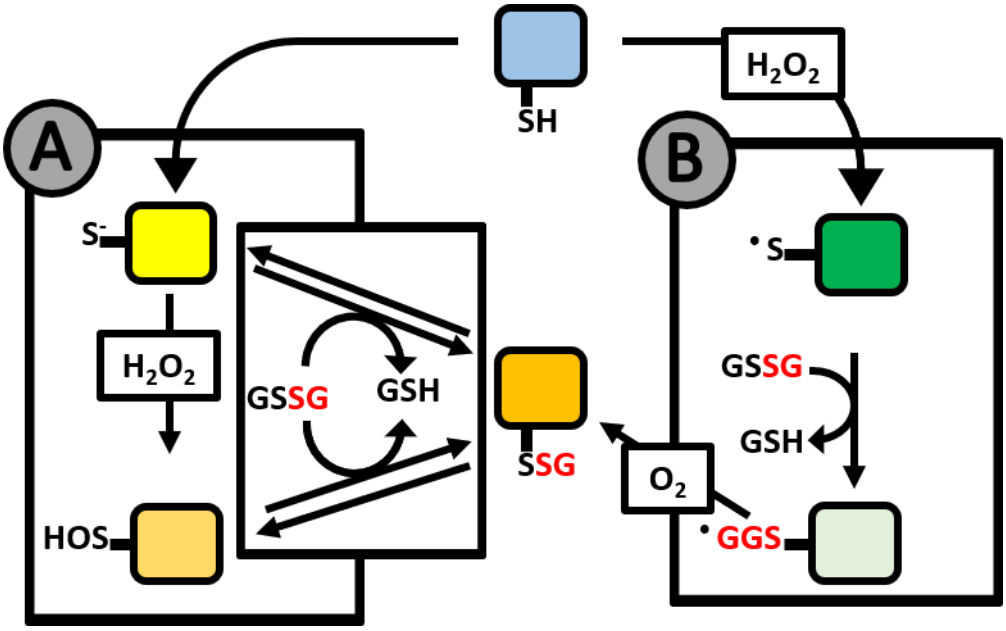

Figure 1.8: Spontaneous S-glutathionylation reactions.

Spontaneous protein S-glutathionylation reactions can proceed via two different pathways. This includes (**A**) ionization and thiolate formation followed by thiol-disulfide exchange reaction between cysteine and GSSG or oxidation of protein cysteine thiolate anion by H_2O_2, forming SOH followed by thiol-disulfide exchange. (**B**) Finally, the formation of a thiyl-radical on a protein cysteine residue can interact with glutathione.

It is important to emphasize that most proteins in normal cells (e.g. not experiencing oxidative distress) have an equilibrium constant for S-glutathionylation (K_{mix}) of approximately 1 (106). This means that spontaneous reactions are not likely in normally functioning mammalian cells. Some exceptions include the protein *c*-Jun, which has a reported $K_{mix} = 15$ (107). In mitochondria, certain proteins like complex II and UCP3 are also basally S-glutathionylated. Proteins that are basally S-glutathionylated may have higher than normal S-glutathionylation coefficients allowing for their spontaneous modification.

Although spontaneous reactions may occur in normal cells for a few proteins, most protein S-glutathionylation reactions are enzymatically driven. The GRX proteins are the chief enzymes that drive these reactions in cells. Glutathione S-transferases have also been shown to mediate these reactions in the cytosol as well (108). Glutaredoxins are a family of small heat-stable thiol oxidoreductases that belong to the thioredoxin superfamily. The first glutaredoxin found to catalyze the deglutathionylation of target proteins was the cytosolic isoform, GRX1. GRX1 can deglutathionylate a target protein at 10^2-10^5 $M^{-1}s^{-1}$ and the rate of deglutathionylation depends on the pKa of the modified cysteine residues (the lower the pKa the higher the rate) (109). GRX1 contains a thioredoxin fold comprised of 4 beta-sheets and 3 alpha-helices. The active site *CXXC* motif is localized in the first loop region and alpha helices of the protein, which is required to drive the first step of deglutathionylation (110). It is important to point out that TRX proteins also contain a *CXXC* motif. However, TRX isozymes are unable to carry out the deglutathionylation of a protein. This is because the enzymatic deglutathionylation of a protein also requires GSH. GRX1 harbors a GSH binding motif in its C-terminus which binds and deprotonates glutathione, facilitating protein deglutathionylation (111). Proteins modified by glutathione also contain glutathionylation motifs, which are recognized and bound by GRX1. The deglutathionylation of a

target protein by GRX1 can occur either through a monothiol or dithiol exchange **(**Figure 1.9**)**. In the monothiol mechanism, GSH binds to GRX1, followed by the nucleophilic attack of GSH on GSH. The result is GSSG formation which is reduced by GR and NADPH (112). Dithiol exchange involves a thiol-disulfide exchange reaction between the *CXXC* motif and the target protein, resulting in the transfer of the glutathionyl moiety to the active site of GRX1 (42). In the second step, glutathione anion located in the C-terminus performs a nucleophilic attack on the GRX1-glutathione disulfide bridge, forming GSSG and a deglutathionylated GRX1 protein. GSSG is then reduced by glutathione reductase (42). The deglutathionylation of target proteins by GRX1 has been found to regulate a wide breadth of cellular functions ranging from inflammatory signaling to apoptosis (42).

The mitochondrial matrix associated GRX1 homolog, GRX2, was discovered in 2001 (113). Although it only shares ~34% homology with GRX1, GRX2 uses a very similar enzymatic mechanism to deglutathionylate a target protein. While GRX2 function and structure are similar to that of GRX1, there are many striking differences that set the two apart. Firstly, GRX2 is capable of mediating both forward and reverse S-glutathionylation in response to changes in 2GSH/GSSG ratio (114). This has not been observed in GRX1. Secondly, GRX2 has demonstrated the capacity to reactivate oxidized TRX2 during TR2 deactivation by oxidative distress (115). Finally, in contrast, to GRX1, GRX2 cannot be deactivated by oxidation. GRX2 lacks the alternate redox-sensitive cysteines present in GRX1 that are oxidized and lead to protein deactivation. Alternatively, GRX2 is activated by mitochondrial $O_2^{\bullet-}$ production. GRX2 exists primarily as an inactive dimer stabilized by a redox-sensitive Fe-S cluster $[2Fe\text{-}2S]^{2+}$. Release of mitochondrial $O_2^{\bullet-}$ results in disassembly of this Fe-S cluster and release of active GRX2 monomers (116).

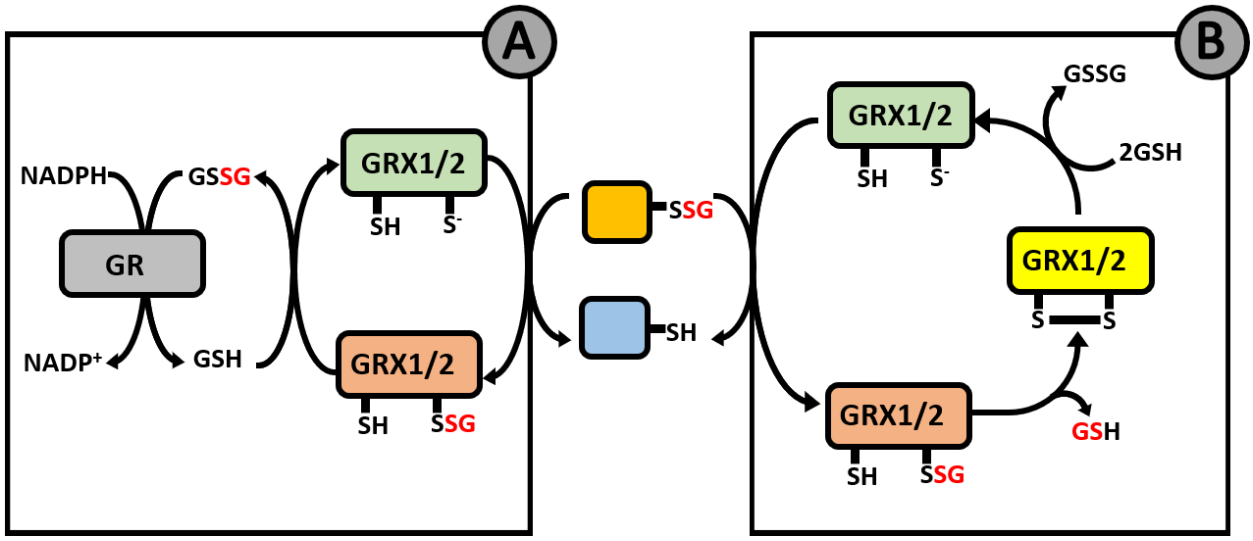

Figure 1.9: Protein deglutathionylation by GRX1/2.

Deglutathionylation can proceed either via a monothiol (**A)** or dithiol **(B)** mechanism.

The GRX2 proteins maintain a Cys-Ser-Tyr-Cys conserved active site. The 3 isozymes GRX2a, GRX2b and GRX2c differ in 5`splicing patterns and are differentially expressed (113). GRX2a is expressed predominantly in the mitochondrial matrix, while GRX2b and GRX2c are localized to the nucleus and are expressed almost exclusively in the testes and some cancerous cell lines (116). The preferred mechanism of GRX2 action is a monothiol exchange due to its high affinity for protein glutathione-mixed disulfides (PSSG) (117).

1.5.2 Mitochondrial S-glutathionylation reactions

Generation of the proton gradient in mitochondria also, in turn, results in the basification of the mitochondrial matrix, creating a unique environment in which thiolate ion formation is favored. As previously mentioned, thiolate ion formation is required for modification of the exposed protein cysteine thiols. In addition, cysteine thiols are the most concentrated thiol in mitochondria at 60 – 90 mM (118). This, coupled with GSH concentrations that fluctuate between 1 to 5 mM and a 2GSH/GSSG redox potential of -280 to -340 mV (41), make the mitochondrial matrix environment prime for S-glutathionylation. These conditions increase the likelihood of spontaneous and enzymatically driven PSSG formation which can reverse SOH formation and prevent excessive irreversible oxidation to SO_2H and SO_3H (119) while simultaneously modifying protein function through conformational changes. GRX2 mediated S-glutathionylation reactions allow mitochondrial bioenergetics, metabolism and ROS production to be modulated in response to physiological changes in redox balance. They demonstrate considerable complexity as a regulatory system.

1.5.2.1 Krebs cycle and associated enzymes

Multiple enzymes within the Krebs cycle link S-glutathionylation and the regulation of metabolism and nutrient oxidation. S-glutathionylation of aconitase decreases its activity and protects from irreversible oxidation of Cys^{126} and Cys^{385} (53). S-glutathionylation of IDH and SCS also decreases their activity in response to oxidative stress (7, 120). Our laboratory has also recently demonstrated that Grx2 controls PDH and OGDH in liver mitochondria (68, 69). Under highly oxidized situations the lipoic acid residue in the E2 subunit of both enzymes is in danger of irreversible oxidation. S-glutathionylation of the lipoic acid residues protects them from excessive oxidation. S-glutathionylation of the lipoic acid residue also leads to decreased activity and ROS production by both enzymes (Figure 1.10). The E2 subunit is the primary site for PDH and OGDH S-glutathionylation; however, work conducted by our group and others has demonstrated that the E1 and E3 subunits can also be modified (68, 69). ROS production by both enzymes is reduced during forward electron flow; however, when metabolizing NADH these enzymes increase ROS with increased GSH concentration (45, 68, 69). Reverse electron flow can occur at physiological concentrations of NADH. Given the importance of these enzymes as entry points for electrons from a large fraction of the available carbon metabolites, these findings suggest they are a key point of control by mitochondrial modulations of redox balance and that Grx2 is the mediator of this control (68).

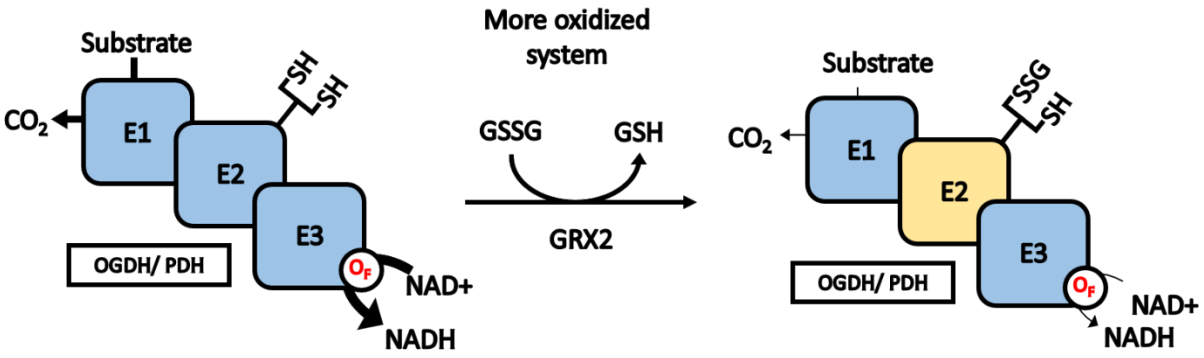

Figure 1.10: GRX 2 mediated S-glutathionylation of OGDH and PDH

S-glutathionylation of the lipoic acid residue of the E2 subunit decreases enzyme activity while simultaneously reducing ROS production.

1.5.2.2 Oxidative Phosphorylation

Complex I was the first identified target of Grx2 targeted S-glutathionylation in skeletal muscle mitochondria and is the most extensively studied. Complex I contains an assortment of glutathionylation sites that elicit flexible physiologically relevant responses (99, 111, 121). Grx2 demonstrated the ability to glutathionylate or deglutathionylate complex I in response to changes in 2GSH/GSSG ratio (42). S-glutathionylation of Cys^{531} and Cys^{704} of NDUSF1 leads to decreased ROS production and decreased enzyme activity (122). Cys^{531} and Cys^{704} are very near to the NADH binding site and it is suggested that GSH conjugation leads to conformational changes that reduce NADH oxidation. It has been suggested that S-glutathionylation of the ND3 subunit of complex I serves as a possible method of regulation of complex I. ND3 is exposed on a transition from A to D configuration in response to low substrate availability (123). Oxidative modification Cys^{39} of this subunit is associated with decreased complex I activity (124). S-glutathionylation of the Ndufv1 in response to increased GSSG concentrations can decrease enzyme activity and decrease ROS production. This has been demonstrated in mitochondria isolated from cardiac skeletal muscle and liver tissue as well as lens epithelia (122, 125–127). In contrast, extended exposure to increased GSSG concentrations results in increased ROS production by the complex (128). Even Ndufa11 required for complex one assembly has displayed altered function as a result of S-glutathionylation reactions (129)

Each of the 5 enzyme complexes of the electron transport chain are modified and modulated in some way by S-glutathionylation reactions in response to altered redox state in physiologically relevant or disease state conditions. Complex II is constitutively S-glutathionylated at Cys^{90} which helps to protect it from excessive oxidation and inactivation by peroxynitrite and $O_2^{\bullet-}$ (130). Deglutathionylation of complex II reduces activity and increases ROS

production suggesting that S-glutathionylation of complex II is required for its activity. Under oxidative stress as in dyssynchronous heart failure, the α subunits of complex V are also reversibly glutathionylated reducing the ATP producing capacity of mitochondria (131). Most recently, S-glutathionylation of complex IV and III have also been demonstrated in an *S. cerevisiae* model (132).

1.5.2.3 Proton leak

The least contentious function of both UCP2 and 3 is their ability to modulate mitochondrial ROS production. Indeed, a non-Ohmic relationship exists between membrane potential and ROS production where small changes in membrane potential can result in drastic modulation of ROS production. Thus, UCP2 and 3 represent key points of control. How mitochondria might implement this control, however, was not known until the demonstration that reversible S-glutathionylation of UCP2 and 3 regulates their activity in thymocytes, promyelocytic leukemia cells, kidney tissue, and skeletal muscle mitochondria (133). UCP2 S-glutathionylation results in increased ROS production in a number of tissues (133–135). Grx2 mediated S-glutathionylation of UCP3 at Cys^{25} and Cys^{295} is required to inhibit proton leak (133). This was confirmed by increased proton leak in skeletal muscle mitochondria isolated from Grx2 haploinsufficient and deficient mice (99). Our laboratory has also demonstrated that the absence of Grx2 leads to constitutive s-glutathionylation of UCP3 (70, 127). As of today, the mechanisms of ROS mediated UCP3 deglutathionylation and activation are not yet known. There is also evidence to show that ANT may be a target for S-glutathionylation, introducing yet another avenue for S-glutathionylation dependent regulation of ROS production. Induction of chemical S-glutathionylation was incapable of modifying UCP1 activity suggesting that UCP1 is not regulated in this way (136).

1.5.2.4 Other mitochondrial functions

The influence of S-glutathionylation reactions extends outside the scope of mitochondrial bioenergetics and ROS production. Indeed S-glutathionylation reactions influence solute import through modulation of the mitochondrial pyruvate carrier-1 (MPC1), MPTP formation as well as transport by CACT. Our laboratory has recently demonstrated that S-glutathionylation of MPC1 almost completely abolishes pyruvate transport (127).

MPTP formation occurs in response to indicators of cellular stress such as increased oxidation or cytoplasmic Ca^{2+} release (137). MPTP formation is essential for apoptosis and mitophagy. Although ANT is a debated component of MPTP, it was demonstrated that S-glutathionylation of ANT prevents pore formation, suggesting that it may play some role in regulating MPTP formation (138). Likewise, S-glutathionylation of cyclophilin-D prevents MPTP formation (139). This is strong evidence for S-glutathionylation as a mechanism of control for MPTP formation and, in turn, MPTP dependent apoptotic pathways.

The regulation of CACT by S-glutathionylation is currently under debate. It was demonstrated that S-glutathionylation of Cys^{136} and Cys^{155} led to inhibition of CACT activity (140). However, our group was unable to recreate these findings (127). Still, there is a possibility that S-glutathionylation reactions regulate fatty acid oxidation in this way.

Lastly, mitochondria have demonstrated the ability to modify their structure in response to physiological demands. Mitochondrial hyperfusion can protect from excessive oxidation through increased electron transfer efficiency (141, 142). Fusion processes are carried out by mitofusin (MTF) 1 and 2 and the autosomal dominant optic atrophy protein 1 (OAP1), each of which have been demonstrated to be S-glutathionylated (143, 144). S-glutathionylation of these proteins leads

to mitochondrial hyperfusion suggesting a role for S-glutathionylation reactions in mediating changes in morphology in response to acute mitochondrial stressors.

1.6 Skeletal muscle physiology

Muscle tissue can be separated into three groups. Smooth, cardiac and skeletal muscle can then be subdivided based on the structures and differences in innervation (10). Skeletal muscle is the most abundant of the three. It constitutes approximately 40% of the adult male's body mass and 20% the body mass of adult mice. Innervation by the somatic nervous system grants voluntary control over skeletal muscle giving organisms a range of movement. Skeletal muscle cells consist of elongated multinucleated cells that are bundled together by connective tissue to create muscle fibers (10). Within each cell is a highly organized cytoskeleton system consisting of thick and thin filaments that work in unison to generate the force required for contraction. These myofibrils make up~80% of the contents of muscle cells and consist of myosin, the thick filaments, actin, and the thin filaments. Along the myofibrils, alternating Z lines and M lines arrange the actin and myosin fibers such that they interlock at the center of each Z-M interval. The myosin fibers extend from their bass at the M line while the actin filaments extend from their base at the Z line. This alternating pattern of Z and M lines creates an alternating pattern of dark and light bands that give skeletal muscle its striated appearance under the microscope. Myosin consists of large numbers of dimers that each contain two identical proteins containing a tail and head domain. The tail domain allows dimerization and formation of the myosin fiber while the head domain contains actin binding and ATPase activity. The actin filament acts as a "scaffold" upon which the myosin fibers climb to elicit contraction. Actin filaments consist of actin tropomyosin and troponin. Troponin and tropomyosin hold regulatory roles. When muscle is relaxed Troponin-tropomyosin and myosin are bound in such a way that it prevents binding of myosin to actin filaments. Ca^{2+} release from

the sarcoplasmic reticulum binds to troponin leading to a conformational change in tropomyosin that removes tropomyosin from the myosin binding site enabling contraction (10).

Once myosin is given access to the actin filaments in response to Ca^{2+} release from the sarcoplasmic reticulum, it binds and conducts what is characterized as a power stroke. Here the head domain bends at a 45° angle to the myosin tail domain. This effectively pulls the actin filaments in towards the stationary M line a small distance. During this process bound ADP and P_i are released. Binding of ATP to the myosin head domain reduces its affinity for actin binding and the myosin head releases and returns to the unbent form. Hydrolysis of this ATP molecule reengages the myosin head and initiates a second power stroke. This cycle repeats continuously as long as ATP and Ca^{2+} are supplied until the muscle is fully contracted. For this reason, skeletal muscle is rich in mitochondria which supply the large volume of ATP required to continue contraction. An interesting consequence of the need for ATP for myosin release from actin filaments is the development of rigor mortis a few hours after death. The lack of ATP production and the inability of the cells to efficiently remove Ca^{2+} leads to a steady cross bridge formed between the myosin heads and actin filaments leading to unyielding and unmoving muscle tissue (10).

Skeletal muscle has always been a prime target for therapeutic strategies to combat obesity and related disorders like diabetes and hypertension due to the fact that skeletal muscle is a major location of fatty acid oxidation for ATP production. Obesity has long since been attributed to a positive energy balance resulting from a sedentary lifestyle coupled with excessive nutrient intake. Indeed, the most effective treatment options for such ailments require the maintenance of a negative energy balance through diet and exercise. During the initial phases of exercise, fatty acid oxidation increases considerably in addition to decreased esterification in adipose tissue, and

increased uptake by skeletal muscle (145). It is important to note, however, that these therapeutic strategies are not always feasible and may result in different outcomes in individuals due to variations in genetic background (146, 147). For this reason, many are trying instead to understand the processes that regulate fatty acid metabolism in skeletal muscle in an attempt to identify pharmaceutical targets for treatment strategies (145). In this regard, skeletal muscle mitochondria are poised as key targets since nutrient metabolism and fatty acid metabolism is centered within the matrix of the mitochondria, and mitochondria have established themselves as effective mediators of cellular control in addition to their primary role as energy producers.

In both humans and mice, high-fat diets have been shown to increase H_2O_2 production in conjunction with an increased oxidative cellular environment (148). The persistence of this increased oxidative state leads to the development of insulin resistance. However, that is only when levels are chronically high. In normal muscle, ROS levels display spatiotemporal increases and decreases which are vital for muscle physiology (61). The subsarcolemmal and intermyofibrillar populations of mitochondria both increase in volume in response to exercise and are capable of mediating fatty acid metabolism and cell signaling (149). These mitochondria also increase ROS production in response to exercise. These ROS generated by skeletal muscle mitochondria have a biphasic relationship with muscle function. Low-level ROS production is essential for normal muscle force production, while excessive ROS production leads to decreased muscle force. These mechanisms of regulation are dependent on post-translational modification and changes in redox balance (61). For example, S-glutathionylation of troponin in skeletal muscle increases its affinity for Ca^{2+} and increased S-glutathionylation of titin, a constituent of M-line in muscle sarcomeres, increases protein elasticity. Together this leads to increased muscle contraction efficiency (61). On the other hand, when antioxidant defense systems are depleted, or during strenuous exercise when

ROS is produced faster than it can be removed muscle force is weakened substantially by the presence of ROS (150). Indeed, sites within the mitochondria are the most affected by protein S-glutathionylation reactions in response to exercise (61). Multiple locations within the TCA and ETC are targeted for S-glutathionylation including complex II, MDH, and ATP synthase. Indeed, our laboratory was the first to demonstrate S-glutathionylation of complex I and inhibition of pyruvate uptake as a consequence of chemical inducers of S-glutathionylation (127). This demonstrates additional points of regulation of metabolism in response to changes in redox balance.

Recent work has also demonstrated that Grx2 was required for the regulation of UCP3 activity in skeletal muscle mitochondria. In the absence of Grx2, UCP3 remained in a deglutathionated state resulting in increased proton leak dependent respiration. Grx2 seems to be required to glutathionylate UCP3 to decrease proton leak. This represents a promising avenue for regulation of fatty acid metabolism since the researchers observed that these mice, deficient and haploinsufficient in Grx2, displayed decreased overall bodyweight, decreased lower gonadal white adipose tissue weight and decreased fat associated with skeletal muscle. This was associated with a more oxidized 2GSH/GSSG ratio and increased ROS production from skeletal muscle mitochondria (99) With the ever-increasing awareness of S-glutathionylation as an effective mediator of cell signaling and metabolic control it is essential that its possible role in the regulation of fatty acid metabolism be further investigated.

1.7 Research objectives

The goal of this project was to assess the role of Grx2 in the regulation of fatty acid metabolism and ROS generation. To do this, the impact of a diet which will cause diet-induced obesity (DIO) on Grx2-haploinsufficient mice was investigated. Diets that induce DIO have been shown to increase ROS production and increase S-glutathionylation events. This model, therefore, provides insight into how dysregulated S-glutathionylation reactions will affect the ability of skeletal muscle mitochondria to respond to challenge with a diet that induces DIO.

1.8 Hypothesis

Decreasing Grx2 availability will protect mice from DIO by increasing muscle fuel metabolism through changes in the S-glutathionylation of proteins.

Chapter 2: Materials and methods

2.1 Chemicals

Chemical	Source
100bp DNA ladder	Invitrogen
2-propanol	ACP
40% acrylamide/Bis	Bio-Rad
Acetic acid	ACP
ADP	Sigma
Ammonium Persulphate	Sigma
Antimycin A	Sigma
Atpenin A5	Santa Cruz
AUR	Invitrogen
BSA	Sigma
Disulfuram	Sigma
DMSO	ACP
EGTA	Sigma
GDP	Sigma
Genapin	Sigma
Glutathione assay Kit	Sigma
Glycine	Sigma
Goat anti-mouse antibody	Abcam
Goat anti-rabbit antibody	Santa Cruz
H_2O_2	Sigma
HCl	Thermo Fisher
HEPES	Sigma
HRP	Sigma
Insulin ELISA Kit	Millipore Sigma
KCL	Thermo Fisher
KMV	Sigma
KOH	Sigma
L-Carnitine Hydrochloride	Sigma
Lammli Buffer	Bio-Rad
Luminol	Thermo Fisher
Malic Acid	Sigma
Mannitol	Sigma
Methanol	Thermo Fisher

Chemical	Source
Monobasic Potassium phosphate	Sigma
$MgCl_2$	Sigma
NaCl	Sigma
NADH	Sigma
NDUSF1 primary antibody	Santa Cruz
Nitrocellulose Membrane	Bio-Rad
Non-fat Dry milk	Lab scientific
Nuclease Free water	Ambion
OGDH primary antibody cocktail	Abcam
Oligomycin	Sigma
OXHOS primary antibody cocktail	Abcam
Palmitoyl-carnitine	Sigma
PDH primary antibody Cocktail	Abcam
Ponceau	Sigma
Pyruvic acid	Sigma
Red extract N AMP PCR kit	Sigma
Ripa buffer	Sigma
Rotenone	Sigma
SOD	Sigma
SOD2 primary antibody	Santa Cruz
Sodium Azide	Sigma
Sodium Dodecyl Sulphate	Sigma
Stable peroxide solution	Thermo Fisher
Subtilisin A	Sigma
Succinic Acid	Sigma
Sucrose	Sigma
SYBR safe	Invitrogen
TEMED	Bio-Rad
Triglyceride Assay kit	Cedarlane
Tris borate EDTA	Thermo Fisher
Trizma Base	Sigma
Tween 20	Bio-Rad
UCP3 primary antibody	Abcam
Ultra-pure Agarose	Thermo Fisher

2.2 Mouse Breeding

Male and female *Grx2*$^{+/-}$ mice were a gift from Dr. Mary-Ellen Harper (University of Ottawa). *Grx2*$^{+/-}$ mice were generated using the C57BL/6N mouse strain as described in Wu *et al.* (121, 126) the physiological and metabolic characteristics of this mouse model was performed previously by Mailloux et al. in 2013 (99). Additional comparisons between the *Grx2*$^{+/-}$ and *Grx2*$^{-/-}$ strains were characterized by this laboratory previously (70). Male and female mice heterozygous for *Grx2* (*Grx2*$^{+/-}$) were paired (age-dependent pairing) for breeding and housed at 25 ºC on a 12-hour day/night light cycle and provided water and chow ad libitum (Teklad Global 18% Protein Rodent Diet, 2018). New litters were weaned at three weeks of age and then ear notched to determine genotype. Ear notches were stored at -20 °C.

2.3 Administration of DIO diets

Female mice were either kept for breeding or used in a separate study. Male *Grx2*$^{+/-}$ mice and wild-type (WT) littermates were fed a high-fat diet (HFD; Teklad diet TD.06415) or matched control diet (CD, Teklad TD.06416) *ad libitum* and given free access to water until 10 weeks of age (Table 2.1). Mouse mass, food, and water consumption were measured once a week until 10 weeks of age. For blood glucose measurements, mice were restrained, and the hind leg extended. The area just above the knee was swabbed with 75% ethanol to sterilize the surface. A small amount of petroleum jelly was then administered, and pressure was applied to the hind leg proximal to the saphenous vein. An A26 gauge ½ inch needle was used to prick the exposed vein and then blood was collected. Glucose levels were measured using a glucose monitoring system glucose test meter (FreeStyle Lite®). At 10 weeks of age, mice were euthanized by cerebral dislocation under heavy anesthesia (5% isoflurane). Blood was collected by cardiac puncture and stored at -80°C for further analysis. Mice were euthanized by cervical dislocation and liver, kidney,

heart, skeletal muscle (pooled forelimb, hindlimb, and pectoral muscles), and abdominal fat were collected, dabbed to remove excess blood, and weighed. Livers were then sectioned and used for histological staining. Gastrocnemius muscle was also used for histological staining and remaining muscle was used for the isolation of mitochondria. Animals were cared for in accordance with the principles and guidelines of the Canadian Council on Animal Care and the Institute of Laboratory Animal Resources (National Research Council). All procedures using mice were approved by the Animal Care and Use Committee at Memorial University of Newfoundland.

Component	TD.06415: HFD	TD.06416: CD
Fat	**44.8 % Kcal**	**10.2% Kcal**
Lard (g/kg)	195	20
Soybean oil (g/kg)	30	20
Protein	**19% Kcal**	**20% Kcal**
Casein (g/kg)	245	210
L-Cystine (g/kg)	3.5	3
Carbohydrate	**36.2% Kcal**	**69.8% Kcal**
Corn starch (g/kg)	85	280
Maltodextrin (g/kg)	115	50
Sucrose (g/kg)	200	325
Other Metabolites	-	-
Cellulose (g/kg)	58	37.15
Mineral mix (g/kg)	43	35
Calcium phosphate (g/kg)	3.4	2
Vitamin mix (g/kg)	19	15
Choline bitartrate (g/kg)	3	2.75

Table 2.1: Distributed diet

Calorie contribution of fat, protein, and carbohydrates and individual component mass in the high-fat diet and matched control diet obtained from Teklab global.

2.4 Genotyping

2.4.1 DNA extraction

Genotyping was carried out using the Extract-N-Amp Tissue PCR kit (Sigma Aldrich) according to the manufacturer's instructions. All pipette tips and Eppendorf tubes utilized in the

genotyping procedures were certified nuclease-free. Ear notches were first treated with 100 µL of extraction solution and 25 µL of preparation solution and then mixed. This mixture was incubated at 25 ºC for 10 minutes followed by a 3-minute incubation at 95 ºC. The mixture was allowed to cool and 100 µL of the neutralization solution was added to stop the reaction.

2.4.2 Polymerase chain reaction

Primer sequences for the *Grx2* gene were produced by Integrated DNA technologies (IDT) and generated according to a previously published study (70). The primer sequences are as follows:

Forward:

5'-GAC CTA GCC TAC CAG ACT TGG CTG AAA TTT ATT C-3' (located in intron 2)

Reverse:

5'-CAT AGA CAC TCT TCA CTT TCA AGC CCA CCC TC-3'

Neo:

5'-CCT ACA TTT TGA ATG GAA GGA TTG GAG CTA CGG G-3'

The following solutions were added to the PCR tube containing the extracted DNA: 1 µL of 0.5 µM *Grx2* forward primer, 1 µM of 0.5 µM *Grx2* reverse primer, 1 µL of 0.5 µM *Grx2* neo primer, 4 µL of DNA solution, 3 µL nuclease-free water and 10 µL of REDExtract-N-Amp Tissue PCR Kit Reaction Mixture, giving a final volume of 20 µL. Tubes were then transferred to an Eppendorf master cycler pro PCR System for sequence amplification. The PCR protocol is as follows; a 3 minute 95 ºC denaturation step followed by 30 cycles of denaturation (94 °C 30 sec), annealing (63°C 1 min), and extension (72°C 1 min) with a final extension (72°C for 7 min).

Step	Process	Temperature (ºC)	Time (min)
Step 1	Denaturation	95	3
Step 2 (30 Cycles)	Denaturation	94	0.5
	Annealing	63	1
	Extension	72	1
Step 3	Final extension	72	7
-	Incubation	4	-

Table 2.2: PCR protocol for the *Grx2*$^{+/-}$ Genotyping procedures.

2.4.3 Gel Electrophoresis.

PCR samples were electrophoresed in a 1.5% (w/v) agarose gel that was produced by heating 0.75 g of agarose powder (Fisher Scientific) in a 0.5 X Tris-Borate-EDTA (TBE) buffer (Fisher Scientific, made by diluting 20 µL 10 X Tris-Borate-EDTA in 340 µL of analytical water). Five microliters of SYBR safe DNA gel stain was added to the gel solution. The molten agarose solution was then poured into the mold and allowed to solidify. Once the gel had solidified, it was placed in a Fisher Biotech Horizontal Electrophoresis Systems gel box. Trackit 100 bp DNA ladder (5 µL)(Invitrogen) was added to the first lane of the gel and 10 µL of the PCR amplified DNA samples were added to subsequent lanes. Electrophoresis was conducted at 90 V for 40 minutes and imaged using the Alpha Innotech ChemiImager Ready System. WT mice produced a single 729 base pair (bp) nucleotide sequence. *Grx2*$^{-/-}$ mice produced a bp fragment 510 bp in size and *Grx2*$^{+/-}$ mice contained both nucleotide sequence fragments (Figure 2.1).

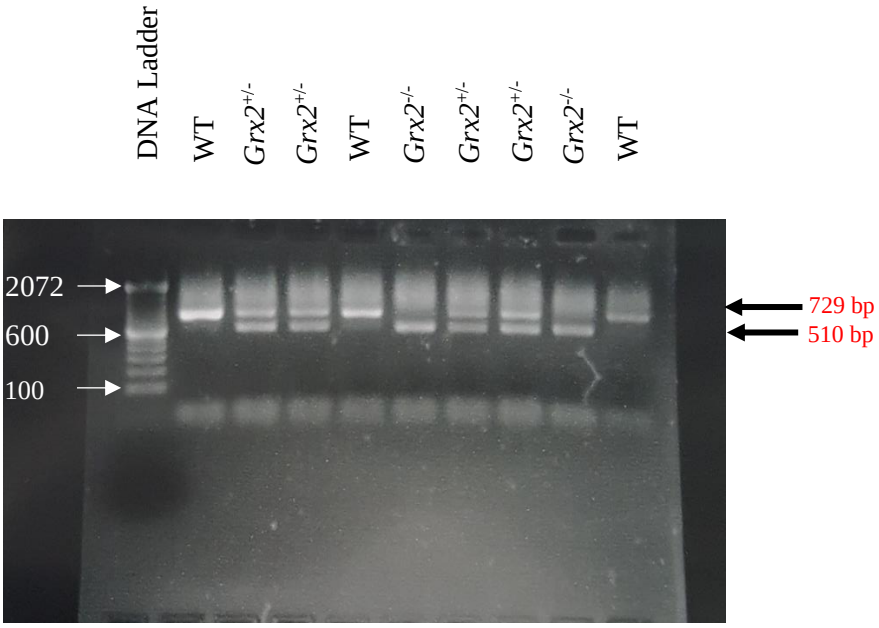

Figure 2.1: Gel electrophoresis

Identification of full length or truncated versions of the *Grx2* gene for WT, *Grx2*$^{+/-}$ and *Grx2*$^{-/-}$ characterization of mice by PCR amplification and gel electrophoresis.

2.5 Histological analysis

Hematoxylin and eosin (H&E) and Oil Red O staining were performed on the liver and muscle sections by the Memorial University of Newfoundland Histology unit. Fixed tissue was processed using the TissueTek 5 automated tissue processor. Using the embedding media Leica Blue Ribbon paraffin. Sections from paraffin embedded tissue were cut at 5µm thickness using the Leica microtome Leica RM2135. The slides were dried at RT and heated at 60 °C oven for 2 hours and stained with HE. Fresh frozen tissue for Oil Red O was embedded in VWR® Premium Frozen Section Compound and cut at 8 µm thickness using the cryostat LeicaCM3050S. slides were then stained for Oil Red O.

2.6 Serum biochemistry

2.7.1 Insulin levels

A Rat/Mouse insulin ELISA kit (MilliporeSigma) was utilized for the measurements of blood serum insulin. Assays were conducted according to the manufacturer's instructions. Blood serum samples were warmed to room temperature. The microliter assay plate containing insulin-specific antibodies was washed with a 1X wash buffer made from the provided 10X concentrate of 50 mM Tris-buffered saline containing Tween-20. First, 10 µL of assay buffer containing 0.05 M phosphosaline, (pH 7.4), 0.025 M EDTA, 0.08% sodium azide, and 1% w/v BSA was added to each well. Ten microliters of matrix solution were added to a blank and control well. This contained charcoal stripped pooled mouse serum. Ten microliters of rat insulin standards were added to separate wells in duplicate. The rat insulin standards contained rat insulin in assay buffer at 0.2, 0.5, 1, 2, 5 and 10 ng/mL, respectively. Quality controls containing rat insulin in Quality Control buffer were added to QC1 and QC2. Unknown samples of mouse insulin from *Grx2*$^{+/-}$ and WT mice were added in duplicate to separate wells. Eighty microliters of detection antibody (Pre-

titered biotinylated anti-insulin antibody) were added to each well and the plate was agitated at a moderate speed for 2 hours at room temperature. Buffer was then removed, and the wells were washed three times with 1X wash buffer. One hundred microliters of enzyme solution (pre-titered streptavidin-horseradish peroxidase conjugate in buffer) were added to each well and the plate was agitated at room temperature for 30 minutes. Wells were then washed 6 times with 1X wash buffer. One hundred microliters of substrate solution (3, 3', 5, 5'-tetramethylbenzidine in buffer) were added to each well and the plate was agitated for 15 minutes. One hundred microliters of stop solution containing 0.3 M HCl were finally added yielding a yellow color. This allowed quantification of immobilized ab-enzyme conjugates by the activity of HRP in the presence of 3, 3', 5, 5'-tetramethylbenzidine. Absorbance was recorded at 450 nm and 590 nm using a SpectraMax M5 plate reader and the difference was used to generate a standard curve based on the standard rat insulin levels.

2.7.2 Triglyceride levels

The L-type Triglyceride M assay kit from Wako Pure Chemical industries was utilized for determinations of plasma triglyceride levels. Assays were conducted according to the manufacturer's instructions. A standard curve was generated with increasing concentrations of Wako MultiCalibrator Lipids (Cat. No. 464-01601). To separate wells 4, 8, 12, and 16 µL of the standard solution were added to generate 110 mg/dL, 220 mg/dL, 330 mg/dL, and 440 mg/dL standard preparations in duplicate. Four microliters of analytical water and the unknown samples were also added to separate wells in duplicate. Ninety microliters of the R1 (color A) solution were added to each well and mixed by gentle rotation at 37 ºC for 5 minutes. This solution contains the following:

- 50 U/mL glycerol kinase
- 8.0 mM ATP
- 5.6 U/mL Glycerol-3-phosphate oxidase
- 150 U/mL Catalase
- 0.4 mM N-(3-isopropyl)-3methoxy-5-methylaniline (HMMPS)
- 2.0 U/mL ascorbate oxidase

Glycerol kinase utilizes ATP to convert free glycerol to glycerol-3-phosphate which is subsequently converted to dihydroxyacetone phosphate coupled with the generation of H_2O_2 by the action of glycerol-3-phosphate oxidase. The H_2O_2 generated is neutralized to H_2O by the action of catalase. The absorbance was measured at 600 nM using a SpectraMax M5 plate reader. This reading is established as the sample blank. Following this 30 µL of R2 (color B) solution was added to each well and mixed by gentle rotation at 37 ºC for 5 minutes. This solution contains the following:

- 250 U/mL lipoprotein lipase
- 25 U/mL Horseradish peroxidase
- 4.6 mM 4-aminoantipyrine

Lipoprotein lipase cleaves triglycerides generating free fatty acids and glycerol. Glycerol is once again converted to dihydroxyacetone phosphate by glycerol kinase and glycerol-3-phosphate oxidase at the expense of ATP and coupled with the generation of H_2O_2. HMMPS and 4-aminantipyrine undergo condensation to form a blue pigment in the presence of HRP and H_2O_2. The absorbance is once again read at 600 nm using a SpectraMax M5 plate reader. The final absorbance is calculated as the difference between the two absorbances and a standard curve is generated to be utilized for the measurement of serum triglyceride levels.

2.7.3 Glutathione/Glutathione disulfide pool

The glutathione assay kit from Sigma Aldrich was used to assess the GSH and GSSG concentrations in isolated blood serum samples. Twenty-five microliters of each plasma sample were transferred to a new Eppendorf tube. Two hundred microliters of 5% 5-sulfosalicylic acid were added to each sample to deproteinize the sample. The samples were incubated at 4 ºC for 10 minutes followed by centrifugation at 10,000 X g for 10 minutes. The supernatant was measured by pipetting and this value was used in future calculations. Samples and standards provided in the kit were loaded into individual wells of a 96 well plate in duplicate. One hundred and fifty microliters of working mix containing 95 mM potassium phosphate buffer, pH 7.0, 0.95 mM EDTA, 0.038 mg/mL (48 µM), 5,5'-dithiobis (2-nitrobenzoic acid) (DTNB), 0.115 U/mL glutathione reductase were added to each well and incubated for 5 minutes with agitation. Following this, 50 µL of the provided NADPH solution (0.16 mg/mL) were added. The GSH in this assay acts as a catalyst for the continuous reduction of DNTB to 5-thio-2-nitrobenzoic acid (TNB), a yellow substance. The absorbance is read at 412 nm using a SpectraMax M5 plate reader and the GSH standards were utilized to generate a standard curve. The GSH concentration in each sample was calculated as follows.

Equation 2.1: Calculation of blood serum GSH concentrations

nmoles GSH per mL of sample: $\frac{\Delta A_{412}/\text{min(sample)} \times \text{dilution}}{\Delta A_{412}/\text{min (1 nmole)} \times \text{volume}}$

Where:

ΔA_{412}/min (sample) = slope generated by sample (after subtracting the values generated by the blank reaction).

ΔA_{412}/min (1 nmole) = slope calculated from the standard curve for 1 nmole of GSH

2.7 Preparation of muscle mitochondria

Skeletal muscle mitochondria were isolated using basic medium (BM) using the differential centrifugation technique as described in (127). BM buffer consisted of KCl (140 mM), HEPES (20 mM), ethylene glycol-bis (β-aminoethyl ether)-N,N,N',N'-tetraacetic acid (EGTA; 1 mM) and $MgCl_2$ (5 mM) dissolved in analytical water (pH 7.0 with 6 N HCl). BM was then stored at 4 °C. On the day of experiments, muscle homogenization medium (HM) was made fresh by adding ATP (1 mM) and 1% (w/v) BSA to ice cold BM. For the isolation of mitochondria, all steps were performed on ice or at 4 °C. ATP is added to promote myofiber depolymerization and the release of intermyofibrillar mitochondria. BSA was included to remove contaminating fatty acids. Pooled muscles were first cleaned of any connective tissue or fat and then dried and weighed. Skeletal muscle was then minced on a Teflon watch glass and placed in 15 mL of HM containing 1 U of the protease subtilisin A. The volume of subtilisin A added was determined using equation 2.2 and was added to promote myofiber degradation. Homogenization was performed using the Potter-Elvejham method using the Variable Speed Reversible Homogenizer (Glas-Col) and transferred to ultracentrifuge tubes on ice.

Equation 2.2: Calculation of amount of Subtilisin A required for muscle extraction.

$$\text{Volume of subtilisin A (1 mg/mL)} = \frac{\text{Muscle (g)}}{1\frac{\text{mg}}{\text{mL}} \times 11.7\frac{\text{mg}}{\text{unit}}}$$

All centrifugation steps were performed with a Thermo Sorvall RC6+Centrifuge. The homogenate was centrifuged at 800 X g for 9 minutes to remove nuclei and undisrupted tissue. The supernatant was subsequently transferred to a second tube and centrifuged at 10,000 X g for 9 minutes. The supernatant was discarded, the sides of the tube carefully wiped to remove any excess fat, and the pellet was resuspended in 1 mL of BM and incubated for 5 minutes at 4 ºC to promote myofiber

repolymerization. Fourteen milliliters of BM were then added to each tube and the homogenate was centrifuged at 800 X g to remove the myofibers. The supernatant was then collected and centrifuged at 10,000 X g for 9 minutes to pellet skeletal muscle mitochondria.

2.8 Bradford Assay

Mitochondrial protein concentrations were estimated using the Bradford assay (Sigma Aldrich). After isolation, 1 µL of isolated mitochondria was diluted in 999 µL of analytical water. The diluted protein sample was vortexed and then 50 µL was transferred to 200 µL of Bradford reagent. The volume of the solution was then adjusted to 1 mL with 750 µL of analytical water. Two hundred microliters of this Bradford solution were transferred to 96-well plate in duplicate and the absorbance was measured at 595 nm using a SpectraMax M5 plate reader. Absorbances were compared to a standard curve prepared previously with 0, 0.125, 0,25, 0.625, 1.25, and 1.875 mg/mL BSA.

2.9 Mitochondrial $O_2^{\bullet-}/H_2O_2$ Production

The Amplex UltraRed (AUR) assay was utilized to measure the rate of $O_2^{\bullet-}/H_2O_2$ production and determine which ROS generating enzymes served as high capacity sites of production. The rate of ROS production can be estimated by the conversion of non-fluorescent AUR to fluorescent resorufin in the presence of H_2O_2 and horseradish peroxidase (HRP). The final volume for all reactions in each well was 200 µL. Assays were prepared by diluting skeletal muscle mitochondria in BM to a final concentration of 1.5 mg/mL. For assays involving palmitoyl-carnitine, mitochondria were first pre-incubated in the presence of carnitine (2 mM) for 5 min. Mitochondria were then incubated for 5 min at room temperature in the presence or absence of different ROS production inhibitors. Reaction chambers were then supplemented with HRP (3

U/mL), SOD1 (25 U/mL) AUR (10 nM). Mitochondria contain endogenous SOD1 and SOD2 which convert $O_2^{\bullet-}$ to H_2O_2. Exogenous SOD1 is added to reactions to ensure the full conversion of $O_2^{\bullet-}$ to H_2O_2 and increase the accuracy of the assay. Exogenous SOD1 is also added to limit the spontaneous production of peroxynitrite, a molecule generated through reaction between $O_2^{\bullet-}$ and nitric oxide that is known to oxidize AUR. Reactions were then initiated by the addition of substrate; pyruvate (50 µM) and malate (50 µM), succinate ((50 µM), or palmitoyl-carnitine (20 µM; note that these reactions also contained carnitine). Changes in resorufin fluorescence were followed at excitation/emission wavelengths (565 nm/600 nm) for 5 minutes with reads taken once every 30 seconds using a SpectraMax M5 plate reader. Sample rates were compared against standard curves generated using 0, 20, 50, 100, 200, 500, and 1000 nM H_2O_2.

For inhibitor studies and to determine which ROS generating site served as the higher capacity enzyme for production, mitochondria were supplemented with different combinations of substrate and $O_2^{\bullet-}/H_2O_2$ generation suppressors. To examine the contributions of OGDH and the respiratory chain, mitochondria were supplied pyruvate/malate with the ROS suppressors KMV (10 mM; OGDH inhibitor), myxothiazol (4 µM; complex III inhibitor) or atpenin A5 (50 µM; complex II inhibitor) (68, 69, 151). To examine ROS release exclusively by the respiratory chain, mitochondria were supplemented with succinate or palmitoyl-carnitine/carnitine and rotenone (4 µM; complex I inhibitor, prevents reverse electron flow), myxothiazol (4 µM), and atpenin A5 (50µM) (68, 69). For a clear representation of the inhibitors and their targets see Figure 2.2.

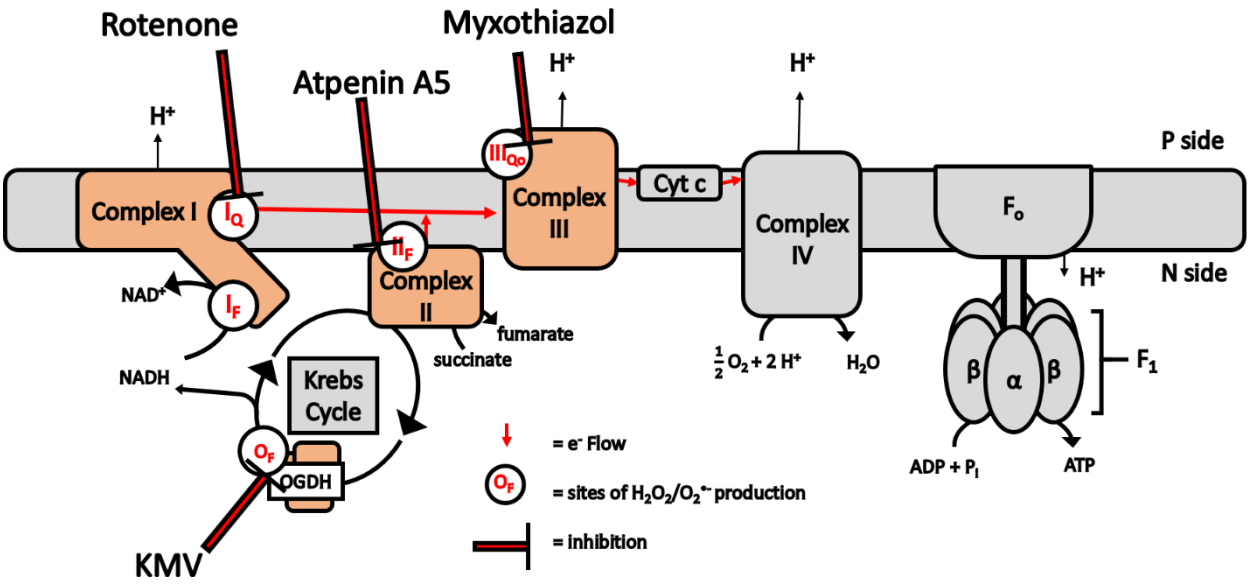

Figure 2.2: Inhibitors
Rotenone (complex I), KMV (OGDH), atpenin A5 (complex II) and myxothiazol (complex III) were utilized to identify the sources of ROS and their sites of inhibition.

2.10 Mitochondrial NAD(P)H levels

The auto-fluorescence of nicotinamide groups allowed NAD(P)H levels to be measured simultaneously with measurement of $O_2^{\bullet -}/H_2O_2$ productions. It is important to note that the NAD(H) pool in mitochondria is substantially more oxidized than the NADP(H) pool which is maintained in a highly reduced state (2). As a result, changes in nicotinamide fluorescence are most often associated with changes in the NAD(H) pool. NAD(P)H was measured at 376 nm:420 nm by endpoint analysis.

2.11 Rates of Oxygen Consumption

2.11.1Assessing the different states of respiration

The Oxytherm Clark-type electrode was utilized to measure the rate of mitochondrial oxygen consumption. Prior to assembly, all the components of the electrode were inspected for signs of oxidation or degradation. The O-rings, and electrode itself were rinsed in analytical water and dried carefully. A drop of KCl (17.5 g/ 100 mL) was placed on the center of the Platinum (Pt) cathode. A small segment of filter paper large enough to cover the electrode was placed on this drop and soaked in KCL. A segment of O_2-permeant polyvinylidene difluoride (PVDF) membrane cut to a similar size was placed on top of the salt bridge and the small O-ring was placed around the Pt cathode. A large O-ring was placed around the outside of the electrode and the space between the two rings was filled with KCl. The area between the large and small O-ring was filled with KCl being careful not to overflow the chamber. The electrode was tightly screwed into place and a stir bead was introduced to the electrode chamber. Two milliliters of analytical water were added to the electrode chamber and the temperature was set to 37 ºC. A calibration of air-saturated water was conducted with the stir bead set at 75 %. Subsequently, a small spatula of sodium dithionite (Sigma Aldrich) was added to the electrode chamber and the

cap was placed to establish a 0% O_2 concentration in the chamber. The chamber was rinsed thoroughly three times with analytical water to remove any remaining sodium dithionite. Mitochondria were then diluted to 0.2 mg/mL in the reaction chamber containing respiration buffer (RB). RB consisted of MESH Mannitol (220 mM), EGTA (1 mM), sucrose (70 mM) and HEPES (20 mM) in addition to 0.5% w/v BSA, 10 mM monobasic potassium phosphate (KH_2PO_4) and 2 mM $MgCl_2$ in analytical water made to pH 7.4 with 6 N HCl. Once a baseline oxygen consumption was established, 10 µL of substrate were added to the chamber to initiate state 2 respiration (Figure 2.3). Substrates included pyruvate/malate (10 mM/2 mM), succinate (5 mM), or palmitoyl-carnitine/carnitine (50 µM/2 mM). Note that mitochondria supplied with palmitoyl-carnitine were incubated with carnitine for 5 minutes prior to palmitoyl-carnitine addition. Oxygen consumption was then measured for ~1 minute. State 3 respiration was then stimulated by adding ADP (1 mM). Oligomycin (4 µg/mL), an inhibitor of ATP synthase was then added to induce state 4 respiration (proton leak dependent respiration) this rate was also recorded. Finally, the reaction was ended with the addition of antimycin A allowing identification and exemption of contaminating oxygen consumption not associated with the respiration (4 µM).

2.11.2 UCP3 dependent proton leak

The suspicion that deregulated S-glutathionylation reactions may influence UCP3 function in skeletal muscle mitochondria led to the utilization of GDP and genipin to assess whether any differences in proton leak between genotypes may be associated with differences in UCP3 activity. Mitochondria were introduced to the chamber in reaction buffer in the same manner as previously discussed. However, the proton leak assay began with the addition of oligomycin (4 mg/mL) followed by pyruvate/malate (10 mM/2 mM) or succinate (5 mM) to establish state 4 respiration.

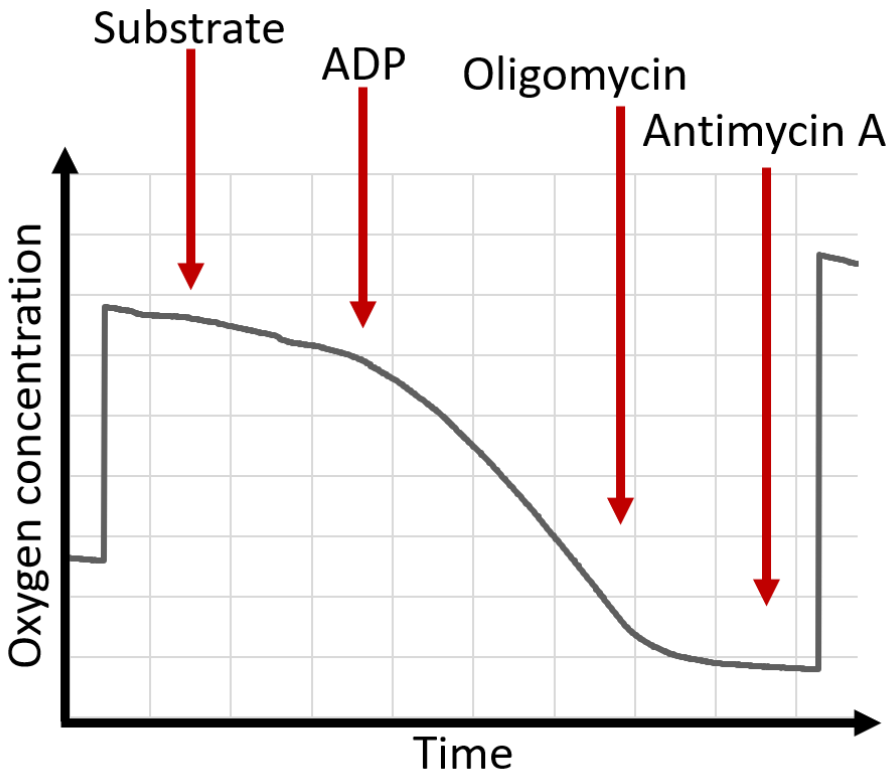

Figure 2.3: Oxytherm assay

Different states of respiration measured using the oxytherm Clark-type electrode as depicted. Substrate and ADP addition initiates state 2 and 3 respiration respectively. Oligomycin an inhibitor of complex V initiates state 4 or proton-leak dependent respiration. Finally, the respiration is hindered by the addition of antimycin A, an inhibitor of complex III.

The rate was taken after 2 minutes of induced proton leak followed by the introduction of GDP (1 mM) genipin (50 µM), or a dimethyl sulfoxide (DMSO) control. Finally, reactions were concluded with the addition of antimycin A (4 µM).

Finally, an S-glutathionylation catalyst disulfiram was utilized to investigate whether the S-glutathionylation state of the UCP3 protein was different between genotypes and diet treatments, and whether or not it had any effect on UCP3 mediated proton leak. Mitochondria were prepared at 0.2 mg/mL in reaction buffer as previously discussed. Once again proton leak was induced with the addition of oligomycin (4 mg/mL) followed by pyruvate/malate (10 mM/2 mM) or succinate (5 mM). The rate was taken after a 2-minute period of induced proton leak followed by the conclusion of the experiment with the addition of antimycin A (4 µM).

2.12 Immunoblot analysis

2.12.1 Protein and gel preparation

Isolated mitochondria were obtained from the -80 ºC storage and allowed to thaw. Samples were diluted to 3 mg/mL in Radioimmunoprecipitation assay (RIPA) buffer to a final volume of 50 mL. RIPA buffer is a lysis buffer that disrupts the mitochondrial membranes making proteins more accessible. This solution was added to 50 µL of Lammli buffer which reduces intracellular disulfide bonds denaturing proteins and gives each an overall negative charge. It also introduces Bromophenol blue, which acts as a marker for how far the proteins have traveled in the electrophoresis unit. The samples are then incubated at 100 ºC for 10 minutes. Resolving Gels were prepared as either 10 % SDS or 12 % SDS for protein targets > 40 kDa and < 40 kDa respectively. The resolving gel was prepared by the addition of 6 mL of 40 % acrylamide solution 5 mL of 4 X Trizma/SDS pH 8.8 solution (1.5 M Trizma base, 0.4 % SDS in 100 mL) and 9 mL

of analytical water. To this solution 75 µL of N,N,N',N'-tetramethylethane-1,2-diamine (TEMED) and 25 µL of 1% (w/v) ammonium persulfate solution (APS) were added to initiate polymerization. Immediately after addition to the gel mold, 2-propanol was added to the surface to create a level gel. The stacking gel was prepared with 1 mL 40% acrylamide solution, 2.5 mL Tris/SDS pH 6.8 solution (0.5 mM Trizma base, 0.4 % SDS in 100 mL), and 6.5 mL analytical water. Once the resolving gel was set, the 2-propanol was removed, polymerization in the stacking gel was initiated with 75 µL TEMED and 25 µL APS. The stacking gel was placed gently on top of the resolving gel. The combs were immediately administered, and the gel was allowed to set.

The 1X electrophoresis buffer consisted of 200 mL of 10 X electrophoresis buffer (250 mM Trizma base, 1920 mM glycine, and 1 % (v/v) SDS) in 1800 mL analytical water. The gels prepared previously were transferred to the electrophoresis apparatus (Mini-protean Tetra System-Bio-Rad). Twenty microliters of PageRuler Plus Pre-stained protein ladder (Fisher Scientific) and previously prepared samples were added to individual wells. This provides 60 µg protein to be probed. Electrophoresis was run at 80 V until the proteins had passed through the stacking gel followed by a 40-minute run at 200 V.

The 1X transfer buffer consisted of 200 mL methanol, 200 mL 10 X transfer buffer (500 mM Trizma base, 380 mM glycine, and 1 % v/v SDS) in 1600 mL analytical water. During this time, the extra thick blotting paper (Bio-Rad), and nitrocellulose membranes (Bio-Rad) were cut to an appropriate size to fit the gel. The electroblotting sponge, the thick blotting paper and nitrocellulose membrane were all equilibrated in transfer buffer for 20 minutes. Once the electrophoresis was complete the gels were transferred to the Mini Trans-Blot Electrophoretic Transfer Cell apparatus (Bio-Rad). Protein was transferred from gels to the nitrocellulose

membrane for 1 hour at 120 V. The Ponceau S dye consisting 0.5 % Ponceau S, 1% Acetic acid made to 200 mL was used to confirm protein transfer.

Tris-buffered saline (TBS; 1mM Trizma base and 68 mM NaCl) with 0.1% (v/v) Tween-20 (TBS-T) was prepared and used to remove excess Ponceau S with 3 washes for 5 minutes. The nitrocellulose membranes were incubated in blocking solutions which contained TBS-T and 5% (w/v) non-fat skim milk. Blocking solution was removed with 3 5-minute washes of TBS-T followed by incubation with the appropriate primary antibody diluted in TBS-T + 5% (w/v) BSA + 2% (w/v) NaN_3. Antibodies were validated previously as in O'Brien et al and Mailloux et al. or through comparison of molecular weight with those of the company issued citations (68, 152). The membranes were probed overnight at -20 ºC with moderate agitation. Membranes were washed 3 times for 5 minutes with TBS-T to remove any unbound primary antibody. Membranes were incubated for 1 hour with secondary antibody diluted in blocking solution TBS-T and 5% (w/v) non-fat skim milk. Membranes were washed 3 times for 5 minutes with TBS-T to remove unbound secondary antibody. A 1:1 Super Signal West Pico plus luminol:Enhancer at 750 µL was added to the surface of each nitrocellulose membrane and the results were visualized using ImageQuant LAS 4000 system. Band intensities were quantified using Image J. Bands were identified using rectangular selections maintaining a constant area throughout. The "plot lanes" command was utilized to identify the relative density of each band. After removing the common background signal the relative area of each peak was quantified using the "wand" tool. The band intensity was expressed as a percentage of respective loading control.

Primary Antibody	Primary Antibody dilution	Secondary Antibody	Secondary Antibody Dilution	Loading control	Loading Control Dilution	Loading Control Secondary Antibody
OGDH	1/3000	Goat anti-mouse	1/3000	SOD 2	1/2000	Goat anti-rabbit 1/3000
PDH	1/3000				1/2000	
OXPHOS	1/3000			NDUSF1	1/3000	Goat anti-mouse
UCP3	1/1000					

Table 2.3: Immunoblot antibodies

2.13 Data Analysis

Graphpad Prism 6 software was utilized for all statistical analysis. All data are represented as the mean ± standard error of the mean (SEM) with $N \geq 4$. Two-way analysis of variance (ANOVA) with a Tukey's posthoc test was employed for all experimental results with the exception of proton leak investigations which utilized Fisher's LSD. No statistical analysis was performed for immunoblot and histological results. Statistical significance was represented as follows:

Not significant	$P > 0.05$
*	$P \leq 0.05$
**	$P \leq 0.01$
***	$P \leq 0.001$
****	$P \leq 0.0001$

Chapter 3: Results

3.1 Physiology and metabolic characteristics of Grx2$^{+/-}$ mice

3.1.1 Impact of HFD on body and tissue mass

To investigate the role of Grx2 in the modulation of fatty acid metabolism, we challenged a Grx2 haploinsofficient mouse model and WT littermates with a HFD consisting of 44.8% Kcal fat or a matched CD diet (10.2% Kcal fat). The successful deletion of *Grx2* was confirmed by PCR amplification and agarose gel electrophoresis in addition to Grx2 protein expression analysis in both *Grx2*$^{+/-}$ and *Grx2*$^{-/-}$ mice in previous work in our laboratory (70). The *Grx2* gene is 720 bp long, whereas the truncated version is 510 bp, allowing easy identification with PCR amplification and agarose gel electrophoresis (Figure 2.1). WT mice yielded a lone band at 720 bp while *Grx2*$^{-/-}$ yielded one band at 510 bp. Samples collected from *Grx2*$^{+/-}$ mice contained both the 720 bp and 510 bp sequences.

The first study to investigate the whole-body effects of *Grx2* deficiency demonstrated decreased body weight and fat mass in *Grx2*$^{-/-}$ mice fed a standard chow diet *ad libitum* when compared to WT littermates (99). This prompted us to ascertain if whole body deletion of the *Grx2* gene protected mice from DIO. For our studies, we decided to use *Grx2*$^{+/-}$ mice and WT littermates since rodents homozygous for this gene develop cardiac disease and hypertension as early as 6 weeks of age (70, 99). No differences in body weight were observed in *Grx2*$^{+/-}$ and WT mice fed a CD over the 7-week period (Figure 3.1 A). This is consistent with previous findings in our laboratory that demonstrated no difference in whole body mass between *Grx2*$^{+/-}$, *Grx2*$^{-/-}$ and WT littermates (70). Interestingly, when challenged with a HFD, *Grx2*$^{+/-}$ and WT littermates displayed different physiological effects. WT mice saw a significant increase in body mass from 4 to 9 weeks of age. By contrast, *Grx2*$^{+/-}$ mice fed a HFD did not differ in mass from WT mice or *Grx2*$^{+/-}$ mice

fed a matched CD (Figure 3.1 A). This was not associated with any significant differences in food (Figure 3.1 B) or water consumption (Figure 3.1 C).

Our observation that *Grx2*$^{+/-}$ mice fed a HFD displayed a weight gain profile that was similar to mice fed a CD diet prompted the measurement of the masses of various organs, including fat tissue. No differences in heart mass were observed between WT and *Grx2*$^{+/-}$ mice fed either diet (Figure 3.2 A). Mouse kidney (Figure 3.2 B) and muscle (Figure 3.2 C) mass were also unaffected by diet or genotype. Interestingly, WT mice fed a HFD demonstrated small but significant decrease in liver mass when compared to WT or *Grx2*$^{+/-}$ mice on a CD (Figure 3.3 A). Liver mass of *Grx2*$^{+/-}$ mice fed a HFD did not differ from WT or *Grx2*$^{+/-}$ mice on CD (Figure 3.3 A). WT mice on HFD had a 2-fold increase in abdominal fat mass (Figure 3.3 B). This increase in abdominal fat mass was absent in *Grx2*$^{+/-}$ mice fed a HFD. Indeed, the abdominal fat mass observed in *Grx2*$^{+/-}$ fed a high fat diet was similar to the mass of the white adipose collected from WT and *Grx2*$^{+/-}$ mice fed a CD (Figure 3.3 B).

3.1.2. Loss of Grx2 prevents intrahepatic lipid accumulation

H&E staining was performed to ascertain if the weight gain observed in WT littermates fed a HFD was associated with any changes in liver and muscle histology. Muscle tissue collected from *Grx2*$^{+/-}$ and WT littermates fed either diet displayed no visible differences (Figure 3.4 A) (99). H&E staining of liver sections from WT mice fed a HFD, however, revealed a high degree of intracellular vacuolization (Figure 3.4 B). This is in contrast to *Grx2*$^{+/-}$ mice fed a HFD, which displayed a staining pattern that was similar to samples collected from rodents fed a CD. It was then hypothesized that the vacuolization observed in samples from WT mice fed a HFD was due to the intrahepatic accumulation of lipids. To test this, liver sections were treated with Oil Red-O, which stains fat droplets a deep red color.

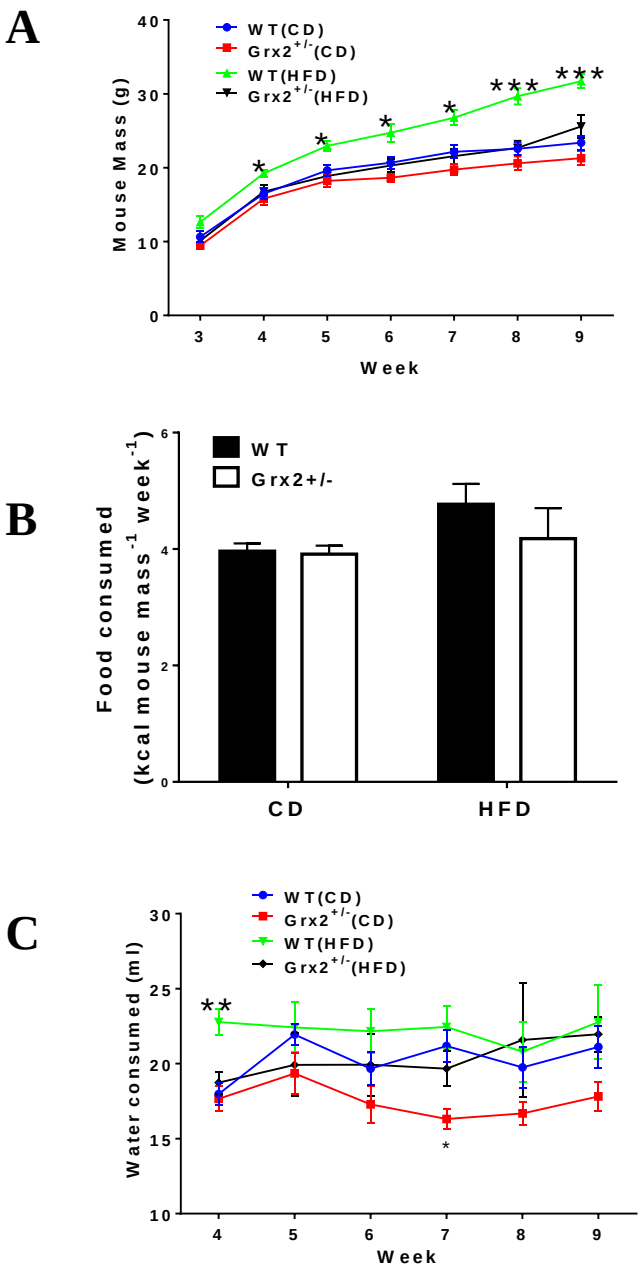

Figure 3.1: Body mass food, and water consumption measurements

Body mass (**A**) and food (**B**), and water consumption measurements (**C**). Changes in mass and food or water consumption were measured weekly from 4-9 weeks of age. N ≧5, mean ± SEM, Two-way ANOVA with a Tukey's post-hoc test. Statistics on mouse mass and water consumption were run on each individual week. "*" Represents a comparison to the WT control while "#" represents a comparison between genotypes.

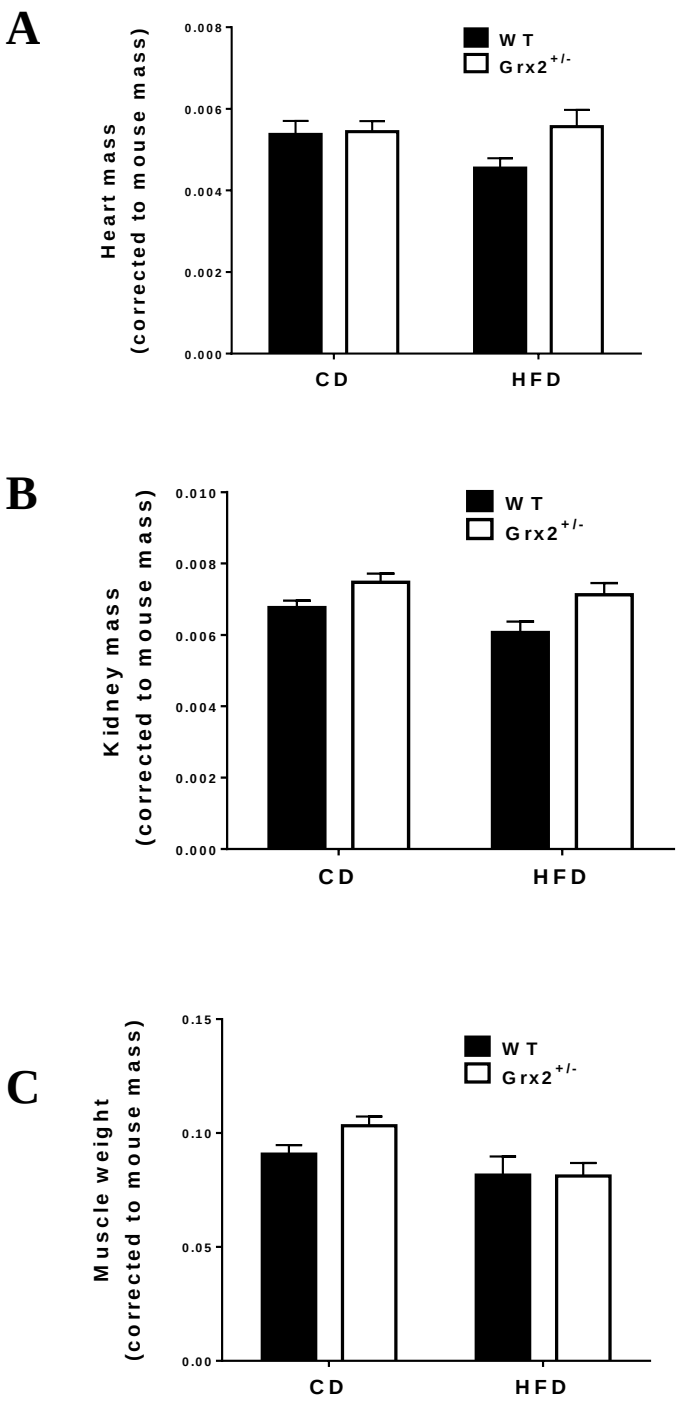

Figure 3.2: Heart, kidney, and skeletal muscle mass

Heart (**A**), kidney (**B**), and skeletal muscle mass (hindlimb, forelimb and pectoral) (**C**). N ≧5, mean ± SEM, Two-way ANOVA with a Tukey's post-hoc test.

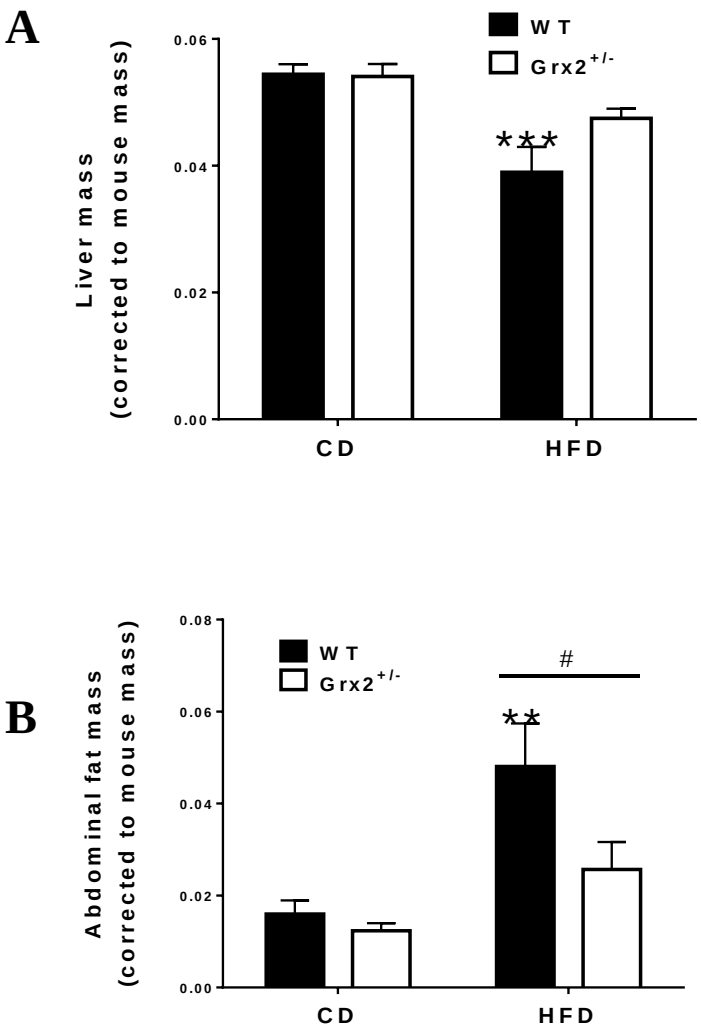

Figure 3.3: Liver, and abdominal fat mass

Liver (**A**), and abdominal fat mass (**B**). N≧5, mean ± SEM, Two-way ANOVA with a Tukey's post-hoc test. "*" Represents a comparison to the WT control while "#" represents a comparison between genotypes.

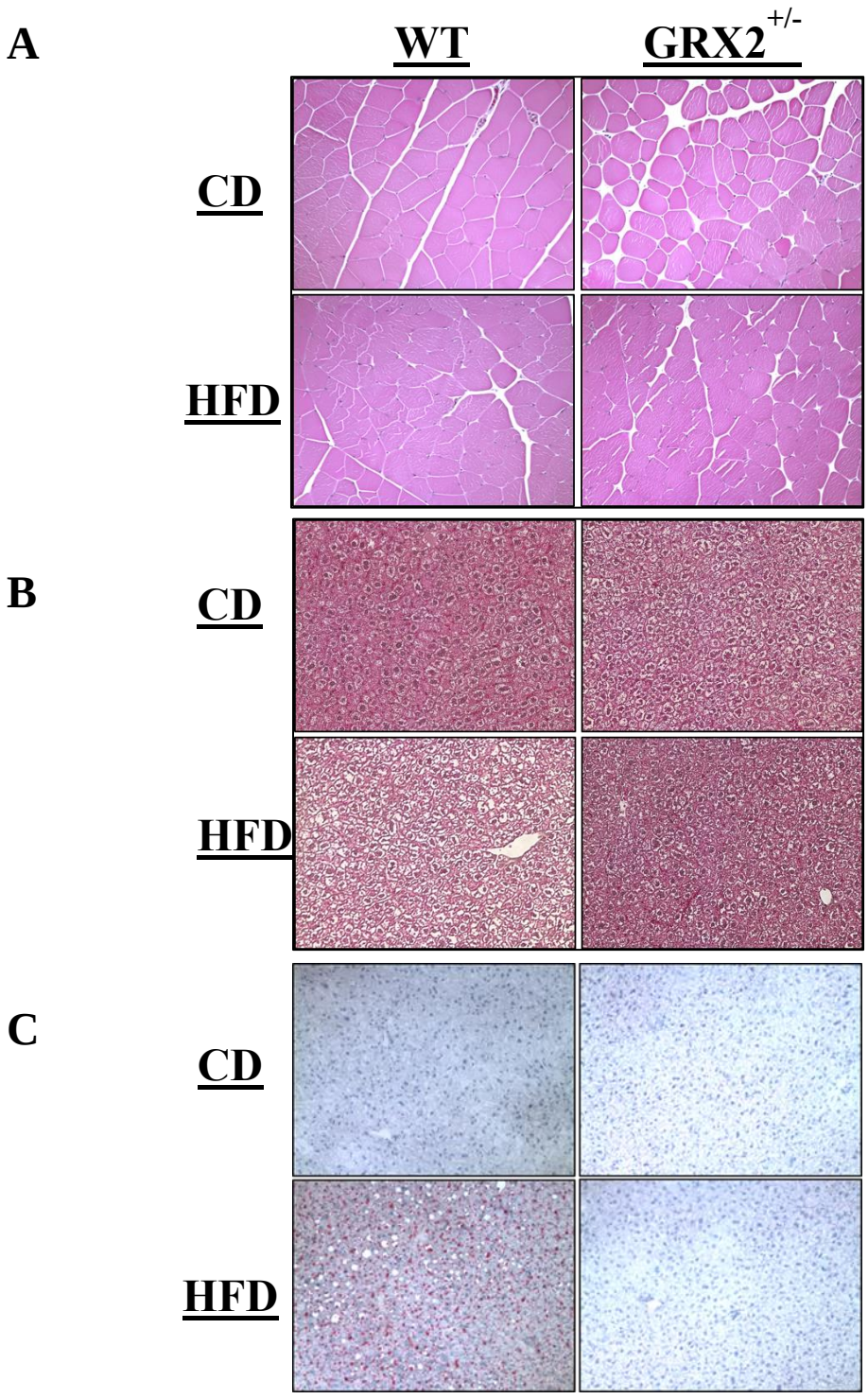

Figure 3.4: Hematoxilin and Eosin and Oil Red-O stains.

H&E staining for muscle (**A**) and liver (**B**) sections and Oil Red-O staining confirm lipid droplet accumulation in WT mice on HFD (**C**) of liver sections. N = 3

Oil red-O staining revealed that exposing WT littermates to a HFD for seven weeks promoted intrahepatocellular lipid accumulation (Figure 3.4 C). By contrast, liver sections from *Grx2*$^{+/-}$ mice displayed a staining pattern similar to mice fed control diets (Figure 3.4 C).

3.1.3. Effect of deleting the Grx2 gene on circulating insulin and metabolites

DIO and intrahepatic lipid accumulation correlate with aberrant changes in circulating metabolite, triglycerides and insulin levels (153). . Blood glucose measurements were performed weekly from 4-8 weeks of ages. Blood glucose concentrations were not significantly altered by diet or genotype (Figure 3.5). Intriguingly, administering a HFD to WT littermates induced a ~3-fold increase in circulating insulin, an effect not observed in *Grx2*$^{+/-}$ mice fed the same diet (Figure 3.6 A). Circulating insulin in *Grx2*$^{+/-}$ mice fed a HFD was significantly higher when compared to the control groups. However, deleting the *Grx2* gene significantly diminished the HFD-mediated increase in blood insulin levels. Next, triglyceride levels were measured. WT littermates fed a HFD contained higher blood triglyceride levels when compared to *Grx2*$^{+/-}$ fed the same diet (Figure 3.6 B). Additionally, triglyceride levels were similar to samples collected from the control groups. Overall, this indicates that *Grx2*$^{+/-}$ are protected from DIO and development of insulin resistance and fatty liver disease, potentially through an augmented capacity to clear triglycerides.

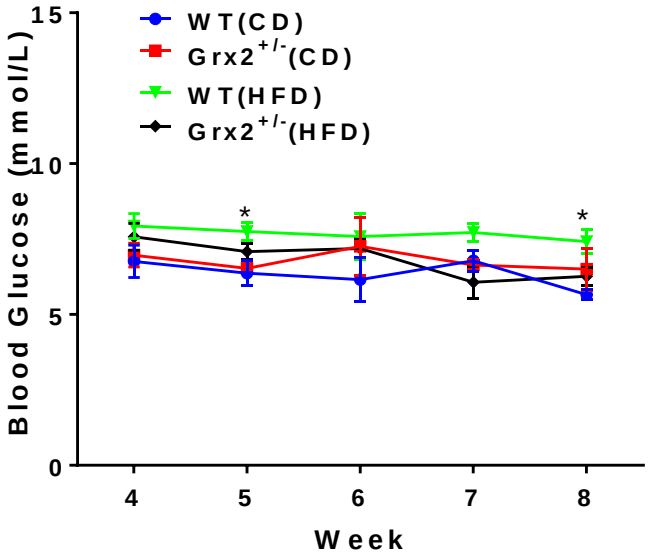

Figure 3.5: Blood glucose levels

Measured weekly from 4 to 8 weeks of age. N ≧5, mean ± SEM, two-way ANOVA with a Tukey's post-hoc test was performed on each individual week. "*" Represents a comparison to the WT control.

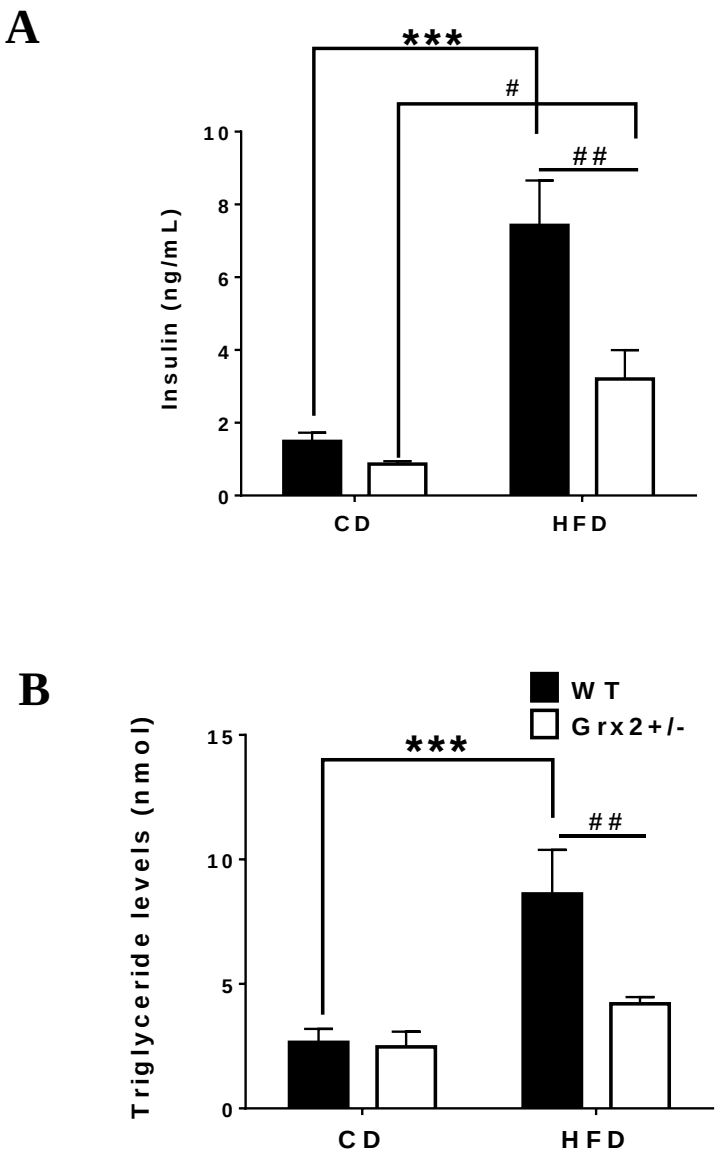

Figure 3.6: Serum insulin and triglyceride levels

Serum insulin (**A**) and triglyceride levels (**B**), measured at 10 weeks of age. N ≧5, mean ± SEM, two-way ANOVA with a Tukey's post-hoc test. "*" Represents a comparison to the WT control while "#" represents a comparison between genotypes.

3.2 Examination of energy metabolism in Grx2$^{+/-}$ mice challenged with HFD.

3.2.1 Phosphorylating and proton leak-dependent respiration are increased in Grx2$^{+/-}$ mice

Muscle plays an integral role in whole body energy homeostasis since it is a major site for fat combustion for the maintenance of ATP levels. The resistance of *Grx2* haploinsufficient mice towards DIO prompted us to examine the fuel combusting capacity of skeletal muscle mitochondria isolated from mice fed a CD or HFD. Fuel combustion capacity was determined by testing state 2, 3, and 4 respiration; indexes for the health of mitochondrial bioenergetics and their capacity to combust fuels to support oxidative phosphorylation. Genotype and diet did not affect state 2 respiration in mitochondria energized with pyruvate (Figure 3.7 A). Mitochondria isolated from *Grx2*$^{+/-}$ mice demonstrated a 2-fold increase in state 3 respiration. This increase occurred both in *Grx2*$^{+/-}$ mice fed a CD or HFD. Likewise, there was a ~2-fold increase in non-phosphorylating respiration in skeletal mitochondria energized with pyruvate isolated from *Grx2*$^{+/-}$ mice fed either diet (Figure 3.7 A).

Succinate supplementation yielded similar results. State 2 respiration remained unchanged by diet or genotype (Figure 3.7 B). However, there was a trend for an increase in state 2 respiration by *Grx2*$^{+/-}$ mice metabolizing succinate. State 3 respiration was increased by 2-fold in *Grx2*$^{+/-}$ mice during succinate supplementation (Figure 3.7 B). This was observed in *Grx2*$^{+/-}$ mice fed either a CD or HFD. Likewise, there was a ~2-fold increase in proton leak-dependent respiration in skeletal muscle mitochondria isolated from *Grx2*$^{+/-}$ mice metabolizing succinate (Figure 3.7 B).

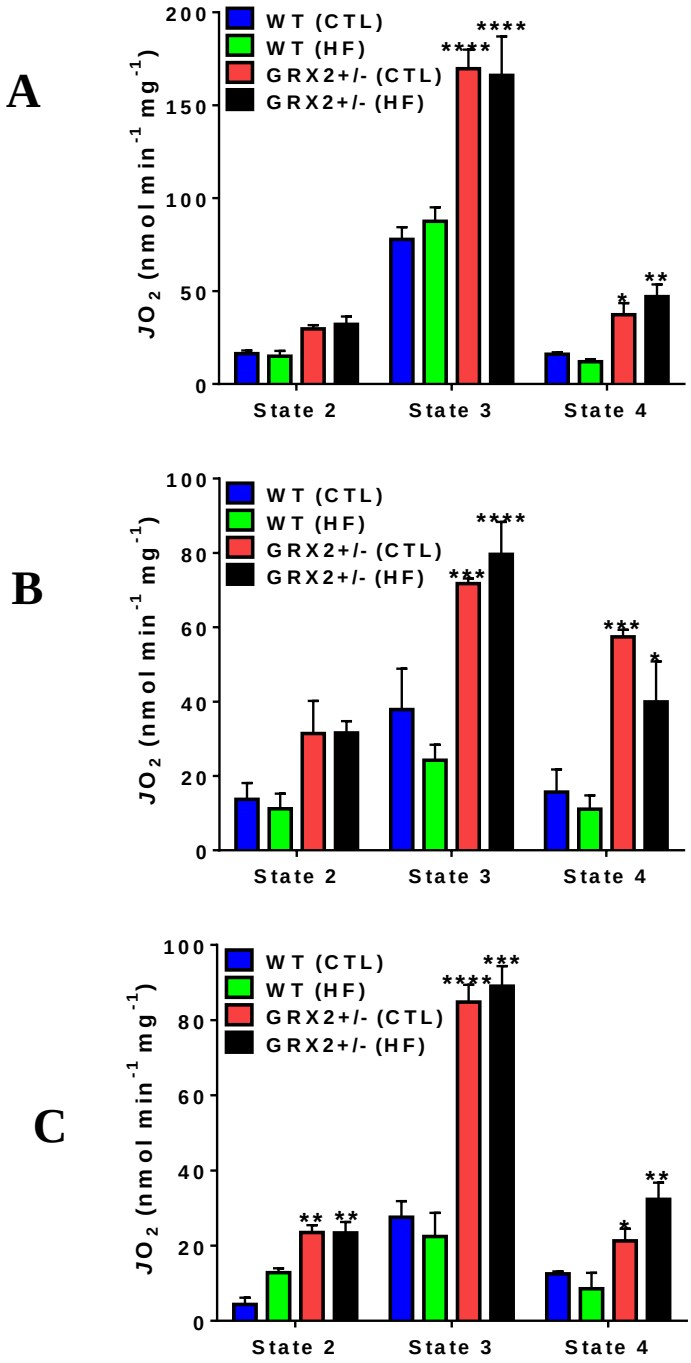

Figure 3.7: Rates of respiration.

Different states of respiration were measured in mitochondria oxidizing pyruvate/malate (**A**), succinate (**B**), palmitoyl-carnitine/carnitine (**C**). State 3 and 4 respiration were subsequently induced by adding ADP and oligomycin. N ≧5, mean ± SEM, one-way ANOVA with a Tukey's post-hoc test. "*" Represents a comparison to the WT control.

Next, the different states of respiration were assessed in mitochondria energized with palmitoyl-carnitine, a common fuel used for fatty acid oxidation in muscle tissue. State 2 respiration was ~2-fold higher in *Grx2*$^{+/-}$ mitochondria collected from mice fed either diet (Figure 3.7 C). Measurement of phosphorylating respiration revealed that mitochondria collected from *Grx2*$^{+/-}$ mice fed either diet displayed a ~4-fold increase in the rate of O_2 consumption (Figure 3.7 C). Similarly, a 2-fold increase in proton leak dependent respiration was observed in *Grx2*$^{+/-}$ mice on CD and HFD (Figure 3.7 C).

3.2.2 Levels of Krebs cycle linked and OXPHOS proteins in Grx2 $^{+/-}$ mice

Changes in the rates of nutrient energy metabolism can often be explained by changes in the expression of enzymes associated with the Krebs cycle and OXPHOS. Therefore, the relative abundance of the major proteins involved in nutrient metabolism was assayed by immunoblot. This included PDH, OGDH and complexes I-V. Here, we discovered an increase in pyruvate dehydrogenase expression in WT mice fed a HFD when compared to WT mice on a matched CD (Figure 3.8). Interestingly, *Grx2*$^{+/-}$ mice on CD and HFD demonstrated a significant increase in PDH expression when compared to the WT on CD, as well (Figure 3.8). On the other hand, we observed no changes in expression of the E1 subunit for OGDH (Figure 3.9). Using an OXPHOS antibody cocktail, we also probed for the different ETC subunits found in complex I-V. We observed no differences in the intensity for the bands corresponding to complex I (NDUFB8), complex II (30 kDa subunit), complex III (core protein 2), complex IV (subunit 1), or complex V (α subunit) (Figure 3.10).

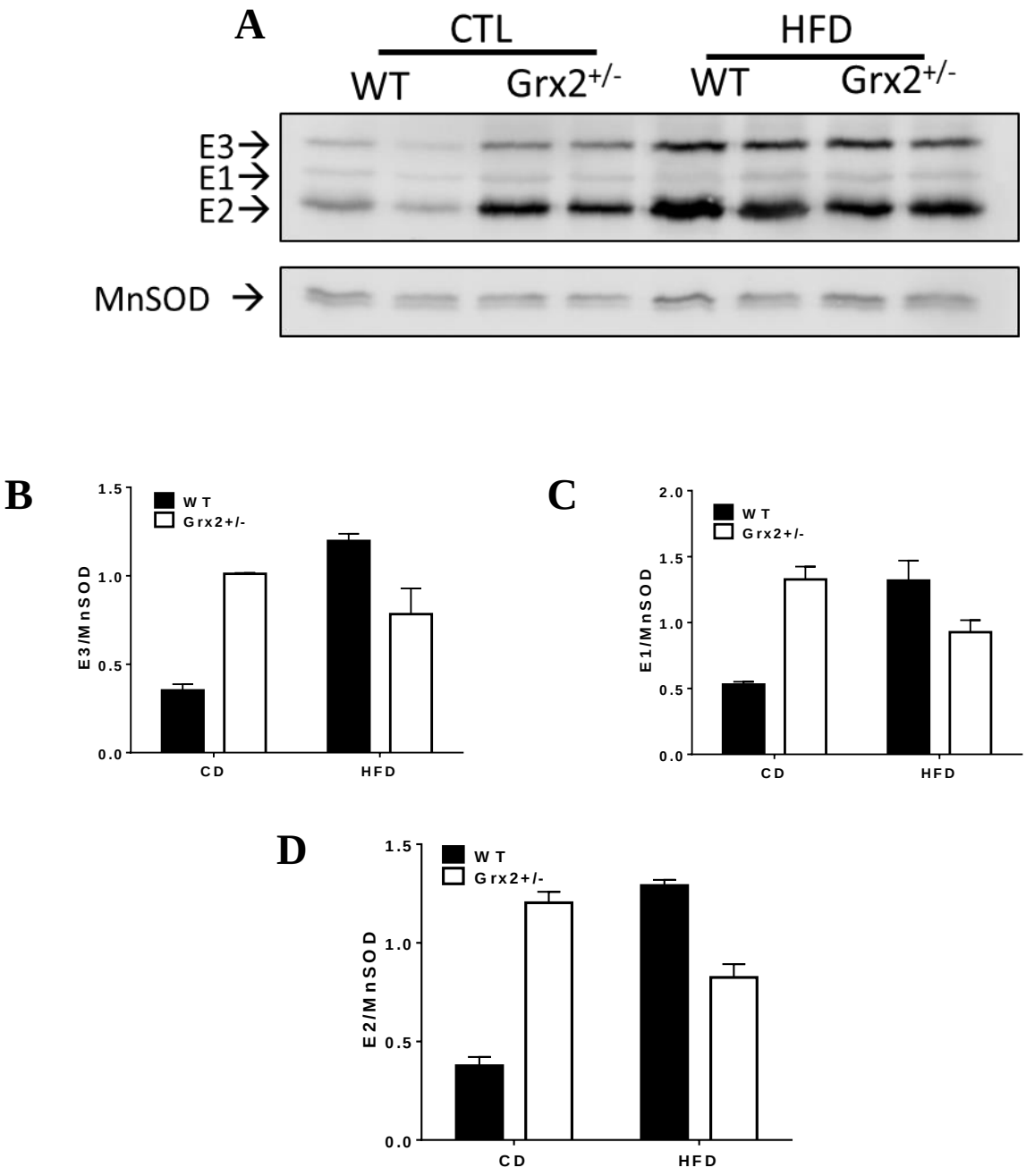

Figure 3.8: PDH protein levels

Immunoblot with skeletal muscle mitochondria using PDH antibody cocktail identifying the E1 E2 and E3 subunits of the PDH complex (A). Densitometry analysis was performed with ImageJ analysis (B)(C)(D). MnSOD was used as a loading control.

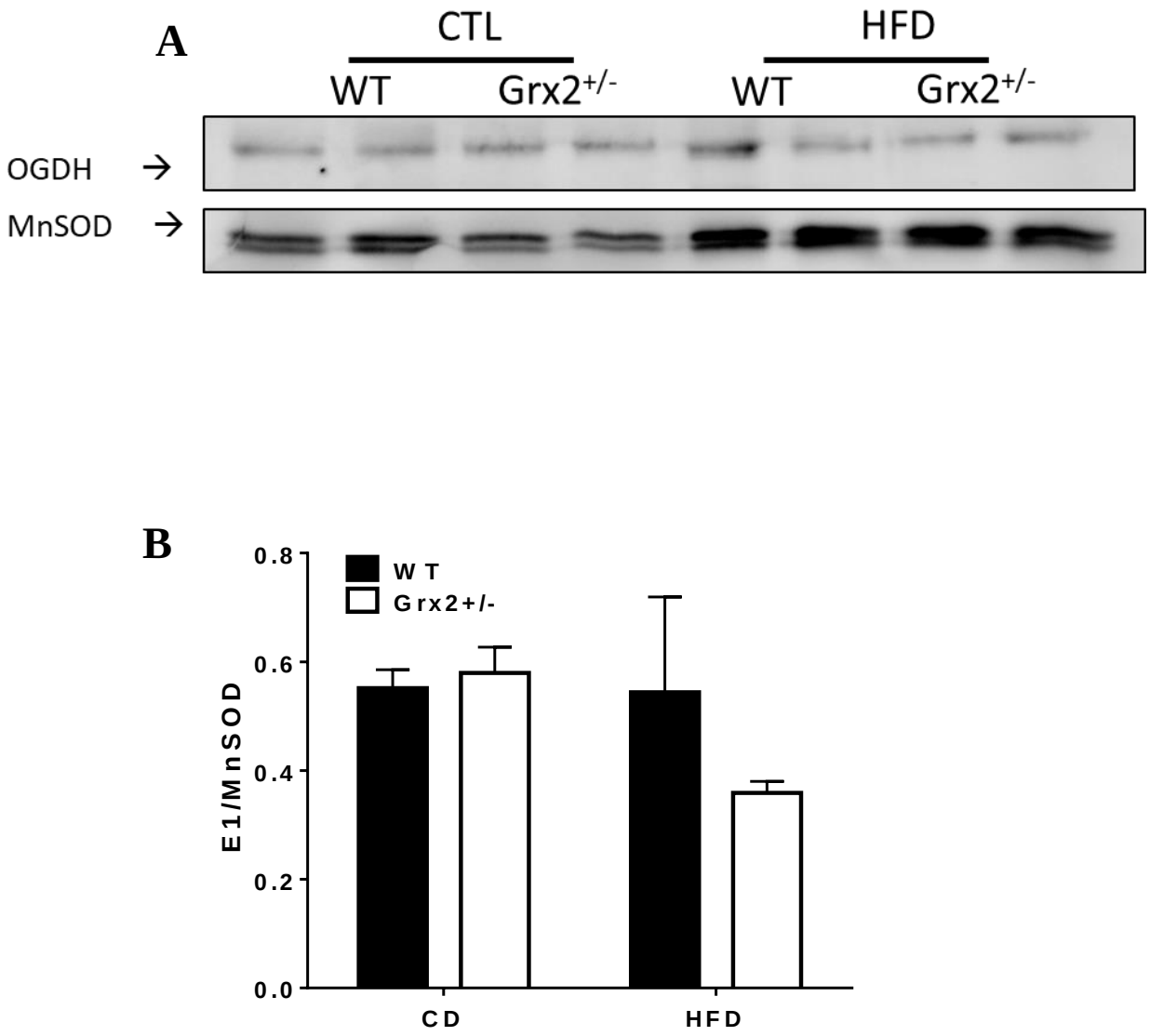

Figure 3.9: OGDH protein levels

Immunoblot with skeletal muscle mitochondria using Anti-OGDH antibody (**A**). Densitometry analysis was performed with ImageJ analysis (**B**). MnSOD was used as a loading control.

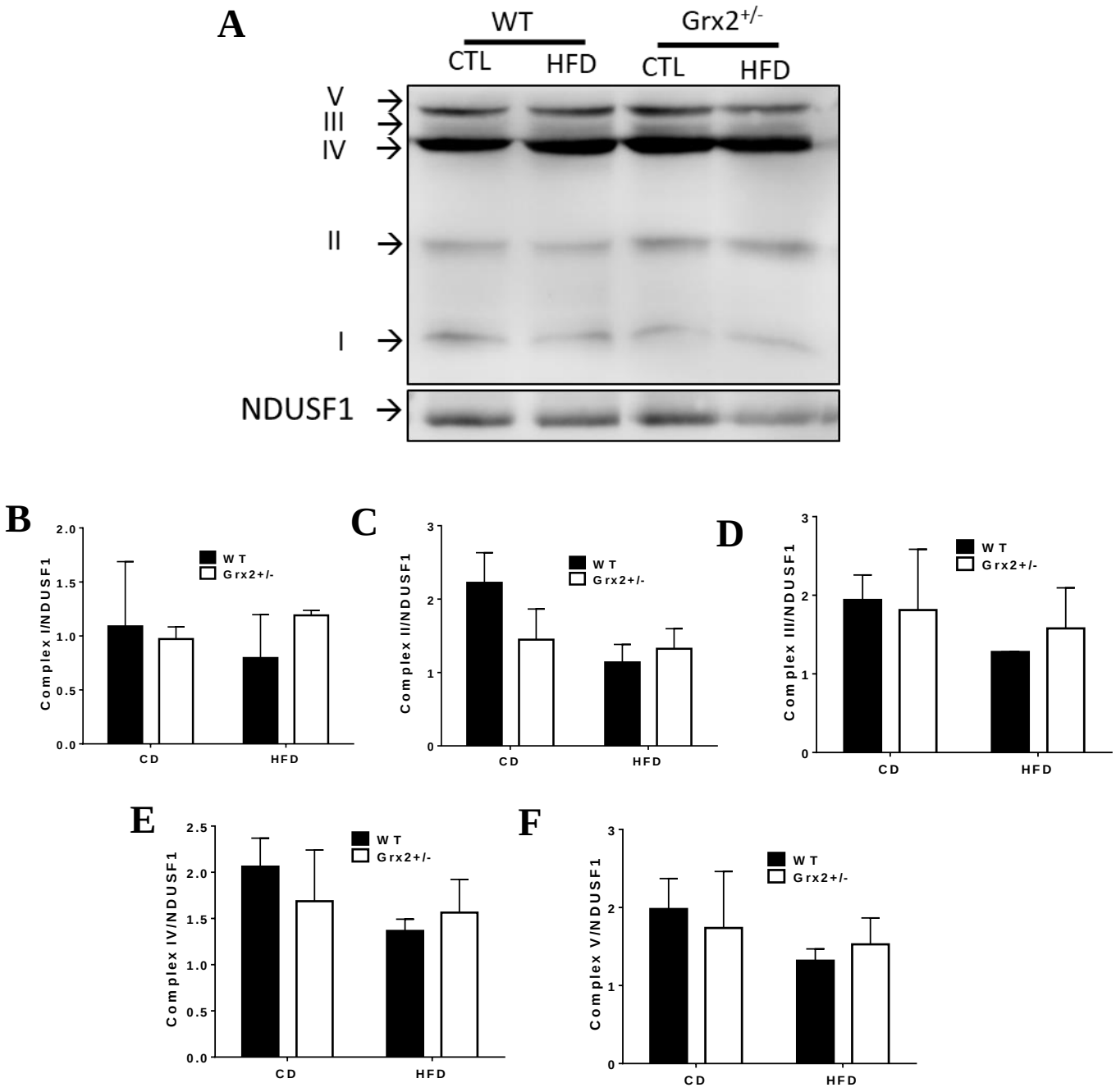

Figure 3.10: OXPHOS protein levels

Immunoblot with skeletal muscle mitochondria using OXPHOS antibody cocktail (A). Densitometry analysis was performed with ImageJ analysis (B-F). NDUSF1 was used as a loading control.

3.2.3 Increase in respiration is due to higher rate of proton return through UCP3

As previously discussed, S-glutathionylation reactions have been shown to regulate proton leak through UCP3 in skeletal muscle mitochondria. Grx2 is required to deactivate leaks through UCP3 through the S-glutathionylation of Cys^{25} and Cys^{256} (99). This prompted us to hypothesize that the increase in mitochondrial respiration and fuel combustion was due, in part, to the maintenance of UCP3 in an active state. To probe this notion, mitochondria were treated with oligomycin to induce proton leak-dependent respiration followed by exposure to GDP and genipin, two site specific inhibitors for UCP3 (154–156).

While metabolizing pyruvate and malate, *Grx2*$^{+/-}$ mice on CD or HFD demonstrated a ~40 % decrease in state 4 (proton leak-dependent) respiration when challenged with GDP (Figure 3.11). This suggests that UCP3 is responsible for the differences in proton-leak observed between WT and Grx2 haploinsufficient mice. To test this further, mitochondria were treated with genipin. (Figure 3.11). Genipin induced a significant decline in state 4 respiration (~50% and ~40%, respectively in *Grx2*$^{+/-}$ mitochondria collected from mice fed a CD or HFD) (Figure 3.11). A small decrease was also observed in mitochondria collected from WT littermates fed either diet, but this effect was not significant.

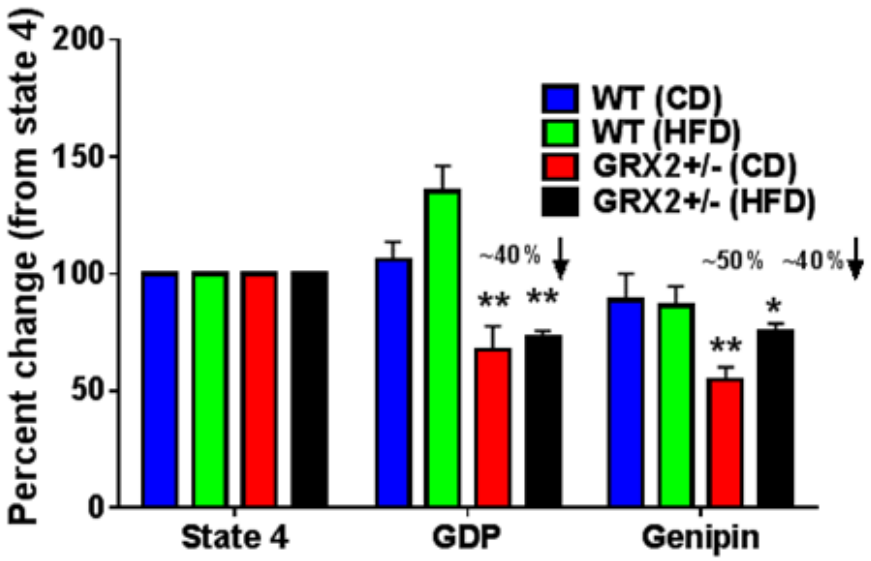

Figure 3.11: Inhibition of state 4 by genipin and GDP

State 4 was induced with the addition of oligomycin (4 µg/ml) followed by addition of pyruvate/malate (10 mM/2 mM). Respiration was measured after the addition of GDP. Reactions were completed with the addition of 4 µM Antimycin A. N ≧4, mean ± SEM, Two-way ANOVA with Fisher's LSD test. "*" Represents a comparison to the WT control.

Next, we decided to conduct immunoblot analyses to determine if changes in leaks were related to differences in the availability of UCP3. There were no changes in UCP3 expression regardless of the diet or genotype (Figure 3.12: UCP3 protein levels).

This result prompted us to hypothesize that the differences in leaks were related to changes in the S-glutathionylation status of UCP3. To test this, state 4 respiratory conditions were induced and then mitochondria were treated with the chemical catalyst for S-glutathionylation reactions, disulfiram. It is important to note that disulfiram is a non-specific catalyst that has also been found to inhibit complex I through S-glutathionylation (157). However, given that leaks are higher in *Grx2*$^{+/-}$ mitochondria, it was anticipated that we would see a much larger disulfiram effect in these samples. We found that disulfiram significantly inhibited state 4 respiration in WT and *Grx2*$^{+/-}$ mitochondria collected from mice fed either diet (Figure 3.13). However, we found that the effect was much larger in *Grx2*$^{+/-}$ mitochondria indicating that it contained more deglutathionylated proteins (Figure 3.13).

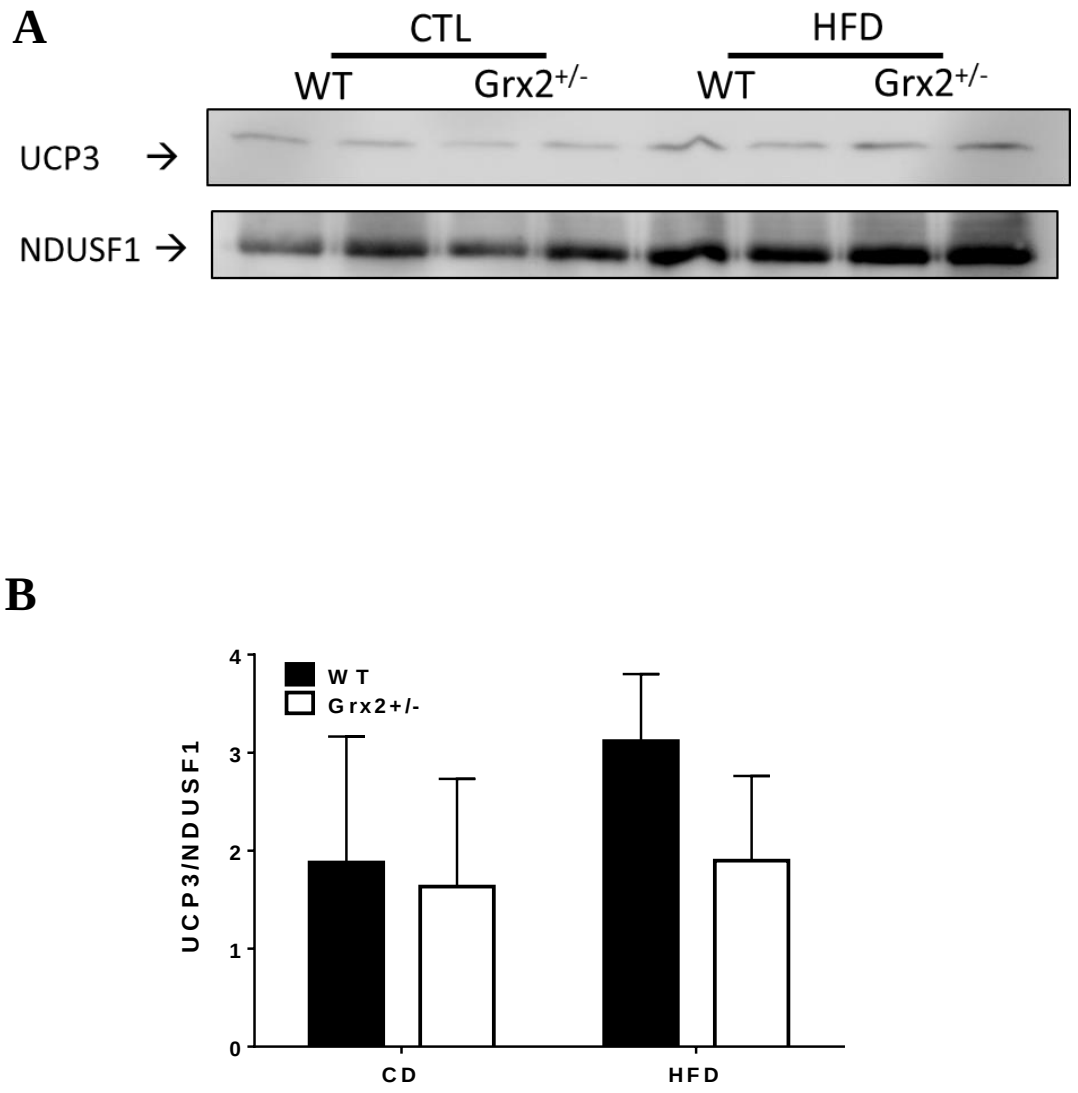

Figure 3.12: UCP3 protein levels

Immunoblot with skeletal muscle mitochondrial using Anti-UCP3 antibody (**A**). Densitometry analysis was performed with ImageJ analysis (**B**). NDUSF1 was used as a loading control.

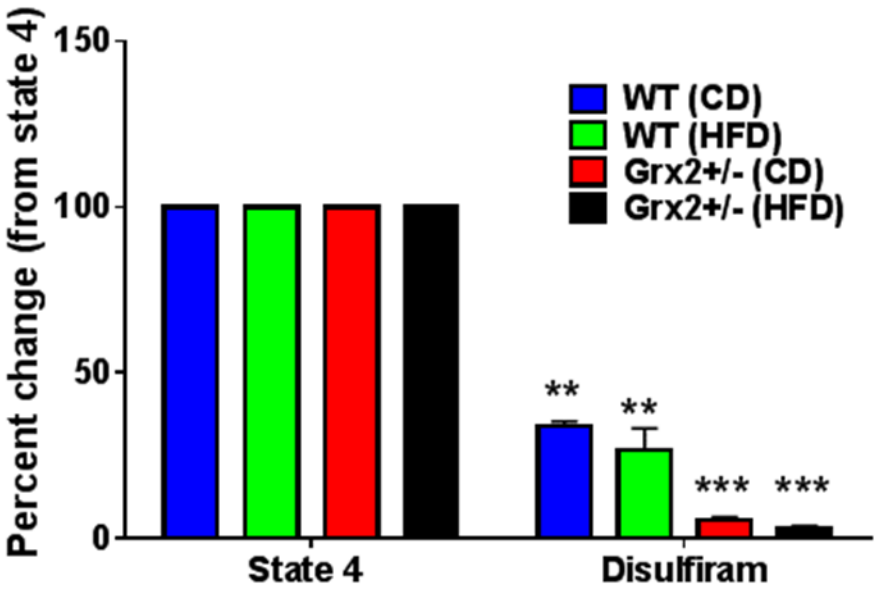

Figure 3.13: Inhibition of state 4 by Disulfiram

State 4 respiration was measured in mitochondria pre-incubated in 500 μM disulfiram. State 4 was induced with the addition of oligomycin (4 μg/ml) followed by addition of pyruvate/malate (10 mM/2 mM). Reactions were completed with the addition of 4 μM Antimycin A. N ≧4, mean ± SEM, Two-way ANOVA with Fisher's LSD test. "*" Represents a comparison to the WT control.

3.3 Examination of redox balance and ROS production profile of Grx2 haploinsufficient mice challenged with HFD.

3.3.1 Glutathione homeostasis

Grx2 activity is intimately linked to the redox status of the mitochondrial glutathione pool and previous work found that deleting the *Grx2* gene alters availability of serum GSH (70, 99). . Additionally, changes in GSH concentration correlate with the development of DIO (158–160). Therefore, we examined circulating GSH and GSSG levels. Here, *Grx2*$^{+/-}$ mice showed no change in GSH concentrations when compared to WT littermates on CD (Figure 3.14 A). In contrast, when challenged with a HFD, *Grx2*$^{+/-}$ mice demonstrated a small but significant increase in GSH concentration. Genotype did not alter GSSG levels. Additionally, no significant change in GSSG concentration was observed after administering a HFD (Figure 3.14 B). A more negative redox potential is associated with maintenance of a high GSH/GSSG ratio, which is required for H_2O_2 detoxification. Calculating the GSH/GSSG ratio revealed that the circulating glutathione pool in *Grx2*$^{+/-}$ mice fed a HFD was significantly more reductive (Figure 3.14 C).

3.3.2 $O_2^{\bullet-}$/H_2O_2 production is increased in Grx2$^{+/-}$ challenged with HFD

Grx2 and protein S-glutathionylation are required to decrease ROS release from several Krebs cycle enzymes, as well as complexes I and II (66, 68–70, 127, 128). Therefore, the impact of CD and HFD on ROS release from skeletal muscle mitochondria isolated from WT and *Grx2*$^{+/-}$ mice was examined. The rate of $O_2^{\bullet-}$/H_2O_2 was first examined using mitochondria energized with pyruvate (50 µM) and malate (50 µM). Mitochondria isolated from the skeletal muscle of *Grx2*$^{+/-}$ mice demonstrated no difference in $O_2^{\bullet-}$/H_2O_2 production when compared to WT littermates (Figure 3.15 A).

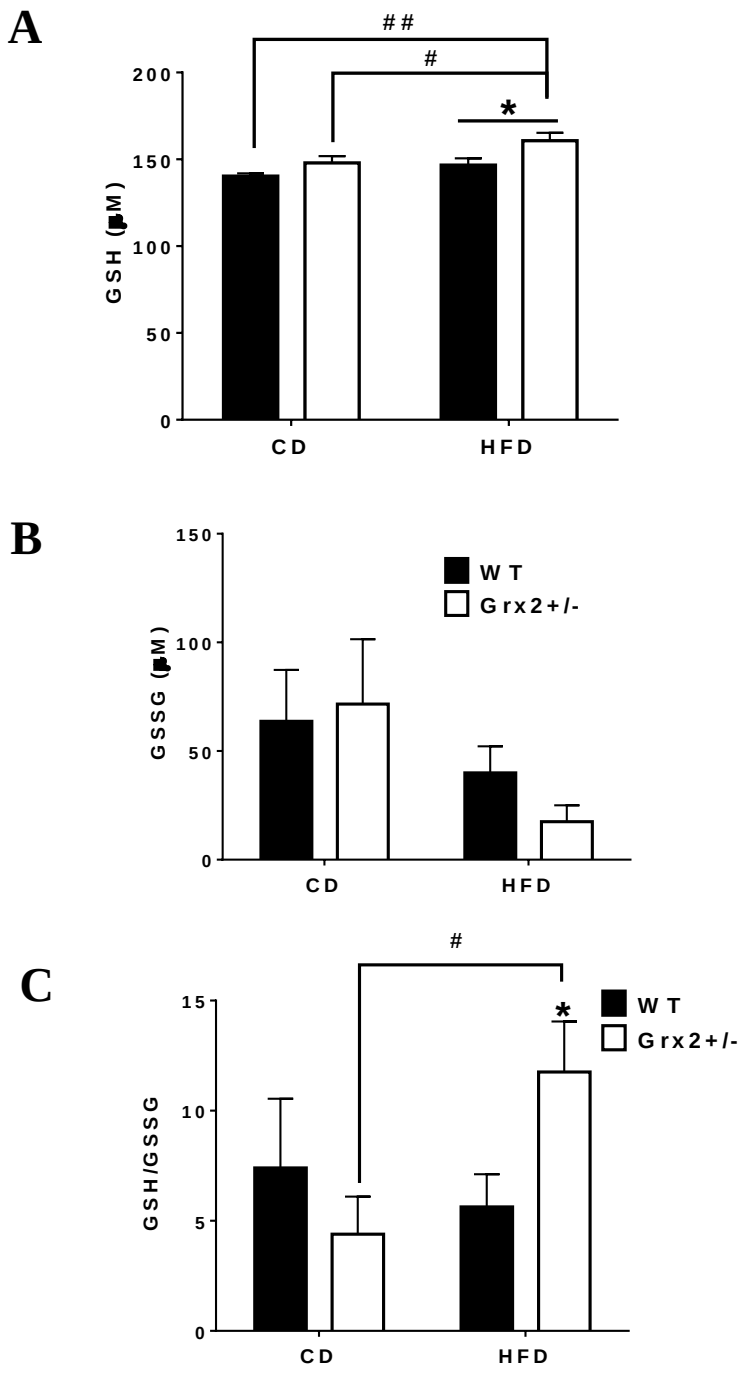

Figure 3.14: Serum levels of GSH, GSSG and GSH/GSSG ratio.

Serum levels of GSH (**A**), GSSG (**B**) GSH/GSSG ratio (**C**) were measured at 10 weeks of age. N ≧5, mean ± SEM, two-way ANOVA with a Tukey's post-hoc test. "*" Represents a comparison to the WT control while "#" represents a comparison between diets or genotypes.

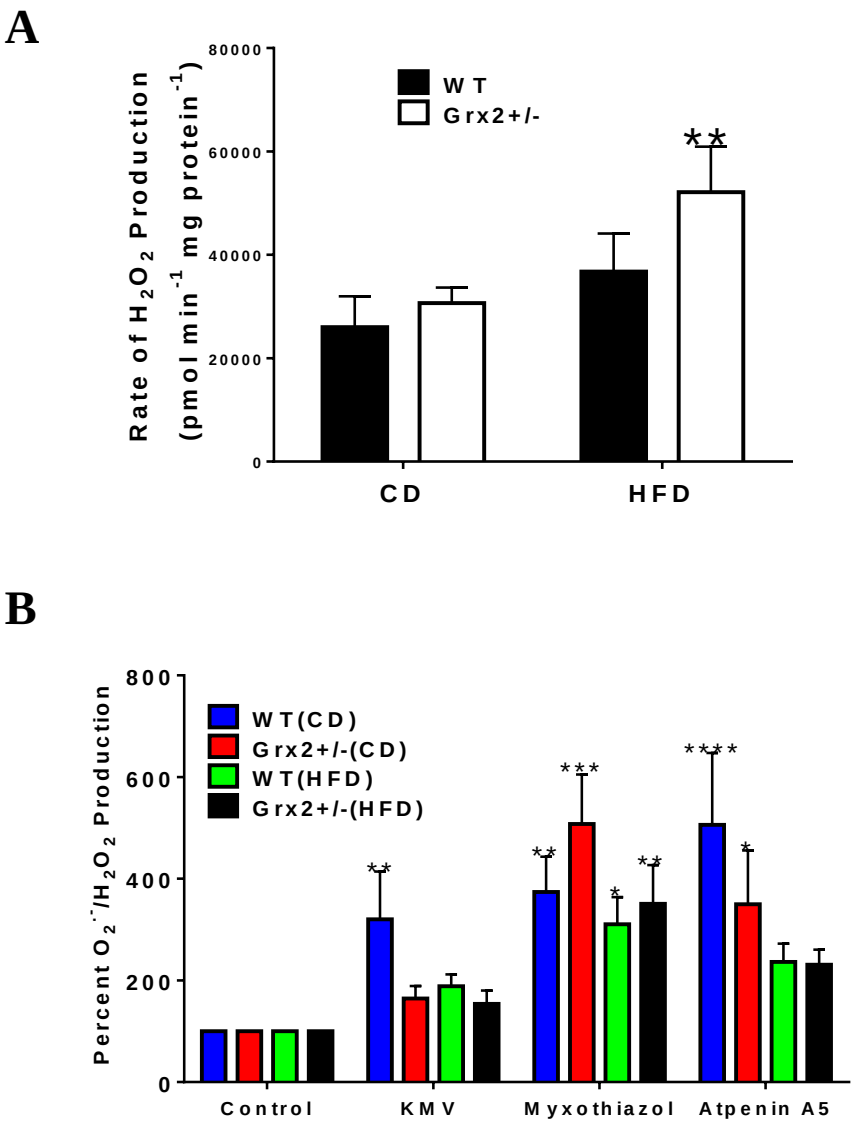

Figure 3.15: $O_2^{\bullet -}/H_2O_2$ release from mitochondria oxidizing pyruvate/malate

Mitochondria in the absence of inhibitors (**A**) and treated with KMV, atpenin A5, and myxothiazol oxidizing pyruvate/malate (**B**). N ≧5, mean ± SEM, two-way ANOVA with a Tukey's post-hoc test. "*" Represents a comparison to the WT control in the absence of inhibitors.

In contrast, there was a 2-fold increase in $O_2^{\bullet-}/H_2O_2$ production by mitochondria isolated from *Grx2*$^{+/-}$ mice challenged with a HFD (Figure 3.15 A). WT mice challenged with a HFD did not show a significant change in $O_2^{\bullet-}/H_2O_2$ production (Figure 3.15 A).

Next, we examined which ROS generating sites in the Krebs cycle and electron transport chain displayed the highest rates for mitochondrial $O_2^{\bullet-}/H_2O_2$ production. This was achieved by using selective inhibitors for OGDH (KMV), atpenin A5 (complex II), and myxothiazol (complex III). KMV, an inhibitor of OGDH, resulted in a 4-fold increase in ROS release by WT mice on CD. In contrast, *Grx2*$^{+/-}$ and WT mice on HFD demonstrated no significant effect on ROS production from skeletal muscle mitochondria (Figure 3.15 B).

Myxothiazol which inhibits electron transfer from the quinone pool to complex III induced a 2-fold increase in mitochondrial $O_2^{\bullet-}/H_2O_2$ production in WT mice on both diets as well as *Grx2*$^{+/-}$ mice on a CD (Figure 3.15 B). This increase was much more pronounced in *Grx2*$^{+/-}$ mice challenged with a HFD where a ~3-fold increase in ROS release was observed (Figure 3.15 B). Atpenin A5, an inhibitor of complex II resulted in a 2-fold increase in $O_2^{\bullet-}/H_2O_2$ production regardless of genotype or diet (Figure 3.15 B). Together, these results indicate that complex I is the major ROS source when mitochondria are energized with pyruvate and malate. The Krebs cycle, likely PDH, is also a major source of ROS in mitochondria from WT mice fed a HFD. This suggests the major sources for ROS during pyruvate supplementation are complex I and possibly complex II. This contrasts with previous findings that suggest that complex III is a major site for $O_2^{\bullet-}/H_2O_2$ production and that PDH and OGDH can produce up to 4 x and 8 x more $O_2^{\bullet-}/H_2O_2$ than complex I when metabolizing Krebs cycle linked substrates (68, 69).

Next, ROS release was examined using mitochondria energized with succinate. Complex II feeds electrons directly into the ETC, bypassing the Krebs cycle completely. Therefore, this approach gave us an opportunity to estimate ROS production from the ETC only. Skeletal muscle mitochondria isolated from *Grx2*$^{+/-}$ mice demonstrated no significant difference from WT littermates (Figure 3.16 A). When challenged with a HFD, however, *Grx2*$^{+/-}$ mice demonstrated a 3-fold increase in $O_2^{\bullet-}/H_2O_2$ production (Figure 3.16 A). This increase was not reflected in WT mice on a HFD although a trend for an increase was apparent (Figure 3.16 A).

Next, sites for $O_2^{\bullet-}/H_2O_2$ production during succinate oxidation were assessed using rotenone, myxothiazol, and atpenin A5. Rotenone blocks reverse electron flow from complex II by blocking the ubiquinone binding site in complex I. Rotenone did not alter $O_2^{\bullet-}/H_2O_2$ production by skeletal muscle mitochondria regardless of diet or genotype (Figure 3.16 B). This suggests that complex I is not a major contributor of $O_2^{\bullet-}/H_2O_2$ production during succinate oxidation. Supplementing mitochondria with myxothiazol induced a significant increase in ROS production by mitochondria from both genotypes fed either diet (Figure 3.16 B). Exposing mitochondria to atpenin A5 resulted in the largest increase in mitochondrial $O_2^{\bullet-}/H_2O_2$ production regardless of genotype or diet. This suggests, that when succinate is being oxidized, complex II is the major location of $O_2^{\bullet-}/H_2O_2$ production in skeletal muscle mitochondria. Succinate has been shown to induce $O_2^{\bullet-}/H_2O_2$ production from complex I through reverse electron transfer (66).

Finally, ROS release was examined using mitochondria energized with palmitoyl-carnitine; electrons supplied by palmitoyl-carnitine are transferred directly to the electron transfer chain through ETFQO (Figure 1.4) allowing investigation of ROS production associated with fatty acid metabolism. There were no significant differences in $O_2^{\bullet-}/H_2O_2$ production observed between mice based on genotype or diet (Figure 3.17 A).

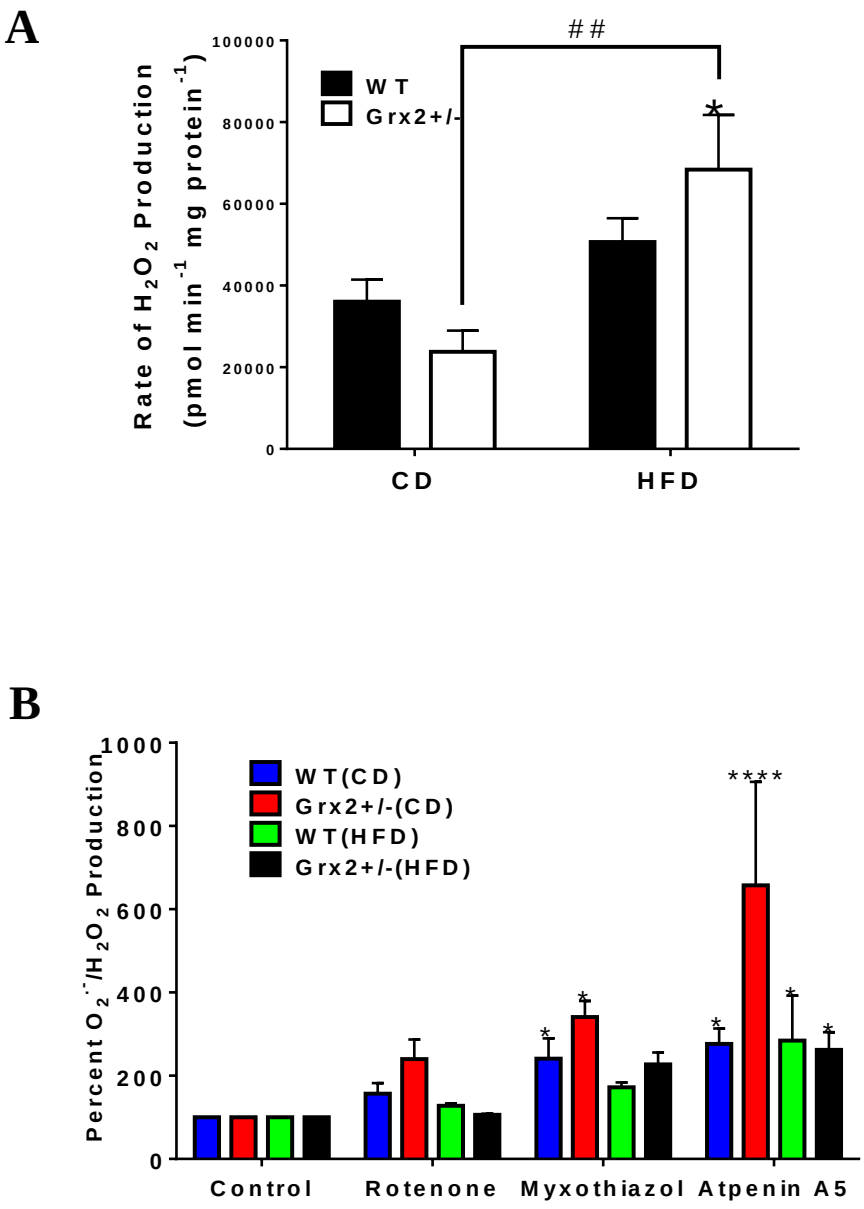

Figure 3.16: $O_2^{\bullet-}/H_2O_2$ release from mitochondria oxidizing succinate

Mitochondria in the absence of inhibitors (**A**) and treated with rotenone, atpenin A5, or myxothiazol oxidizing succinate (**B**). N ≧5, mean ± SEM, two-way ANOVA with a Tukey's post-hoc test. "*" Represents a comparison to the WT control while "#" represents a comparison between genotypes.

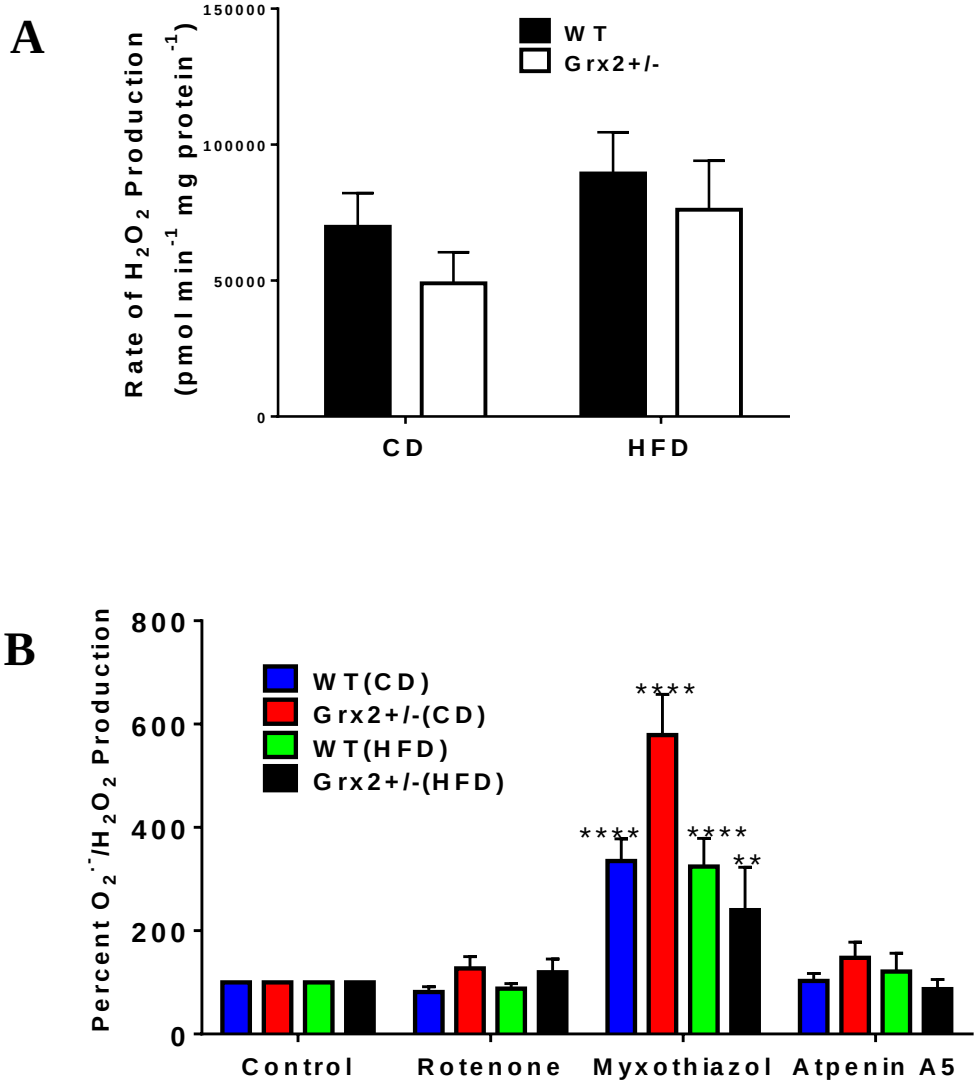

Figure 3.17: $O_2^{\bullet -}/H_2O_2$ release from mitochondria oxidizing palmitoyl carnitine

Mitochondria in the absence of inhibitors (**A**) or treated with rotenone, atpenin A5, or myxothiazol oxidizing palmitoyl carnitine (**B**). N ≧5, mean ± SEM, two-way ANOVA with a Tukey's post-hoc test. "*" Represents a comparison to the WT control while "#" represents a comparison between genotypes.

The sites for $O_2^{\bullet-}/H_2O_2$ production during palmitoyl-carnitine oxidation were also assessed using rotenone, myxothiazol, and atpenin A5. Inhibition by rotenone did not alter mitochondrial $O_2^{\bullet-}/H_2O_2$ production regardless of diet or genotype. The case was similar for inhibition of complex II by atpenin A5 (Figure 3.17 B). Inhibition of complex III by myxothiazol led to a 2-fold increase in mitochondrial $O_2^{\bullet-}/H_2O_2$ production in isolated skeletal muscle mitochondria regardless of diet or genotype (Figure 3.17 B). Given these results, it is likely that complex I is a major location of ROS production during palmitoyl-carnitine oxidation.

3.3.3 NADH levels are not significantly altered by Grx2 haploinsufficiency or HFD

NADH is produced by multiple Krebs cycle associated enzymes and bridges electron transport between Krebs cycle intermediates and the ETC (Figure 1.4). It has been demonstrated that elevated NADH levels can induce $H_2O_2/O_2^{\bullet-}$ production from OGDH and PDH (8, 41, 151). This coupled with the fact that OGDH and PDH have previously been identified as major sources for $O_2^{\bullet-}/H_2O_2$ production in liver and skeletal muscle mitochondria (67–69), means it was essential that NADH levels be monitored in addition to measurement of $O_2^{\bullet-}/H_2O_2$ production.

Overall, NADH levels appeared to be decreased in *Grx2*$^{+/-}$ mice on the control diet when compared to the WT on control diet but the effect was not significant (Figure 3.18). Interestingly, NADH levels of the *Grx2*$^{+/-}$ mice on HFD saw similar NADH levels as WT mice on control diet. During pyruvate supplementation, KMV led to decreased NADH levels. This is not unexpected since electron transfer from the Krebs cycle relies on NADH production from OGDH, PDH, and IDH. Myxothiazol inhibition of complex III led to an increase in NADH levels (Figure 3.18 A). This was also not unexpected since inhibiting electron transfer to complex III will slow the ETC leading to a decreased complex I activity and increased NADH. Inhibition of complex II had no effect on NADH levels (Figure 3.18 A). During succinate oxidation, inhibitors rotenone,

myxothiazol, and atpenin A5 had no effect on NADH (Figure 3.18 B). This is not surprising since electron transfer to succinate does not require NADH. During palmitoyl-carnitine supplementation, rotenone inhibition of complex I results in an increase in NADH levels (Figure 3.18 C). This is likely due to the fact that, during palmitoyl oxidation, NADH and acetyl CoA are generated. Acetyl CoA can feed into the Krebs cycle generating additional NADH.

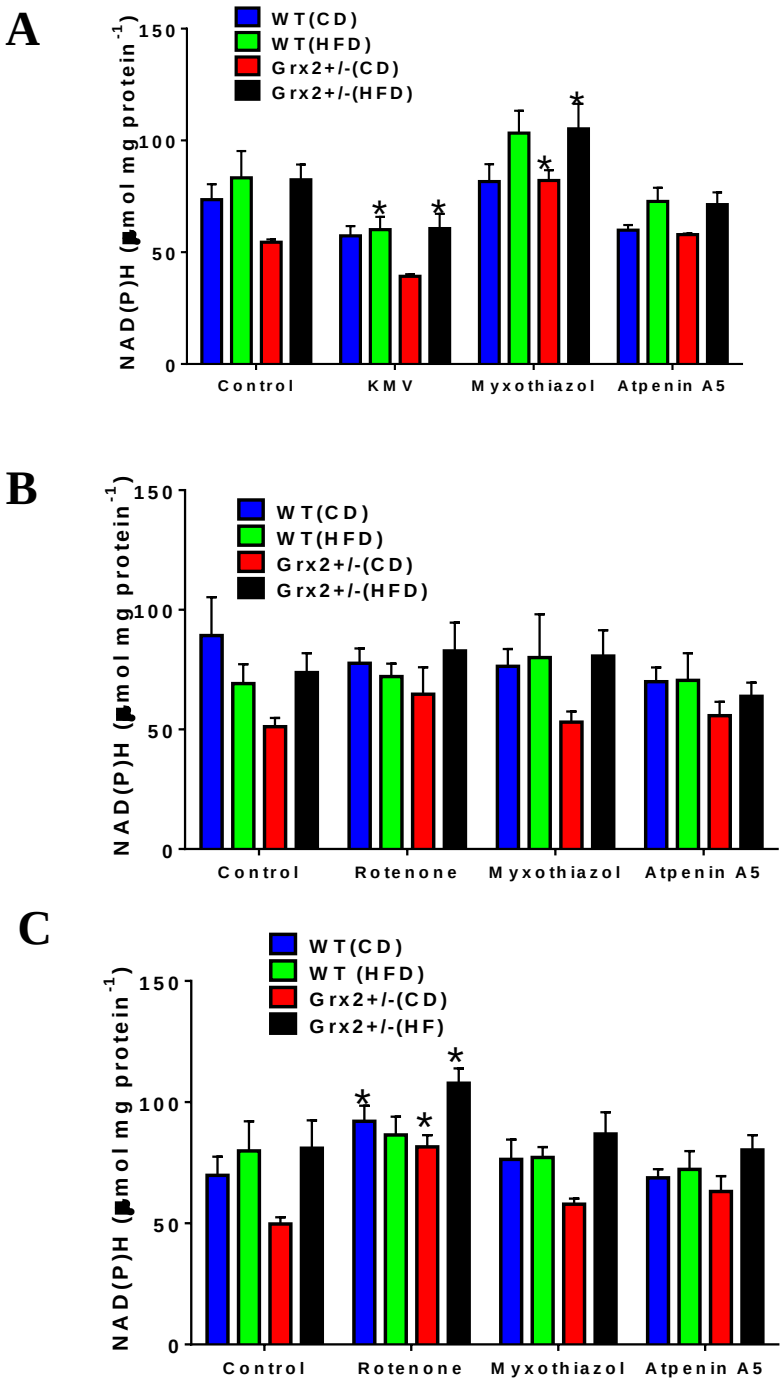

Figure 3.18: NADH levels in isolated skeletal muscle mitochondria.

Mitochondria were treated KMV, rotenone, atpenin A5, and myxothiazol oxidizing pyruvate/malate (**A**), succinate (**B**), or palmitoyl carnitine and carnitine (**C**). N ≧5, mean ± SEM, two-way ANOVA with a Tukey's post-hoc test. "*" Represents a comparison to the WT control while "#" represents a comparison between genotypes.

`

Chapter 4: Discussion

4.1 Summary

The purpose of this investigation was to examine the role of Grx2 in regulating fat metabolism and ROS production in skeletal muscle mitochondria. To do so, Grx2 haploinsufficient mice and WT littermates were challenged with HFD or matched CD. A comparison of the physiological and metabolic characteristics of the mice was performed in addition to redox balance, ROS production, and bioenergetics analyses. It is important to note that while previous works have probed these aspects in *Grx2*$^{-/-}$ mice (70, 99), this is the first time that it has been shown that Grx2 haploinsufficent male mice are protected from DIO. Indeed, the body mass of *Grx2*$^{+/-}$ mice was unchanged when challenged with a HFD. By contrast, WT mice fed a HFD displayed an increase in overall body mass, hypertrophy of white adipose tissue, increased serum insulin and triglyceride levels, and intrahepatic lipid accumulation. Insulin resistance is an important step in the development of metabolic syndrome and leads to dysregulation of peripheral lipolysis increasing circulating fatty acids (161). Additionally, the liver plays a central role in metabolic homeostasis acting as a major site for lipid synthesis and storage. High-fat diets have been shown to lead to increased fatty acid accumulation in the liver leading to lipotoxicity and the development of non-alcoholic fatty liver disease (NAFLD) which can, in turn, progress to non-alcoholic steatohepatitis.

The protection experienced by mice haploinsufficient for Grx2 was attributed to the augmentation of fuel metabolism by muscle mitochondria. Indeed *Grx2*$^{+/-}$ mice demonstrated a ~2 to ~3-fold increase in ADP dependent respiration, as well as proton leak dependent respiration through UCP3 regardless of diet or substrate being oxidized. These findings are consistent with previous work demonstrating that UCP3 is controlled through S-glutathionylation reactions (99, 133). Indeed, Grx2 is required to S-glutathionylate UCP3 to reduce its activity. In the absence of

Grx2, UCP3 is maintained in a deglutathionylated and active state leading to increased proton leak, which subsequently increases fuel metabolism (99). This notion is supported further by work from our laboratory showing that chemical S-glutathionylation catalysts can inhibit non-phosphorylating respiration (127). Here, we utilized selective inhibitors for UCP3, GDP and genipin, to confirm that UCP3 is responsible for increased proton leak in *Grx2*$^{+/-}$ mice. GDP reduced UCP3-mediated proton leak in *Grx2*$^{+/-}$ mice but had no significant effect on WT mice. Genipin elicited a similar effect.

Grx2$^{+/-}$ mitochondria also exhibited an enhanced capacity to combust palmitoyl-carnitine to support oxidative phosphorylation. It is likely that the augmentation of fatty acid combustion is due to increased proton return through UCP3 to the matrix, which contributes to the maintenance of normal body mass when challenged with a HFD. In conjunction with increased fuel metabolism, *Grx2*$^{+/-}$ mice demonstrated an altered redox state and increased mitochondrial ROS. The increase in ROS production is likely related to the augmentation of mitochondrial fuel combustion. Although ROS can be dangerous, these molecules also play a vital role in normal muscle physiology, namely, adaptation to exercise. This is achieved through the induction of signaling cascades that bolster antioxidant defenses, activate muscle repair programs, and induce the expression of genes involved in muscle growth. Overall, this indicates that manipulating mitochondrial redox signals may serve as an “exercise mimetic”.

4.2 Pharmacotherapeutic strategies that activate proton leaks for the treatment of obesity.

4.2.1 Current strategies to prevent and treat obesity

There are a number of strategies to prevent and treat obesity including methods that manipulate the balance between energy intake and expenditure, surgery, behavioral modifications, and pharmacological interventions. While some of these interventions can be effective, they often suffer from significant limitations. Increased physical activity and diet restriction is still the gold standard in weight loss intervention since it is non-invasive and can be highly effective at promoting increased whole-body energy metabolism. However, such interventions can have highly variable outcomes. The degree of weight loss is a function of the individual's ability to stick to a strict diet and exercise regimen (162) and the efficacy of altering physical activity and diet restriction depends on external factors such as social, economic, and cultural influences (163). Additionally, the effectiveness of diet and exercise is highly variable due to genetic and epigenetic differences, making it more difficult for individuals to lose weight or maintain new energy balances following weight loss.

Bariatric surgery has seen increased favor and employment due to promising results (164). Current strategies include Roux-en-Y gastric bypass, sleeve gastrectomy, and laparoscopic adjustable gastric band. The drawbacks of these procedures stem from cost, and complications that result from invasive surgery, and a selection criterion that requires patients to fall within a weight class, usually within a Body mass index of 30-35 (165). Patients often develop infections, gastrointestinal bleeding and blockage, gastroesophageal reflux, and nutritional deficiencies (166).

Pharmaceutical strategies have multiple targets that modify appetite, nutrient uptake, and removal through modulation of the serotonergic, noradrenergic and dopaminergic systems. Targets of the serotoninergic system include serotonin 2C receptor (5-HT_{2C}) (167), melanocortin receptor (MC4) agonists (168), and arcuate neuro peptide Y receptor (NPY) antagonists (169). Targets of the noradrenergic system activate α1- and β2-adrenoreceptors. Other targets that influence appetite include the endocannabinoid system, the Y2 receptor, and the circulating hormones, glucagon-like peptide-1 (GLP-1), amylin and ghrelin (170–173). These interventions are effective; however, their adverse effects include increased blood pressure and the development of heart valvulopathy (174, 175). Phentermine, for example, is highly addictive and can lead to cardiovascular toxicity (171).

Some intervention strategies have turned to pharmacological activation of AMP-activated protein kinase (AMPK). AMPK is activated by muscle contraction and signaling pathways initiated by its activation mediate metabolic adaptations that protect from the development of metabolic disorder (176). AMPK activation by metformin, leptin, and adiponectin have demonstrated the ability to increase insulin sensitivity, glucose transport, mitochondrial content and protein expression in skeletal muscle and decreased gluconeogenesis in hepatic tissue (177–181). AMPK activation has garnered considerable interest for its potential as exercise and calorie restriction mimetics; however, there is much that is still not well understood.

Lastly, there are strategies that convert white adipose tissue (WAT) to brown adipose tissue (BAT). Accumulation of WAT is associated with the development of obesity and related disorders (182, 183). WAT has functions in long term lipid storage for times of caloric need in addition to immune function and hormone production (183). BAT cells appear brown in color due to a greater number of mitochondria and reduced lipid content in comparison to WAT cells. BAT is required

for non-shivering thermogenesis through UCP1 activity. This action increases energy expenditure since fuels are burned at a high rate to support heat production through the provision of a protonmotive force. As a result, research is being conducted to "brown" white fat by increasing its mitochondrial content. Indeed, the browning of white fat correlates with increased insulin sensitivity and a lower BMI (182, 184). Some browning agents include beta-amino isobutyric acid, gamma amino butyric acid, PPARγ, and irisin (185–188). Phase II clinical trials for leptin amylin analogs pramlintide and metreleptin were ended due to the development of severe adverse side effects (189). Currently, enough information has not been gathered to make the browning of WAT an effective treatment option.

4.2.2 Uncoupling strategies

The concept of inducing proton leaks for weight loss is not new. Early anti-obesity therapeutic strategies utilized chemical uncoupling agents such as 2,4 dinitrophenol (DNP), carbonylcyanide m-chloro phenylhydrazone (CCCP), and p-trifluoromethoxycarbonylcyanide phenylhydrazone (FCCP). DNP was used for a greater part of the 1930s with promising results (190). DNP shuttles protons across the MIM, dissipating the PMF leading to a 20-30% increase in energy expenditure that persisted for 24 hours. Unfortunately, DNP has a narrow therapeutic window and thus had some dire side effects, causing cataract and death by hyperplasia at doses near pharmacologically relevant concentrations. Consequently, use of chemical uncouplers for weight loss was banned in many countries. Nonetheless, there is still a lot of interest in exploiting leaks to promote weight loss through the activation of the body's genetically encoded leakers, the uncoupling proteins (UCPs).

The first uncoupling protein that was discovered was UCP1, which is required for the induction of thermogenesis in brown fat following cold exposure (191). Thermogenesis in BAT

relies on the activation of proton leaks through UCP1, which is induced by norepinephrine release (192). Indeed, β_3-adrenergic agonist can increase energy expenditure significantly, likely through activation of UCP1 (146). Fatty acids also modulate the activity of UCP2 and UCP3. Indeed, increased fatty acid availability has been demonstrated to increase UCP2 and UCP3 mRNA availability (193). This suggests some role for UCP2 and 3 in the regulation of fatty acid metabolism. Most intriguing are the number of lines that can be drawn between the previously discussed treatment options for obesity and the UCP2 and UCP3 proteins. The promoter for UCP2 expression is regulated by AMPK (194) and PPARγ agonists can also lead to increased UCP3 expression (195). Additionally, acute exercise, leptin, and β_3-adrenergic agonists induce increased transcription of both UCP2 and UCP3 (192, 196).

Still, the field surrounding the regulation of UCP2 and 3 and their ability to conduct protons has undergone great scrutiny and is entwined with controversy (197, 198). As previously mentioned, the mechanism by which UCP2 and 3 conduct protons across the MIM is not yet fully understood. The histidine pair required for UCP1 mediated proton conductance is not present in the UCP2 and UCP3 homologs complicating our understanding of their function (199). Additionally, changes in UCP2 and UCP3 expression did not correlate with changes in proton leak, bringing into question whether or not these proteins conduct protons (200). This led several groups to ascertain if UCP2 and 3 fulfill other functions. For instance, it has been observed that UCP2 and 3 are capable of transferring calcium anions, monovalent anions, fatty acids, and hydroperoxide anions (155, 201–203). Despite this, it has been firmly established that UCP2 and 3 are required to stem the effects of oxidative stress. Indeed, it has also been established that UCP2 and 3-dependent proton leak is activated by fatty acids, $O_2^{\bullet-}$, lipid peroxides and 4-hydroxynonenal (32, 89, 99, 204). Also, recent work has found that *Ucp3* gene expression is controlled by NRF2,

a critical transcription factor required for bolstering cellular antioxidant defenses in response to oxidative stress (205). Activating UCP3 or increasing its expression also has positive metabolic effects. Mice overexpressing UCP3 have reduced adiposity and increased insulin sensitivity while $UCP3^{-/-}$ mice have impaired fatty acid metabolism (98, 206). This suggests a role in the regulation of ROS production in addition to facilitating fatty acid oxidation.

The increased proton leak-dependent respiration observed in $Grx2^{+/-}$ mice in this study is likely associated with the activation of UCP3. Treatment of mitochondria from $Grx2^{+/-}$ mice with GDP induced a significant decrease in non-phosphorylating respiration whereas it had no effect on the rate of O_2 consumption in samples enriched from WT littermates. This suggests that UCP3 is more active in $Grx2^{+/-}$ muscle mitochondria. It is important to point out that GDP is often considered a selective inhibitor for UCP3. Indeed, the structure of UCP2 in the presence of GDP has been determined using nuclear magnetic resonance (207). However, some studies have shown that GDP can also inhibit ANT, another source of leaks in mitochondria (208, 209). This prompted us to test the effect of genipin on non-phosphorylating respiration. Genipin was first identified as a membrane permeable inhibitor of UCP2 for applications in regulating insulin signaling in pancreatic β cells (210). Researchers demonstrated that genipin did not inhibit basal proton conductance by ANT and could be a specific inhibitor of UCP2 in liver and pancreatic β cells (210). It has also been suggested that genipin may inhibit UCP3 due to its similarity in structure and function to UCP2. Treatment of mitochondria from $Grx2^{+/-}$ mice elicited a similar effect; there was ~40% decrease in the rate of O_2 consumption under state 4 respiratory conditions. Additionally, there was little to no effect on WT mitochondria. Together, these results indicate that UCP3 is more active in muscle mitochondria isolated from $Grx2^{+/-}$ mice.

Increased proton leak-dependent respiration as a result of Grx2 haploinsufficiency mirrors previous findings that characterized the physiology and ROS production profile of *Grx2*$^{-/-}$ mice (99) and ties together the current understanding of the functions and regulation of UCP3 in skeletal muscle mitochondria. In past research, while UCP3$^{-/-}$ mice did not demonstrate higher susceptibility to obesity (211), mice overexpressing human UCP3 protein demonstrated increases in weight loss (98). Additionally, a study using human subjects found that muscles from patients who had a greater rate of weight loss displayed a 51% increase in proton leak dependent respiration associated and a 25% increase in UCP3 mRNA expression. In previous work describing the characteristics of *Grx2*$^{-/-}$, increases in proton leak were attributed to the maintenance of UCP3 in a deglutathionylated state (99). Here, we also found the increase in leaks in muscle mitochondria from *Grx2*$^{+/-}$ mice was associated with the deglutathionylation of UCP3. Indeed, treatment of mitochondria with the S-glutathionylation catalyst disulfiram induced a profound decrease in state 4 respiration in WT and *Grx2*$^{+/-}$ mitochondria. However, the effect was significantly larger in *Grx2*$^{+/-}$ mitochondria. Note that disulfiram is a non-specific S-glutathionylation catalyst, and it is thus not surprising that it inhibited respiration in WT and *Grx2*$^{+/-}$ mitochondria. Indeed, in a previous study published by our group, it was found that disulfiram inhibited respiration in muscle mitochondria from C57BL6N mice through the S-glutathionylation of NDUFS1, a subunit required for complex I activity (127). However, it is worthwhile to point out here there was a stark difference in the effect between WT and *Grx2*$^{+/-}$ mitochondria, with the latter being suppressed by an additional ~40%, a decrease in state 4 respiration that was also observed with mitochondria treated with GDP or genipin. Taken together, these results indicate that the deglutathionylation of UCP3 and the resulting increase in proton leak-dependent respiration is, in part, responsible for

the increase in mitochondrial fat combustion in muscles from *Grx2*$^{+/-}$, which likely contributes to its resistance to DIO.

4.2.3 Altered S-glutathionylation reactions influence fuel metabolism

Under normal physiological conditions, mitochondria respond to nutritional and physiological cues that dictate the metabolism of the favored substrate for any given condition. In obese individuals there exists inflexibility and impaired fuel switching capacity, which is referred to as metabolic gridlock (212). It is hypothesized that excessive competition between substrates leads to mitochondrial indecision leading to acyl-carnitine accumulation, the over production of ROS, and lipid and protein damage. Antioxidant systems help to alleviate substrate competition through cysteine modification and the regulation of various enzymes involved in nutrient metabolism, resulting in the control of metabolic flux and bioenergetics (212). Metabolic diseases are associated with alterations in redox buffering capacity and the inability to sustain the spatiotemporal flexibility of cellular redox signaling (148). Indeed, preservation or restoration of mitochondrial redox buffering networks and signals have been suggested to serve as a means of treating metabolic diseases such as obesity by alleviating metabolic gridlock (148, 212).

A critical observation made in this study was that there was an increase in both state 3 and state 4 respiration in mitochondria oxidizing either Krebs cycle linked substrates, succinate, or palmitoyl-carnitine. As noted above, this increase in mitochondrial fuel combustion is related, in part, to deglutathionylation and activation of UCP3. However, induction of leaks through UCP3 cannot be the only factor driving this increase in fuel oxidation. Outside of UCP3, there are multiple S-glutathionylation targets associated with the respiratory chain and nutrient metabolism that could explain this increase in respiration. The first is complex I, which our group recently identified as a target of S-glutathionylation in muscle mitochondria (70, 157). Indeed, it was found

that the disulfiram induced decrease in state 3 respiration in mitochondria oxidizing pyruvate was associated with the S-glutathionylation of NDUFS1, a key subunit required for the catalytic activity of complex I (70). Previous studies have shown that modifying this subunit with glutathione decreases the activity of complex I (114, 152). Moreover, the S-glutathionylation of NDUFS1, due to defective *Grx2* activity, has been associated with the development of heart disease and cataracts (121, 152). This is associated with a ~50% drop in mitochondrial ATP output, demonstrating that the reversible glutathionylation of complex I plays a vital role in regulating bioenergetics (152). A recent study also found that complex I is a target for S-glutathionylation during fatiguing muscle contraction and relaxation (61). In particular, Cys^{125} and Cys^{142} of NADH dehydrogenase flavoprotein 1 (NDUFV1), a well-known target for S-glutathionylation, was found to be modified (61). Therefore, although not measured here, it is likely that complex I is in a deglutathionylated state in $Grx2^{+/-}$ mitochondria, promoting increased respiration and fuel combustion.

Outside of complex I, there are other important targets for S-glutathionylation in mitochondria that can alter rates of fuel combustion and respiration. For example, we recently discovered that mitochondrial pyruvate carrier is also a target for S-glutathionylation in muscle (127). In this case, induction of S-glutathionylation inhibits pyruvate uptake while deglutathionylation has the opposite effect (127). Another important target for S-glutathionylation is carnitine/acyl-carnitine carrier, which is required to facilitate the uptake of fatty acids for beta-oxidation. Glutathionylation inhibits the antiport of acyl-carnitine and carnitine, an effect that is reversed by exogenous GRX1 (140). It is also important to point out that Kramer *et al* found that several complex II subunits as well as ATP synthase α-subunit and ANT were also targets for S-glutathionylation in muscle during fatiguing exercise (61). Glutathionylation of ATP synthase has

been documented to decrease its activity and prolonged modification is associated with metabolic dysfunction and heart disease (213). Therefore, it is also possible that maintenance of these proteins in a deglutathionylated state may also facilitate the high rates of fuel combustion observed in *Grx2*$^{+/-}$ muscle mitochondria.

The increase in respiration in *Grx2*$^{+/-}$ mitochondria oxidizing pyruvate or palmitoyl-CoA also indicates that the glutathionylation state of Krebs cycle and fatty acid oxidation enzymes may also be altered. Candidates include PDH and OGDH, which have both been demonstrated to be important targets for S-glutathionylation in multiple tissues (70, 112, 214). Protein S-glutathionylation of the E2 subunits of PDH and OGDH plays a vital role in regulating mitochondrial ROS production by blocking electron transfer from the E2 to the E3 subunits (68, 70). The trade-off is a decrease in the activity of both enzyme complexes. Our group has also shown for the first time that Grx2 is integral for facilitating the reversible S-glutathionylation of PDH and OGDH in liver and heart (70). Additionally, oxidation of mitochondrial redox buffering networks also compromises PDH activity in permeabilized muscle fibers, which has been linked to diet-induced obesity and insulin resistance (215). In this particular study, it was postulated that the alteration in PDH activity was related to its protein S-glutathionylation (215). Therefore, it is anticipated that both complexes may be maintained in a deglutathionylated state facilitating increased fuel combustion in mice heterozygous for Grx2. It is also important to note here that partial loss of Grx2 in this study induced an increase in PDH expression. This could also account for the increase in fuel combustion. Although PDH also increased in WT mice fed a HFD, it is likely that most of it is in a glutathionylated state, which would be consistent with previous observations made by our group (70). This would mean that in *Grx2*$^{+/-}$ mitochondria, PDH is more deglutathionylated rendering it more active thereby facilitating higher rates of fuel combustion.

Kramer *et al* also identified a number of S-glutathionylation targets involved in nutrient metabolism in muscle mitochondria (61). One intriguing observation made was that ETFQO was a target for S-glutathionylation in muscle (61). Fatty acid oxidation enzymes are known to undergo S-nitrosylation but to our knowledge this is the first time ETFQO, a crucial component of the beta-oxidation machinery in the matrix of mitochondria, is modified by S-glutathionylation (61, 216). It was recently proposed that protein S-glutathionylation serves as the linchpin for the regulation of mitochondrial bioenergetics in response to changes in environmental cues (112). This does appear to be the case since alterations in S-glutathionylation can impact mitochondrial function. Additionally, based on the findings presented herein, it would also seem that manipulating these pathways can serve as a means of increasing fuel metabolism.

S-glutathionylation reactions also operate beyond mitochondrial metabolism to regulate nutrient oxidation and whole-body energy expenditure. S-glutathionylation of protein kinase A (PKA) desensitizes cAMP signaling reactions (217). This may explain why deregulation of S-glutathionylation reactions demonstrates similar results to AMPK related treatment options for obesity. In fact, AMPK itself is S-glutathionylated and activated by GRX1 on the α and β subunits in response to changes in cellular H_2O_2 levels (218). Understanding how AMPK activators may influence the S-glutathionylation reactions may provide some insight into the mode of action of these pharmaceutical interventions. In skeletal muscle, S-glutathionylation reactions are necessary to maintain normal muscle function during fatiguing exercise. Approximately 1,290 peptides were glutathionylated in response to simulated fatiguing exercise (61). S-glutathionylation reactions regulate calcium release by the sarcoplasmic reticulum as well as calcium sensitivity of troponin. These S-glutathionylation reactions mediated muscle adaptation to exercise. Recent work has suggested that these adaptations towards exercise are facilitated, in part, through the modulation

of mitochondrial bioenergetics through redox signals and S-glutathionylation. Indeed, one intriguing study by Campbell *et al* showed that mitochondrial redox signals through S-glutathionylation are integral for muscle physiology and deregulation of these pathways is linked to sarcopenia, an age-related degenerative muscle disorder which is characterized by dysfunctional bioenergetics (219). Additionally, Kramer *et al* found that mitochondrial S-glutathionylation reactions are vital in the adaption of muscle towards exercise (61). Taken together, mitochondrial S-glutathionylation reactions for the control of fuel metabolism are integral for normal muscle physiology and manipulation of these pathways may serve as a new means for promoting weight loss.

4.3 Measurement and identification of mitochondrial sources of ROS

4.3.1 Pyruvate driven ROS production in skeletal muscle mitochondria.

Previous work with *Grx2*$^{-/-}$ mice demonstrated elevated ROS production in mitochondria isolated from liver but not skeletal muscle when compared to WT littermates (99). This observation was reversed with the addition of dithiothreitol. However, measurement of ROS production by mitochondria in this particular study was done using dihydrodichlorofluorescein diacetate, which is now known to be a non-specific fluorescent probe for the measurement of cell free radicals (220). Additionally, dichlorofluoresceins do not detect hydrogen peroxide. To avoid this pitfall in the present study, we used Amplex UltraRed to measure the rate of hydrogen peroxide production by skeletal muscle mitochondria isolated from WT and *Grx2*$^{+/-}$ mice fed either a HFD or CD. In this study, mitochondria isolated from *Grx2*$^{+/-}$ mice only demonstrated elevated levels of ROS production when mice were challenged with a HFD. This is consistent with past research demonstrating that increased fatty acid availability can lead to increased $O_2^{\bullet-}$ production.

Mitochondria are quantifiably the most important sources of ROS in most mammalian cells (221). Although ROS are dangerous to cells at high levels, short bursts in H_2O_2 production by mitochondria fulfill important cell signaling functions. Indeed, ROS are important for normal muscle physiology, a characteristic that is underscored by the fact that myocytes rely on multiple H_2O_2 in and outside of mitochondria for adaptation and contraction. For instance, it was recently found that bursts in ROS release from mitochondria play an integral role in muscle repair following injury (222). In skeletal muscle in particular, mitochondrial ROS and S-glutathionylation reactions are necessary for normal muscle force production (61, 127). Additionally, H_2O_2 has been shown to be vital for adaptation to exercise which includes bolstering antioxidant defenses and inducing muscle growth and myocyte proliferation (216). In this study, we found that mitochondria from *Grx2*$^{+/-}$ mice fed a high-fat diet emit more ROS in comparison to WT mice treated with either diet. Although speculative at this point, it may be that the manipulation of mitochondrial redox signals may serve as an "exercise mimetic" through the promotion of increased ROS production. This type of response would demand that skeletal muscle bolster antioxidant defenses to help buffer the increase in mitochondrial ROS release. In the present study, we did find that when fed a HFD, *Grx2*$^{+/-}$ mice likely demonstrated augmentation of the biosynthesis of GSH which increases the GSH/GSSG. This indicates that decreasing the Grx2 avaialability may activate the NRF2 signaling cascade to increase the expression of antioxidant genes. Indeed, recent work has found that manipulating mitochondrial glutathione buffering systems leads to the stabilization of NRF2 and the induction of antioxidant defense gene expression through increased ROS production (223). Furthermore, Campbell *et al* recently demonstrated that preservation of mitochondrial redox signals in the muscles of aged mice facilitates mitochondria-to-cell communication for the maintenance of muscle contractility (219). Furthermore, manipulation of the redox state of

glutathione pools protects rodents from diet-induced obesity (224). Taken together, we propose that manipulating mitochondrial redox environments and altering protein S-glutathionylation patterns may serve as a means of promoting an exercise effect in muscles, which could potentially be exploited for the prevention or reversal of weight gain.

One critical issue that needs to be addressed is our contradictory observation that mitochondria from Grx2 haploinsufficient mice produce more ROS but also have a higher rate of non-phosphorylating respiration (e.g. proton leaks). An increase in proton leaks is often viewed as a countermeasure towards increased ROS production. For instance, an increase in leaks diminishes protonic back pressure on the respiratory chain augmenting electron flow through the chain which in turn diminishes the number of electrons available for ROS production (99). Numerous studies have demonstrated that leaks are integral for diminishing ROS release from the electron transport chain (90, 136, 146, 225, 226). However, the relationship between mitochondria and ROS production is far more complicated and is not simply a "tug-of-war" between protonic pressure and the rate of electron flow through the ETC. For instance, mitochondria contain 16 ROS sources, 12 of which are associated with nutrient metabolism and respiration (227–229). Secondly, these individual sites of production are subjected to heavy regulation by allosteric modulators and covalent modifications, which can alter the rate of production. The rate of production also depends on substrate availability, type, and the concentration of the electron donor (e.g. the amount of enzyme) (112). Increased fuel metabolism has also been linked to higher rates of ROS production in muscle (230). Finally, it is now accepted that protonmotive force may not be a major determinant for dictating ROS production. This concept is underscored by the fact that activation of UCP1 leads to increased ROS production (231). Indeed, leaders in the field have indicated that a direct relationship between mitochondrial ROS and membrane potential is not as simple as it seems

(227). Therefore, it is likely that the increase in ROS production is related to the augmentation in fuel oxidation in response to feeding mice a high fat diet.

In the present study, we also examined which ROS source associated with fuel metabolism made the largest contribution to overall production. Here, we examined the rate of ROS production by PDH and OGDH and complexes I-III, which our group and others had previously identified as major sources in liver, muscle, and heart tissue (66, 68–70). First, using pyruvate and malate as substrates, we found that complex I was a major source of ROS. This is attributed to the observation that myxothiazol, which inhibits ROS production by complex III, augmented the rate of H_2O_2 production. We attribute this effect to the accumulation of electrons upstream from complex III. Secondly, atpenin A5 elicited a similar effect, increasing ROS production. Together, these findings indicate that complex I is a major site of production. We also observed that KMV, an inhibitor for ROS production by OGDH, also increased the rate of production, although in some cases the augmentation was not significant relative to the control. This indicates that complex I and to a lesser extent PDH are major sources of ROS in muscle mitochondria. These observations are in line with several studies that have found PDH and complex I are critical mitochondrial ROS sources. For instance, Fisher-Wellman *et al* demonstrated that PDH is a critical ROS supplier in mouse, rat, and human muscle tissue (232). Furthermore, several other studies have provided evidence that PDH and complex I are also major sources (68–70, 151).

It has also been shown by Goncalves *et al.* that mitochondria from muscle can adopt a diverse ROS release profile in response to changes in substrate type and supply (227). For instance, the major sites of production in muscles oxidizing succinate are complexes I-III whereas when glutamate and malate are substrates, other sources, such as OGDH, are critical ROS generators (229). Here, in mitochondria oxidizing succinate, we found that complex II was the major ROS

source. This was made clear due to the atpenin A5 effect, which inhibits complex II by competitively blocking the UQ binding site. Indeed, treating mitochondria with atpenin A5 induced a robust increase in ROS production. By contrast, rotenone had little effect indicating the source of ROS was generated by complex I due to reverse electron flow from succinate. Myxothiazol also elevated ROS production, indicating that the source was upstream from complex III and was most likely complex II.

Finally, we tested which respiratory complex served as the major source of production when palmitoyl-carnitine was the substrate. Treating mitochondria with rotenone and atpenin A5 elicited no change in ROS production, indicating reverse flow to complexes I and II were not sources during fatty acid oxidation. This is surprising since a study conducted by Perevoshchikova *et al.* found that both complexes I and II were potent sources in permeabilized rat mitochondria oxidizing palmitate (233). However, we did find that treatment with myxothiazol induced an increase in ROS production. This is intriguing since it would suggest that complex III is not a major source during fat oxidation either. Based on this evidence, ETFQO is the major ROS generator in mouse muscle mitochondria oxidizing palmitate. It is worthwhile to note that our group has observed that there is a strong strain effect for which ROS generating sites make major contributions to overall production in mitochondria (234). For example, in C57BL6N mice, OGDH, PDH, and complex II are important sources in liver mitochondria whereas in the 6J strain branched chain keto acid dehydrogenase is a major generator (234). This concept of a strain effect on rates of production from different enzymes may also apply to what organism is being used to study ROS genesis. For example, most of the studies dedicated to measuring the rate of ROS production from the 12 different sites associated with nutrient metabolism have been conducted using Sprague-Dawley rats (229). In these studies, ETFQO was characterized as a minor site.

However, our group has found that ETFQO is a critical source in mouse mitochondria from male and female mice (this study and unpublished work in a separate study). Taken together, this would indicate that sites of production need to be carefully considered when studying ROS release profiles in different model systems for human diseases.

4.4 Conclusion and future directions

Here we have demonstrated that S-glutathionylation reactions have a major role in the modulation of fat metabolism and ROS release in skeletal muscle mitochondria. haploinsufficiency in Grx2 granted protection from diet-induced weight gain and associated disorders including insulin resistance and fatty liver disease. These advantages stemmed from dysregulation of S-glutathionylation reactions leading to three main modifications of normal mitochondrial function. This included 1) increased fuel metabolism associated with dysregulation of enzymes and complexes of the ETC and Krebs cycle, 2) constitutive glutathionylation of UCP3 leading to increased state 4 respiration and energy expenditure and 3) increased ROS production and redox buffering capacity initiating stress signaling pathways that amplify fatty acid metabolism and protect from metabolic gridlock. These findings introduce a new avenue for treating and preventing DIO through manipulation of redox signaling in skeletal muscle. However, further investigation is required before pharmacotherapeutic strategies can be explored. Future directions currently involve investigating skeletal muscle, liver and cardiac mitochondria isolated from *Grx2*$^{+/-}$ mice challenged with a HFD. Comparisons will be made to the WT mice on CD and HFD to investigate the effect of this challenge on liver and cardiac mitochondria in addition to investigation of the possibility of sexual dimorphism in mitochondrial regulation by Grx2.

References:

1. Nelson, D. L. (David L., Cox, M. M., and Lehninger, A. L. (2008) *Lehninger principles of biochemistry*, 5th ed, W.H. Freeman and Company, New York
2. Nicholls, D. G., and Ferguson, S. G. (2014) *Bioenergetics*, 4th ed, Academic Press, San Diego
3. Li, X.-B., Gu, J.-D., and Zhou, Q.-H. (2015) Review of aerobic glycolysis and its key enzymes - new targets for lung cancer therapy. *Thorac. cancer*. **6**, 17–24
4. Chaudhry, R., and Bhimji, S. S. (2018) *Biochemistry, Carbohydrate, Glycolysis*, StatPearls Publishing, [online] http://www.ncbi.nlm.nih.gov/pubmed/29493928 (Accessed September 6, 2018)
5. Krebs, H. A. (1940) The citric acid cycle: A reply to the criticisms of F. L. Breusch and of J. Thomas. *Biochem. J.* **34**, 460–3
6. Patel, M. S., Nemeria, N. S., Furey, W., and Jordan, F. (2014) The pyruvate dehydrogenase complexes: structure-based function and regulation. *J. Biol. Chem.* **289**, 16615–23
7. Kil, I. S., and Park, J.-W. (2005) Regulation of mitochondrial NADP+-dependent isocitrate dehydrogenase activity by glutathionylation. *J. Biol. Chem.* **280**, 10846–54
8. Mailloux, R. J., Gardiner, D., O'Brien, M., and O'Brien, M. (2016) 2-Oxoglutarate dehydrogenase is a more signincant source of $O_2^{\bullet-}$ /H_2O_2 than pyruvate dehydrogenase in cardiac and liver tissue. *Free Radic. Biol. Med.* **97**, 501–512
9. Messner, K. R., and Imlay, J. A. (2002) Mechanism of superoxide and hydrogen peroxide formation by fumarate reductase, succinate dehydrogenase, and aspartate oxidase. *J. Biol. Chem.* **277**, 42563–71
10. Sherwood, L., and Kell, R. T. (2009) *Human physiology : from cells to systems*, Nelson Education
11. Chideckel, E. W., Goodner, C. J., Koerker, D. J., Johnson, D. G., and Ensinck, J. W. (1977) Role of glucagon in mediating metabolic effects of epinephrine. *Am. J. Physiol. Metab.* **232**, E464
12. Green, C. R., Wallace, M., Divakaruni, A. S., Phillips, S. A., Murphy, A. N., Ciaraldi, T. P., and Metallo, C. M. (2016) Branched-chain amino acid catabolism fuels adipocyte differentiation and lipogenesis. *Nat. Chem. Biol.* **12**, 15–21
13. Carta, G., Murru, E., Banni, S., and Manca, C. (2017) Palmitic Acid: Physiological Role, Metabolism and Nutritional Implications. *Front. Physiol.* **8**, 902
14. Cases, S., Smith, S. J., Zheng, Y. W., Myers, H. M., Lear, S. R., Sande, E., Novak, S., Collins, C., Welch, C. B., Lusis, A. J., Erickson, S. K., and Farese, R. V (1998) Identification of a gene encoding an acyl CoA:diacylglycerol acyltransferase, a key enzyme in triacylglycerol synthesis. *Proc. Natl. Acad. Sci. U. S. A.* **95**, 13018–23
15. Jogl, G., Hsiao, Y.-S., and Tong, L. (2004) Structure and Function of Carnitine Acyltransferases. *Ann. N. Y. Acad. Sci.* **1033**, 17–29
16. Indiveri, C., Iacobazzi, V., Tonazzi, A., Giangregorio, N., Infantino, V., Convertini, P., Console, L., and Palmieri, F. (2011) The mitochondrial carnitine/acylcarnitine carrier: Function, structure and physiopathology. *Mol. Aspects Med.* **32**, 223–233
17. Swigonová, Z., Mohsen, A.-W., and Vockley, J. (2009) Acyl-CoA dehydrogenases: Dynamic history of protein family evolution. *J. Mol. Evol.* **69**, 176–93
18. Bogdawa, H., Delessert, S., and Poirier, Y. (2005) Analysis of the contribution of the β-

oxidation auxiliary enzymes in the degradation of the dietary conjugated linoleic acid 9-cis-11-trans-octadecadienoic acid in the peroxisomes of *Saccharomyces cerevisiae*. *Biochim. Biophys. Acta - Mol. Cell Biol. Lipids*. **1735**, 204–213
19. Watmough, N. J., and Frerman, F. E. The electron transfer flavoprotein: Ubiquinone oxidoreductases. *Biochim. Biophys. Acta - Bioenerg.* **1797**, 1910–1916
20. Mohamad Fairus, A. K., Choudhary, B., Hosahalli, S., Kavitha, N., and Shatrah, O. (2017) Dihydroorotate dehydrogenase (DHODH) inhibitors affect ATP depletion, endogenous ROS and mediate S-phase arrest in breast cancer cells. *Biochimie*. **135**, 154–163
21. Ramzan, R., Weber, P., Linne, U., and Vogt, S. (2013) GAPDH: the missing link between glycolysis and mitochondrial oxidative phosphorylation? *Biochem. Soc. Trans.* **41**, 1294–1297
22. Scialò, F., Fernández-Ayala, D. J., and Sanz, A. (2017) Role of mitochondrial reverse electron transport in ROS signaling: potential roles in health and disease. *Front. Physiol.* **8**, 428
23. Mitchell, P. (1975) The protonmotive Q cycle: a general formulation. *FEBS Lett.* **59**, 137–9
24. Iwata, S., Lee, J. W., Okada, K., Lee, J. K., Iwata, M., Rasmussen, B., Link, T. A., Ramaswamy, S., and Jap, B. K. (1998) Complete structure of the 11-subunit bovine mitochondrial cytochrome bc1 complex. *Science*. **281**, 64–71
25. Ow, Y.-L. P., Green, D. R., Hao, Z., and Mak, T. W. (2008) Cytochrome c: functions beyond respiration. *Nat. Rev. Mol. Cell Biol.* **9**, 532–542
26. Li, Y., Park, J.-S., Deng, J.-H., and Bai, Y. (2006) Cytochrome c oxidase subunit IV is essential for assembly and respiratory function of the enzyme complex. *J. Bioenerg. Biomembr.* **38**, 283–91
27. Hammes-Schiffer, S., and Stuchebrukhov, A. A. (2010) Theory of coupled electron and proton transfer reactions. *Chem. Rev.* **110**, 6939–60
28. Perry, S. W., Norman, J. P., Barbieri, J., Brown, E. B., and Gelbard, H. A. (2011) Mitochondrial membrane potential probes and the proton gradient: a practical usage guide. *Biotechniques*. **50**, 98–115
29. Mitchell, P., and Moyle, J. (1969) Estimation of membrane potential and pH difference across the cristae membrane of rat liver mitochondria. *Eur. J. Biochem.* **7**, 471–84
30. McCommis, K. S., and Finck, B. N. (2015) Mitochondrial pyruvate transport: a historical perspective and future research directions. *Biochem. J.* **466**, 443–54
31. Ho, H.-Y., Lin, Y.-T., Lin, G., Wu, P.-R., and Cheng, M.-L. (2017) Nicotinamide nucleotide transhydrogenase (NNT) deficiency dysregulates mitochondrial retrograde signaling and impedes proliferation. *Redox Biol.* **12**, 916–928
32. Stuart, J. A., Brindle, K. M., Harper, J. A., and Brand, M. D. (1999) Mitochondrial proton leak and the uncoupling proteins. *J. Bioenerg. Biomembr.* **31**, 517–25
33. Mailloux, R. J. (2018) Mitochondrial antioxidants and the maintenance of cellular hydrogen peroxide levels. *Oxid. Med. Cell. Longev.* **2018**, 7857251
34. Ferguson, S. J. (2010) ATP synthase: from sequence to ring size to the P/O ratio. *Proc. Natl. Acad. Sci. U. S. A.* **107**, 16755–6
35. Nesci, S., Trombetti, F., Ventrella, V., and Pagliarani, A. (2016) The c-Ring of the F_1F_O-ATP Synthase: Facts and Perspectives. *J. Membr. Biol.* **249**, 11–21
36. Fillingame, R. H., Angevine, C. M., and Dmitriev, O. Y. (2002) Coupling proton movements to c-ring rotation in F_1F_o ATP synthase: aqueous access channels and helix

rotations at the a–c interface. *Biochim. Biophys. Acta - Bioenerg.* **1555**, 29–36
37. Wittig, I., and Schägger, H. (2008) Structural organization of mitochondrial ATP synthase. *Biochim. Biophys. Acta - Bioenerg.* **1777**, 592–598
38. Liu, S., Charlesworth, T. J., Bason, J. V, Montgomery, M. G., Harbour, M. E., Fearnley, I. M., and Walker, J. E. (2015) The purification and characterization of ATP synthase complexes from the mitochondria of four fungal species. *Biochem. J.* **468**, 167–75
39. Nakamoto, R. K., Baylis Scanlon, J. A., and Al-Shawi, M. K. (2008) The rotary mechanism of the ATP synthase. *Arch. Biochem. Biophys.* **476**, 43–50
40. Murphy, M. P. (2009) How mitochondria produce reactive oxygen species. *Biochem. J.* **417**, 1–13
41. Mailloux, R. J., McBride, S. L., and Harper, M.-E. (2013) Unearthing the secrets of mitochondrial ROS and glutathione in bioenergetics. *Trends Biochem. Sci.* **38**, 592–602
42. Mailloux, R. J., Jin, X., and Willmore, W. G. (2014) Redox regulation of mitochondrial function with emphasis on cysteine oxidation reactions. *Redox Biol.* **2**, 123–39
43. Starkov, A. A., Fiskum, G., Chinopoulos, C., Lorenzo, B. J., Browne, S. E., Patel, M. S., and Beal, M. F. (2004) Mitochondrial α-ketoglutarate dehydrogenase complex generates reactive oxygen species. *J. Neurosci.* **24**, 7779–7788
44. Zhang, J., Ye, Z., Singh, S., Townsend, D. M., and Tew, K. D. (2018) An evolving understanding of the S-glutathionylation cycle in pathways of redox regulation. *Free Radic. Biol. Med.* **120**, 204–216
45. Kuksal, N., Chalker, J., and Mailloux, R. J. (2017) Progress in understanding the molecular oxygen paradox – function of mitochondrial reactive oxygen species in cell signaling. *Biol. Chem.* **398**, 1209–1227
46. Watts, R. J., Washington, D., Howsawkeng, J., Loge, F. J., and Teel, A. L. (2003) Comparative toxicity of hydrogen peroxide, hydroxyl radicals, and superoxide anion to Escherichia coli. *Adv. Environ. Res.* **7**, 961–968
47. Buechter, D. D. (1988) Free radicals and oxygen toxicity. *Pharm. Res.* **5**, 253–60
48. Esterbauer, H., Schaur, R. J., and Zollner, H. (1991) Chemistry and biochemistry of 4-hydroxynonenal, malonaldehyde and related aldehydes. *Free Radic. Biol. Med.* **11**, 81–128
49. Kohen, R., Yamamoto, Y., Cundy, K. C., and Ames, B. N. (1988) Antioxidant activity of carnosine, homocarnosine, and anserine present in muscle and brain. *Proc. Natl. Acad. Sci.* **85**, 3175–3179
50. Heffern, C. T. R., Pocivavsek, L., Birukova, A. A., Moldobaeva, N., Bochkov, V. N., Lee, K. Y. C., and Birukov, K. G. (2013) Thermodynamic and kinetic investigations of the release of oxidized phospholipids from lipid membranes and its effect on vascular integrity. *Chem. Phys. Lipids*. **175**–**176**, 9–19
51. Catalá, A., and Díaz, M. (2016) Editorial: Impact of lipid peroxidation on the physiology and pathophysiology of cell membranes. *Front. Physiol.* **7**, 423
52. Moini, H., Packer, L., and Saris, N.-E. L. (2002) Antioxidant and Prooxidant Activities of α-Lipoic Acid and Dihydrolipoic Acid. *Toxicol. Appl. Pharmacol.* **182**, 84–90
53. Derick Han, ‡, Raffaella Canali, §, Jerome Garcia, ⦀, Rodrigo Aguilera, ⦀, Timothy K. Gallaher, ⦀ and, and Enrique Cadenas*, ⦀ (2005) Sites and mechanisms of aconitase inactivation by peroxynitrite: modulation by citrate and glutathione†. 10.1021/BI0509393
54. Cadenas, E. (2004) Mitochondrial free radical production and cell signaling. *Mol. Aspects Med.* **25**, 17–26

55. Radi, R. (2013) Peroxynitrite, a stealthy biological oxidant. *J. Biol. Chem.* **288**, 26464–72
56. Niki, E. (2016) Oxidative stress and antioxidants: Distress or eustress ? *Arch. Biochem. Biophys.* **595**, 19–24
57. Diebold, L., and Chandel, N. S. (2016) Mitochondrial ROS regulation of proliferating cells. *Free Radic. Biol. Med.* **100**, 86–93
58. Shadel, G. S., and Horvath, T. L. (2015) Mitochondrial ROS signaling in organismal homeostasis. *Cell*. **163**, 560–569
59. Katz, A. (2007) Modulation of glucose transport in skeletal muscle by reactive oxygen species. *J. Appl. Physiol.* **102**, 1671–1676
60. Latres, E., Amini, A. R., Amini, A. A., Griffiths, J., Martin, F. J., Wei, Y., Lin, H. C., Yancopoulos, G. D., and Glass, D. J. (2005) Insulin-like growth factor-1 (IGF-1) inversely regulates atrophy-induced genes via the Phosphatidylinositol 3-kinase/Akt/mammalian target of rapamycin (PI3K/Akt/mTOR) pathway. *J. Biol. Chem.* **280**, 2737–2744
61. Kramer, P. A., Duan, J., Gaffrey, M. J., Shukla, A. K., Wang, L., Bammler, T. K., Qian, W.-J., and Marcinek, D. J. (2018) Fatiguing contractions increase protein S-glutathionylation occupancy in mouse skeletal muscle. *Redox Biol.* **17**, 367–376
62. Leloup, C., Tourrel-Cuzin, C., Magnan, C., Karaca, M., Castel, J., Carneiro, L., Colombani, A.-L., Ktorza, A., Casteilla, L., and Penicaud, L. (2009) Mitochondrial reactive oxygen species are obligatory signals for glucose-induced insulin secretion. *Diabetes*. **58**, 673–681
63. Brand, M. D. (2016) Mitochondrial generation of superoxide and hydrogen peroxide as the source of mitochondrial redox signaling. *Free Radic. Biol. Med.* **100**, 14–31
64. Hirst, J., King, M. S., and Pryde, K. R. (2008) The production of reactive oxygen species by complex I. *Biochem. Soc. Trans.* **36**, 976–980
65. Bleier, L., and Dröse, S. (2013) Superoxide generation by complex III: From mechanistic rationales to functional consequences. *Biochim. Biophys. Acta - Bioenerg.* **1827**, 1320–1331
66. Kuksal, N., Gardiner, D., Qi, D., and Mailloux, R. J. (2018) Partial loss of complex I due to NDUFS4 deficiency augments myocardial reperfusion damage by increasing mitochondrial superoxide/hydrogen peroxide production. *Biochem. Biophys. Res. Commun.* **498**, 214–220
67. Quinlan, C. L., Goncalves, R. L. S., Hey-Mogensen, M., Yadava, N., Bunik, V. I., and Brand, M. D. (2014) The 2-oxoacid dehydrogenase complexes in mitochondria can produce superoxide/hydrogen peroxide at much higher rates than complex I. *J. Biol. Chem.* **289**, 8312–25
68. O'Brien, M., Chalker, J., Slade, L., Gardiner, D., Mailloux, R. J., O'Brien, M., Chalker, J., Slade, L., Gardiner, D., and Mailloux, R. J. (2017) Protein S-glutathionylation alters superoxide/hydrogen peroxide emission from pyruvate dehydrogenase complex. *Free Radic. Biol. Med.* **106**, 302–314
69. Slade, L., Chalker, J., Kuksal, N., Young, A., Gardiner, D., and Mailloux, R. J. (2017) Examination of the superoxide/hydrogen peroxide forming and quenching potential of mouse liver mitochondria. *Biochim. Biophys. Acta - Gen. Subj.* **1861**, 1960–1969
70. Chalker, J., Gardiner, D., Kuksal, N., and Mailloux, R. J. (2018) Characterization of the impact of glutaredoxin-2 (GRX2) deficiency on superoxide/hydrogen peroxide release from cardiac and liver mitochondria. *Redox Biol.* **15**, 216–227
71. Kanter, M. (1998) Free radicals, exercise and antioxidant supplementation. *Proc. Nutr.*

Soc. **57**, 9–13
72. Cardinale, D. A., Larsen, F. J., Schiffer, T. A., Morales-Alamo, D., Ekblom, B., Calbet, J. A. L., Holmberg, H.-C., and Boushel, R. (2018) Superior intrinsic mitochondrial respiration in women than in men. *Front. Physiol.* **9**, 1133
73. Zhou, Z., and Kang, Y. J. (2000) Cellular and subcellular localization of catalase in the heart of transgenic mice. *J. Histochem. Cytochem.* **48**, 585–594
74. Salvi, M., Battaglia, V., Brunati, A. M., La Rocca, N., Tibaldi, E., Pietrangeli, P., Marcocci, L., Mondovì, B., Rossi, C. A., and Toninello, A. (2007) Catalase takes part in rat liver mitochondria oxidative stress defense. *J. Biol. Chem.* **282**, 24407–24415
75. Radi, R., Turrens, J. F., Chang, L. Y., Bush, K. M., Crapo, J. D., and Freeman, B. A. (1991) Detection of catalase in rat heart mitochondria. *J. Biol. Chem.* **266**, 22028–34
76. Heck, D. E., Shakarjian, M., Kim, H. D., Laskin, J. D., and Vetrano, A. M. (2010) Mechanisms of oxidant generation by catalase. *Ann. N. Y. Acad. Sci.* **1203**, 120–5
77. Vergauwen, B., Pauwels, F., and Van Beeumen, J. J. (2003) Glutathione and catalase provide overlapping defenses for protection against respiration-generated hydrogen peroxide in Haemophilus influenzae. *J. Bacteriol.* **185**, 5555–62
78. Rhee, S. G., Kang, S. W., Chang, T. S., Jeong, W., and Kim, K. (2001) Peroxiredoxin, a novel family of peroxidases. *IUBMB Life*. **52**, 35–41
79. Netto, L. E. S., and Antunes, F. (2016) The roles of peroxiredoxin and thioredoxin in hydrogen peroxide sensing and in signal transduction. *Mol. Cells*. **39**, 65–71
80. Brechbuhl, H. M., Gould, N., Kachadourian, R., Riekhof, W. R., Voelker, D. R., and Day, B. J. (2010) Glutathione transport is a unique function of the ATP-binding cassette protein ABCG2. *J. Biol. Chem.* **285**, 16582–7
81. Fernández-Checa, J. C., Kaplowitz, N., García-Ruiz, C., and Colell, A. (1998) Mitochondrial glutathione: importance and transport. *Semin. Liver Dis.* **18**, 389–401
82. Murphy, M. P. (2012) Mitochondrial thiols in antioxidant protection and redox signaling: distinct roles for glutathionylation and other thiol modifications. *Antioxid. Redox Signal.* **16**, 476–495
83. Parker, N., Affourtit, C., Vidal-Puig, A., and Brand, M. D. (2008) Energization-dependent endogenous activation of proton conductance in skeletal muscle mitochondria. *Biochem. J.* **412**, 131–9
84. Korshunov, S. S., Skulachev, V. P., and Starkov, A. A. (1997) High protonic potential actuates a mechanism of production of reactive oxygen species in mitochondria. *FEBS Lett.* **416**, 15–8
85. Jastroch, M., Divakaruni, A. S., Mookerjee, S., Treberg, J. R., and Brand, M. D. (2010) Mitochondrial proton and electron leaks. *Essays Biochem.* **47**, 53–67
86. Chinopoulos, C., Gerencser, A. A., Mandi, M., Mathe, K., Töröcsik, B., Doczi, J., Turiak, L., Kiss, G., Konràd, C., Vajda, S., Vereczki, V., Oh, R. J., and Adam-Vizi, V. (2010) Forward operation of adenine nucleotide translocase during F0F1-ATPase reversal: critical role of matrix substrate-level phosphorylation. *FASEB J.* **24**, 2405–16
87. Brand, M. D., and Esteves, T. C. (2005) Physiological functions of the mitochondrial uncoupling proteins UCP2 and UCP3. *Cell Metab.* **2**, 85–93
88. Kwong, J. Q., and Molkentin, J. D. (2015) Physiological and pathological roles of the mitochondrial permeability transition pore in the heart. *Cell Metab.* **21**, 206–214
89. Azzu, V., and Brand, M. D. (2010) The on-off switches of the mitochondrial uncoupling proteins. *Trends Biochem. Sci.* **35**, 298–307

90. Echtay, K. S., Roussel, D., St-Pierre, J., Jekabsons, M. B., Cadenas, S., Stuart, J. A., Harper, J. A., Roebuck, S. J., Morrison, A., Pickering, S., Clapham, J. C., and Brand, M. D. (2002) Superoxide activates mitochondrial uncoupling proteins. *Nature*. **415**, 96–99
91. Echtay, K. S., Esteves, T. C., Pakay, J. L., Jekabsons, M. B., Lambert, A. J., Portero-Otín, M., Pamplona, R., Vidal-Puig, A. J., Wang, S., Roebuck, S. J., and Brand, M. D. (2003) A signalling role for 4-hydroxy-2-nonenal in regulation of mitochondrial uncoupling. *EMBO J.* **22**, 4103–10
92. Chouchani, E. T., Methner, C., Nadtochiy, S. M., Logan, A., Pell, V. R., Ding, S., James, A. M., Cochemé, H. M., Reinhold, J., Lilley, K. S., Partridge, L., Fearnley, I. M., Robinson, A. J., Hartley, R. C., Smith, R. A. J., Krieg, T., Brookes, P. S., and Murphy, M. P. (2013) Cardioprotection by S-nitrosylation of a cysteine switch on mitochondrial complex I. *Nat. Med.* **19**, 753–759
93. Mailloux, R. J., Dumouchel, T., Aguer, C., deKemp, R., Beanlands, R., and Harper, M.-E. (2011) Hexokinase II acts through UCP3 to suppress mitochondrial reactive oxygen species production and maintain aerobic respiration. *Biochem. J.* **437**, 301–311
94. Chan, C. B., MacDonald, P. E., Saleh, M. C., Johns, D. C., Marbàn, E., and Wheeler, M. B. (1999) Overexpression of uncoupling protein 2 inhibits glucose-stimulated insulin secretion from rat islets. *Diabetes*. **48**, 1482–6
95. Arsenijevic, D., Onuma, H., Pecqueur, C., Raimbault, S., Manning, B. S., Miroux, B., Couplan, E., Alves-Guerra, M.-C., Goubern, M., Surwit, R., Bouillaud, F., Richard, D., Collins, S., and Ricquier, D. (2000) Disruption of the uncoupling protein-2 gene in mice reveals a role in immunity and reactive oxygen species production. *Nat. Genet.* **26**, 435–439
96. Bechmann, I., Diano, S., Warden, C. H., Bartfai, T., Nitsch, R., and Horvath, T. L. (2002) Brain mitochondrial uncoupling protein 2 (UCP2): a protective stress signal in neuronal injury. *Biochem. Pharmacol.* **64**, 363–7
97. Teshima, Y., Akao, M., Jones, S. P., and Marbán, E. (2003) Uncoupling protein-2 overexpression inhibits mitochondrial death pathway in cardiomyocytes. *Circ. Res.* **93**, 192–200
98. Clapham, J. C., Arch, J. R. S., Chapman, H., Haynes, A., Lister, C., Moore, G. B. T., Piercy, V., Carter, S. A., Lehner, I., Smith, S. A., Beeley, L. J., Godden, R. J., Herrity, N., Skehel, M., Changani, K. K., Hockings, P. D., Reid, D. G., Squires, S. M., Hatcher, J., Trail, B., Latcham, J., Rastan, S., Harper, A. J., Cadenas, S., Buckingham, J. A., Brand, M. D., and Abuin, A. (2000) Mice overexpressing human uncoupling protein-3 in skeletal muscle are hyperphagic and lean. *Nature*. **406**, 415–418
99. Mailloux, R. J., Xuan, J. Y., Beauchamp, B., Jui, L., Lou, M., and Harper, M.-E. M.-E. (2013) Glutaredoxin-2 Is required to control proton leak through uncoupling protein-3. *J. Biol. Chem.* **288**, 8365–8379
100. Stamler, J. S., Simon, D. I., Osborne, J. A., Mullins, M. E., Jaraki, O., Michel, T., Singel, D. J., and Loscalzo, J. (1992) S-nitrosylation of proteins with nitric oxide: synthesis and characterization of biologically active compounds. *Proc. Natl. Acad. Sci. U. S. A.* **89**, 444–8
101. Kulandavelu, S., Balkan, W., and Hare, J. M. (2015) Regulation of oxygen delivery to the body via hypoxic vasodilation. *Proc. Natl. Acad. Sci. U. S. A.* **112**, 6254–5
102. Piantadosi, C. A. (2012) Regulation of mitochondrial processes by protein S-nitrosylation. *Biochim. Biophys. Acta - Gen. Subj.* **1820**, 712–721

103. Brown, G. C. (2001) Regulation of mitochondrial respiration by nitric oxide inhibition of cytochrome c oxidase. *Biochim. Biophys. Acta - Bioenerg.* **1504**, 46–57
104. Mitchell, D. A., Morton, S. U., Fernhoff, N. B., and Marletta, M. A. (2007) Thioredoxin is required for S-nitrosation of procaspase-3 and the inhibition of apoptosis in Jurkat cells. *Proc. Natl. Acad. Sci. U. S. A.* **104**, 11609–14
105. Rhee, S. G., and Kil, I. S. (2016) Mitochondrial H2O2 signaling is controlled by the concerted action of peroxiredoxin III and sulfiredoxin: Linking mitochondrial function to circadian rhythm. *Free Radic. Biol. Med.* **100**, 73–80
106. Gallogly, M. M., and Mieyal, J. J. (2007) Mechanisms of reversible protein glutathionylation in redox signaling and oxidative stress. *Curr. Opin. Pharmacol.* **7**, 381–391
107. Klatt, P., Molina, E. P., De Lacoba, M. G., Padilla, C. A., Martinez-Galesteo, E., Barcena, J. A., and Lamas, S. (1999) Redox regulation of c-Jun DNA binding by reversible S-glutathiolation. *FASEB J.* **13**, 1481–90
108. Klaus, A., Zorman, S., Berthier, A., Polge, C., Ramirez, S., Michelland, S., Sève, M., Vertommen, D., Rider, M., Lentze, N., Auerbach, D., and Schlattner, U. (2013) Glutathione S-transferases interact with AMP-activated protein kinase: evidence for S-glutathionylation and activation in vitro. *PLoS One*. **8**, e62497
109. Cox, A. G., Winterbourn, C. C., and Hampton, M. B. (2010) Mitochondrial peroxiredoxin involvement in antioxidant defence and redox signalling. *Biochem. J.* **425**, 313–325
110. Ströher, E., and Millar, A. H. (2012) The biological roles of glutaredoxins. *Biochem. J.* **446**, 333–48
111. Gallogly, M. M., Starke, D. W., Leonberg, A. K., Ospina, S. M. E., and Mieyal, J. J. (2008) Kinetic and mechanistic characterization and versatile catalytic properties of mammalian glutaredoxin 2: implications for intracellular roles †. *Biochemistry*. **47**, 11144–11157
112. Young, A., Gill, R., and Mailloux, R. J. R. J. (2019) Protein S-glutathionylation: The linchpin for the transmission of regulatory information on redox buffering capacity in mitochondria. *Chem. Biol. Interact.* **299**, 151–162
113. Lundberg, M., Johansson, C., Chandra, J., Enoksson, M., Jacobsson, G., Ljung, J., Johansson, M., and Holmgren, A. (2001) Cloning and expression of a novel human glutaredoxin (Grx2) with mitochondrial and nuclear isoforms. *J. Biol. Chem.* **276**, 26269–26275
114. Beer, S. M., Taylor, E. R., Brown, S. E., Dahm, C. C., Costa, N. J., Runswick, M. J., and Murphy, M. P. (2004) Glutaredoxin 2 catalyzes the reversible oxidation and glutathionylation of mitochondrial membrane thiol proteins. *J. Biol. Chem.* **279**, 47939–47951
115. Zhang, H., Du, Y., Zhang, X., Lu, J., and Holmgren, A. (2014) Glutaredoxin 2 reduces both thioredoxin 2 and thioredoxin 1 and protects cells from apoptosis induced by auranofin and 4-hydroxynonenal. *Antioxid. Redox Signal.* **21**, 669–681
116. Lönn, M. E., Hudemann, C., Berndt, C., Cherkasov, V., Capani, F., Holmgren, A., and Lillig, C. H. (2008) Expression pattern of human glutaredoxin 2 isoforms: identification and characterization of two testis/cancer cell-specific isoforms. *Antioxid. Redox Signal.* **10**, 547–558
117. Mashamaite, L. N., Rohwer, J. M., and Pillay, C. S. (2015) The glutaredoxin mono- and di-thiol mechanisms for deglutathionylation are functionally equivalent: implications for

redox systems biology. *Biosci. Rep.* 10.1042/BSR20140157
118. Requejo, R., Hurd, T. R., Costa, N. J., and Murphy, M. P. (2010) Cysteine residues exposed on protein surfaces are the dominant intramitochondrial thiol and may protect against oxidative damage. *FEBS J.* **277**, 1465–1480
119. Nulton-Persson, A. C., Starke, D. W., Mieyal, J. J., and Szweda, L. I. (2003) Reversible inactivation of α-ketoglutarate dehydrogenase in response to alterations in the mitochondrial glutathione status †. *Biochemistry*. **42**, 4235–4242
120. Garcia, J., Han, D., Sancheti, H., Yap, L.-P., Kaplowitz, N., and Cadenas, E. (2010) Regulation of mitochondrial glutathione redox status and protein glutathionylation by respiratory substrates. *J. Biol. Chem.* **285**, 39646–54
121. Wu, H., Yu, Y., David, L., Ho, Y.-S., and Lou, M. F. (2014) Glutaredoxin 2 (Grx2) gene deletion induces early onset of age-dependent cataracts in mice. *J. Biol. Chem.* **289**, 36125–39
122. Hurd, T. R., Requejo, R., Filipovska, A., Brown, S., Prime, T. A., Robinson, A. J., Fearnley, I. M., and Murphy, M. P. (2008) Complex I within oxidatively stressed bovine heart mitochondria is glutathionylated on Cys-531 and Cys-704 of the 75-kDa subunit. *J. Biol. Chem.* **283**, 24801–24815
123. Grivennikova, V. G., Kapustin, A. N., and Vinogradov, A. D. (2001) Catalytic activity of NADH-ubiquinone oxidoreductase (complex I) in intact mitochondria. evidence for the slow active/inactive transition. *J. Biol. Chem.* **276**, 9038–44
124. Babot, M., Birch, A., Labarbuta, P., and Galkin, A. (2014) Characterisation of the active/de-active transition of mitochondrial complex I. *Biochim. Biophys. Acta - Bioenerg.* **1837**, 1083–1092
125. Passarelli, C., Tozzi, G., Pastore, A., Bertini, E., and Piemonte, F. (2010) GSSG-mediated Complex I defect in isolated cardiac mitochondria. *Int. J. Mol. Med.* **26**, 95–9
126. Wu, H., Lin, L., Giblin, F., Ho, Y.-S., and Lou, M. F. (2011) Glutaredoxin 2 knockout increases sensitivity to oxidative stress in mouse lens epithelial cells. *Free Radic. Biol. Med.* **51**, 2108–2117
127. Gill, R. M., O'Brien, M., Young, A., Gardiner, D., and Mailloux, R. J. (2018) Protein S-glutathionylation lowers superoxide/hydrogen peroxide release from skeletal muscle mitochondria through modification of complex I and inhibition of pyruvate uptake. *PLoS One*. **13**, e0192801
128. Mailloux, R. J., and Willmore, W. G. (2014) S-glutathionylation reactions in mitochondrial function and disease. *Front. Cell Dev. Biol.* **2**, 68
129. Kumar, V., Kleffmann, T., Hampton, M. B., Cannell, M. B., and Winterbourn, C. C. (2013) Redox proteomics of thiol proteins in mouse heart during ischemia/reperfusion using ICAT reagents and mass spectrometry. *Free Radic. Biol. Med.* **58**, 109–117
130. Chen, Y.-R., Chen, C.-L., Pfeiffer, D. R., and Zweier, J. L. (2007) Mitochondrial complex II in the post-ischemic heart: oxidative injury and the role of protein S-glutathionylation. *J. Biol. Chem.* **282**, 32640–54
131. Wang, S.-B., Foster, D. B., Rucker, J., O'Rourke, B., Kass, D. A., and Van Eyk, J. E. (2011) Redox regulation of mitochondrial ATP synthase: implications for cardiac resynchronization therapy. *Circ. Res.* **109**, 750–757
132. Gergondey, R., Garcia, C., Marchand, C. H., Lemaire, S. D., Camadro, J.-M., and Auchère, F. (2017) Modulation of the specific glutathionylation of mitochondrial proteins in the yeast *Saccharomyces cerevisiae* under basal and stress conditions. *Biochem. J.* **474**,

1175–1193
133. Mailloux, R. J., Seifert, E. L., Bouillaud, F., Aguer, C., Collins, S., and Harper, M.-E. (2011) Glutathionylation acts as a control switch for uncoupling proteins UCP2 and UCP3. *J. Biol. Chem.* **286**, 21865–75
134. Pfefferle, A., Mailloux, R. J., Adjeitey, C. N.-K., and Harper, M.-E. (2013) Glutathionylation of UCP2 sensitizes drug resistant leukemia cells to chemotherapeutics. *Biochim. Biophys. Acta - Mol. Cell Res.* **1833**, 80–89
135. Mailloux, R. J., Fu, A., Robson-Doucette, C., Allister, E. M., Wheeler, M. B., Screaton, R., and Harper, M.-E. (2012) Glutathionylation state of uncoupling protein-2 and the control of glucose-stimulated insulin secretion. *J. Biol. Chem.* **287**, 39673–85
136. Mailloux, R. J., and Harper, M.-E. (2011) Uncoupling proteins and the control of mitochondrial reactive oxygen species production. *Free Radic. Biol. Med.* **51**, 1106–1115
137. Kowaltowski, A. J., Castilho, R. F., and Vercesi, A. E. (2001) Mitochondrial permeability transition and oxidative stress. *FEBS Lett.* **495**, 12–15
138. Queiroga, C. S. F., Almeida, A. S., Martel, C., Brenner, C., Alves, P. M., and Vieira, H. L. A. (2010) Glutathionylation of adenine nucleotide translocase induced by carbon monoxide prevents mitochondrial membrane permeabilization and apoptosis. *J. Biol. Chem.* **285**, 17077–88
139. Itani, H. A., Dikalova, A. E., McMaster, W. G., Nazarewicz, R. R., Bikineyeva, A. T., Harrison, D. G., and Dikalov, S. I. (2016) Mitochondrial cyclophilin D in vascular oxidative stress and hypertension. *Hypertension*. **67**, 1218–1227
140. Giangregorio, N., Palmieri, F., and Indiveri, C. (2013) Glutathione controls the redox state of the mitochondrial carnitine/acylcarnitine carrier Cys residues by glutathionylation. *Biochim. Biophys. Acta - Gen. Subj.* **1830**, 5299–5304
141. Liesa, M., and Shirihai, O. S. (2013) Mitochondrial dynamics in the regulation of nutrient utilization and energy expenditure. *Cell Metab.* **17**, 491–506
142. Willems, P. H. G. M., Rossignol, R., Dieteren, C. E. J., Murphy, M. P., and Koopman, W. J. H. (2015) Redox homeostasis and mitochondrial dynamics. *Cell Metab.* **22**, 207–218
143. Shutt, T., Geoffrion, M., Milne, R., and McBride, H. M. (2012) The intracellular redox state is a core determinant of mitochondrial fusion. *EMBO Rep.* **13**, 909–915
144. Thaher, O., Wolf, C., Dey, P. N., Pouya, A., Wüllner, V., Tenzer, S., and Methner, A. (2018) The thiol switch C684 in Mitofusin-2 mediates redox-induced alterations of mitochondrial shape and respiration. *Neurochem. Int.* **117**, 167–173
145. Jeukendrup, A. E. (2002) Regulation of fat metabolism in skeletal muscle. *Ann. N. Y. Acad. Sci.* **967**, 217–35
146. Harper, M.-E., Green, K., and Brand, M. D. (2008) The efficiency of cellular energy transduction and its implications for obesity. *Annu. Rev. Nutr.* **28**, 13–33
147. Thrush, A. B., Dent, R., McPherson, R., and Harper, M.-E. (2013) Implications of mitochondrial uncoupling in skeletal muscle in the development and treatment of obesity. *FEBS J.* **280**, 5015–5029
148. Anderson, E. J., Lustig, M. E., Boyle, K. E., Woodlief, T. L., Kane, D. A., Lin, C.-T., Price, J. W., Kang, L., Rabinovitch, P. S., Szeto, H. H., Houmard, J. A., Cortright, R. N., Wasserman, D. H., Neufer, P. D., and Neufer, P. D. (2009) Mitochondrial H_2O_2 emission and cellular redox state link excess fat intake to insulin resistance in both rodents and humans. *J. Clin. Invest.* **119**, 573–81
149. Koves, T. R., Noland, R. C., Bates, A. L., Henes, S. T., Muoio, D. M., and Cortright, R.

N. (2005) Subsarcolemmal and intermyofibrillar mitochondria play distinct roles in regulating skeletal muscle fatty acid metabolism. *Am. J. Physiol. Physiol.* **288**, C1074–C1082

150. Reid, M. B. (2001) Invited Review: Redox modulation of skeletal muscle contraction: what we know and what we don't. *J. Appl. Physiol.* **90**, 724–731
151. Mailloux, R. J., Craig Ayre, D., Christian, S. L., Ayre, C. D., and Christian, S. L. (2016) Induction of mitochondrial reactive oxygen species production by GSH mediated S-glutathionylation of 2-oxoglutarate dehydrogenase. *Redox Biol.* **8**, 285–297
152. Mailloux, R. J., Xuan, J. Y., McBride, S., Maharsy, W., Thorn, S., Holterman, C. E., Kennedy, C. R. J., Rippstein, P., DeKemp, R., da Silva, J., Nemer, M., Lou, M., and Harper, M.-E. M.-E. (2014) Glutaredoxin-2 Is required to control oxidative phosphorylation in cardiac muscle by mediating deglutathionylation reactions. *J. Biol. Chem.* **289**, 14812–14828
153. Ress, C., and Kaser, S. (2016) Mechanisms of intrahepatic triglyceride accumulation. *World J. Gastroenterol.* **22**, 1664
154. Echtay, K. S., Winkler, E., Frischmuth, K., and Klingenberg, M. (2001) Uncoupling proteins 2 and 3 are highly active H(+) transporters and highly nucleotide sensitive when activated by coenzyme Q (ubiquinone). *Proc. Natl. Acad. Sci. U. S. A.* **98**, 1416–21
155. Jabůrek, M., Varecha, M., Gimeno, R. E., Dembski, M., Jezek, P., Zhang, M., Burn, P., Tartaglia, L. A., and Garlid, K. D. (1999) Transport function and regulation of mitochondrial uncoupling proteins 2 and 3. *J. Biol. Chem.* **274**, 26003–7
156. Žáčková, M., Škobisová, E., Urbánková, E., and Ježek, P. (2003) Activating ω-6 polyunsaturated fatty acids and inhibitory purine nucleotides are high affinity ligands for novel mitochondrial uncoupling proteins UCP2 and UCP3. *J. Biol. Chem.* **278**, 20761–20769
157. Gill, R. M., O'Brien, M., Young, A., Gardiner, D., and Mailloux, R. J. (2018) Protein S-glutathionylation lowers superoxide/hydrogen peroxide release from skeletal muscle mitochondria through modification of complex I and inhibition of pyruvate uptake. *PLoS One*. 10.1371/journal.pone.0192801
158. Chung, A. P. Y. S., Gurtu, S., Chakravarthi, S., Moorthy, M., and Palanisamy, U. D. (2018) Geraniin protects high-fat diet-induced oxidative stress in sprague dawley rats. *Front. Nutr.* **5**, 17
159. Noeman, S. A., Hamooda, H. E., and Baalash, A. A. (2011) Biochemical study of oxidative stress markers in the liver, kidney and heart of high fat diet induced obesity in rats. *Diabetol. Metab. Syndr.* **3**, 17
160. Echeverría, F., Valenzuela, R., Bustamante, A., Álvarez, D., Ortiz, M., Soto-Alarcon, S. A., Muñoz, P., Corbari, A., and Videla, L. A. (2018) Attenuation of high-fat Diet-induced rat liver oxidative stress and steatosis by combined hydroxytyrosol- (HT-) eicosapentaenoic acid supplementation mainly relies on HT. *Oxid. Med. Cell. Longev.* **2018**, 1–13
161. Donnelly, K. L., Smith, C. I., Schwarzenberg, S. J., Jessurun, J., Boldt, M. D., and Parks, E. J. (2005) Sources of fatty acids stored in liver and secreted via lipoproteins in patients with nonalcoholic fatty liver disease. *J. Clin. Invest.* **115**, 1343–1351
162. Dansinger, M. L., Gleason, J. A., Griffith, J. L., Selker, H. P., and Schaefer, E. J. (2005) Comparison of the Atkins, Ornish, weight watchers, and zone diets for weight loss and heart disease risk reduction. *JAMA.* **293**, 43

163. Lean, M., Lara, J., and Hill, J. O. (2006) ABC of obesity. Strategies for preventing obesity. *BMJ*. **333**, 959–62
164. Karlsson, J., Taft, C., Rydén, A., Sjöström, L., and Sullivan, M. (2007) Ten-year trends in health-related quality of life after surgical and conventional treatment for severe obesity: the SOS intervention study. *Int. J. Obes.* **31**, 1248–1261
165. Dixon, J. B., Zimmet, P., Alberti, K. G., Rubino, F., and International Diabetes Federation Taskforce on Epidemiology and Prevention (2011) Bariatric surgery: an IDF statement for obese Type 2 diabetes. *Diabet. Med.* **28**, 628–642
166. Kang, J. H., and Le, Q. A. (2017) Effectiveness of bariatric surgical procedures: A systematic review and network meta-analysis of randomized controlled trials. *Medicine (Baltimore)*. **96**, e8632
167. Sohn, J.-W., Xu, Y., Jones, J. E., Wickman, K., Williams, K. W., and Elmquist, J. K. (2011) Serotonin 2C receptor activates a distinct population of arcuate pro-opiomelanocortin neurons via TRPC channels. *Neuron*. **71**, 488–497
168. Krishna, R., Gumbiner, B., Stevens, C., Musser, B., Mallick, M., Suryawanshi, S., Maganti, L., Zhu, H., Han, T. H., Scherer, L., Simpson, B., Cosgrove, D., Gottesdiener, K., Amatruda, J., Rolls, B. J., Blundell, J., Bray, G. A., Fujioka, K., Heymsfield, S. B., Wagner, J. A., and Herman, G. A. (2009) Potent and selective agonism of the melanocortin receptor 4 With MK-0493 does not induce weight loss in obese human subjects: energy intake predicts lack of weight loss efficacy. *Clin. Pharmacol. Ther.* **86**, 659–666
169. Erondu, N., Gantz, I., Musser, B., Suryawanshi, S., Mallick, M., Addy, C., Cote, J., Bray, G., Fujioka, K., Bays, H., Hollander, P., Sanabria-Bohórquez, S. M., Eng, W., Långström, B., Hargreaves, R. J., Burns, H. D., Kanatani, A., Fukami, T., MacNeil, D. J., Gottesdiener, K. M., Amatruda, J. M., Kaufman, K. D., and Heymsfield, S. B. (2006) Neuropeptide Y5 receptor antagonism does not induce clinically meaningful weight loss in overweight and obese adults. *Cell Metab.* **4**, 275–282
170. Chronaiou, A., Tsoli, M., Kehagias, I., Leotsinidis, M., Kalfarentzos, F., and Alexandrides, T. K. (2012) Lower ghrelin levels and exaggerated postprandial peptide-YY, glucagon-like peptide-1, and insulin responses, after gastric fundus resection, in patients undergoing Roux-en-Y gastric bypass: A randomized clinical trial. *Obes. Surg.* **22**, 1761–1770
171. Derosa, G., and Maffioli, P. (2012) Anti-obesity drugs: a review about their effects and their safety. *Expert Opin. Drug Saf.* **11**, 459–471
172. Kunos, G., and Tam, J. (2011) The case for peripheral CB_1 receptor blockade in the treatment of visceral obesity and its cardiometabolic complications. *Br. J. Pharmacol.* **163**, 1423–31
173. Lutz, T. A. (2012) Control of energy homeostasis by amylin. *Cell. Mol. Life Sci.* **69**, 1947–1965
174. Elangbam, C. S. (2010) Drug-induced valvulopathy: an update. *Toxicol. Pathol.* **38**, 837–848
175. Greenfield, J. R. (2011) Melanocortin signalling and the regulation of blood pressure in human obesity. *J. Neuroendocrinol.* **23**, 186–193
176. Hayashi, T., Hirshman, M. F., Kurth, E. J., Winder, W. W., and Goodyear, L. J. (1998) Evidence for 5' AMP-activated protein kinase mediation of the effect of muscle contraction on glucose transport. *Diabetes*. **47**, 1369–73

177. Zhou, G., Myers, R., Li, Y., Chen, Y., Shen, X., Fenyk-Melody, J., Wu, M., Ventre, J., Doebber, T., Fujii, N., Musi, N., Hirshman, M. F., Goodyear, L. J., and Moller, D. E. (2001) Role of AMP-activated protein kinase in mechanism of metformin action. *J. Clin. Invest.* **108**, 1167–74
178. Fisher, J. S., Gao, J., Han, D.-H., Holloszy, J. O., and Nolte, L. A. (2002) Activation of AMP kinase enhances sensitivity of muscle glucose transport to insulin. *Am. J. Physiol. Metab.* **282**, E18–E23
179. Bergeron, R., Russell, R. R., Young, L. H., Ren, J.-M., Marcucci, M., Lee, A., and Shulman, G. I. (1999) Effect of AMPK activation on muscle glucose metabolism in conscious rats. *Am. J. Physiol. Metab.* **276**, E938–E944
180. Wellman, P. J. (2000) Norepinephrine and the control of food intake. *Nutrition*. **16**, 837–42
181. Viollet, B., and Andreelli, F. (2011) AMP-activated protein kinase and metabolic control. *Handb. Exp. Pharmacol.* 10.1007/978-3-642-17214-4_13
182. Gil, A., Olza, J., Gil-Campos, M., Gomez-Llorente, C., and Aguilera, C. M. (2011) Is adipose tissue metabolically different at different sites? *Int. J. Pediatr. Obes.* **6**, 13–20
183. Giralt, M., and Villarroya, F. (2013) White, brown, beige/brite: different adipose cells for different functions? *Endocrinology*. **154**, 2992–3000
184. Stanford, K. I., Middelbeek, R. J. W., Townsend, K. L., An, D., Nygaard, E. B., Hitchcox, K. M., Markan, K. R., Nakano, K., Hirshman, M. F., Tseng, Y.-H., and Goodyear, L. J. (2013) Brown adipose tissue regulates glucose homeostasis and insulin sensitivity. *J. Clin. Invest.* **123**, 215–223
185. Roberts, L. D., Boström, P., O'Sullivan, J. F., Schinzel, R. T., Lewis, G. D., Dejam, A., Lee, Y.-K., Palma, M. J., Calhoun, S., Georgiadi, A., Chen, M.-H., Ramachandran, V. S., Larson, M. G., Bouchard, C., Rankinen, T., Souza, A. L., Clish, C. B., Wang, T. J., Estall, J. L., Soukas, A. A., Cowan, C. A., Spiegelman, B. M., and Gerszten, R. E. (2014) β-Aminoisobutyric acid induces browning of white fat and hepatic β-oxidation and is inversely correlated with cardiometabolic risk factors. *Cell Metab.* **19**, 96–108
186. Jeremic, N., Chaturvedi, P., and Tyagi, S. C. (2017) Browning of white fat: novel insight into factors, mechanisms, and therapeutics. *J. Cell. Physiol.* **232**, 61–68
187. Koppen, A., and Kalkhoven, E. (2010) Brown vs white adipocytes: The PPARγ coregulator story. *FEBS Lett.* **584**, 3250–3259
188. Zafrir, B. (2013) Brown adipose tissue: research milestones of a potential player in human energy balance and obesity. *Horm. Metab. Res.* **45**, 774–785
189. Seoane, L., Barja-Fenández, S., Leis, R., and Casanueva, F. F. (2014) Drug development strategies for the treatment of obesity: how to ensure efficacy, safety, and sustainable weight loss. *Drug Des. Devel. Ther.* **8**, 2391
190. Grundlingh, J., Dargan, P. I., El-Zanfaly, M., and Wood, D. M. (2011) 2,4-Dinitrophenol (DNP): A weight loss agent with significant acute toxicity and risk of death. *J. Med. Toxicol.* **7**, 205–212
191. Nicholls, D. G. (2008) Forty years of Mitchell's proton circuit: From little grey books to little grey cells. *Biochim. Biophys. Acta - Bioenerg.* **1777**, 550–556
192. Scarpace, P. J., Matheny, M., Moore, R. L., and Kumar, M. V (2000) Modulation of uncoupling protein 2 and uncoupling protein 3: regulation by denervation, leptin and retinoic acid treatment. *J. Endocrinol.* **164**, 331–7
193. Rial, E., and González-Barroso, M. M. (2001) Physiological regulation of the transport

activity in the uncoupling proteins UCP1 and UCP2. *Biochim. Biophys. Acta*. **1504**, 70–81
194. Yoshitomi, H., Yamazaki, K., and Tanaka, I. (1999) Mechanism of ubiquitous expression of mouse uncoupling protein 2 mRNA: control by cis-acting DNA element in 5'-flanking region. *Biochem. J.* **340 (Pt 2)**, 397–404
195. Son, C., Hosoda, K., Matsuda, J., Fujikura, J., Yonemitsu, S., Iwakura, H., Masuzaki, H., Ogawa, Y., Hayashi, T., Itoh, H., Nishimura, H., Inoue, G., Yoshimasa, Y., Yamori, Y., and Nakao, K. (2001) Up-Regulation of uncoupling protein 3 gene expression by fatty acids and agonists for PPARs in L6 myotubes. *Endocrinology*. **142**, 4189–4194
196. Cortright, R. N., Zheng, D., Jones, J. P., Fluckey, J. D., DiCarlo, S. E., Grujic, D., Lowell, B. B., and Dohm, G. L. (1999) Regulation of skeletal muscle UCP-2 and UCP-3 gene expression by exercise and denervation. *Am. J. Physiol. Metab.* **276**, E217–E221
197. Ricquier, D., and Bouillaud, F. (2000) Mitochondrial uncoupling proteins: from mitochondria to the regulation of energy balance. *J. Physiol.* **529 Pt 1**, 3–10
198. Klingenberg, M., and Echtay, K. S. (2001) Uncoupling proteins: the issues from a biochemist point of view. *Biochim. Biophys. Acta*. **1504**, 128–43
199. Bienengraeber, M., Echtay, K. S., and Klingenberg, M. (1998) H + Transport by uncoupling protein (UCP-1) is dependent on a histidine pair, absent in UCP-2 and UCP-3 †. *Biochemistry*. **37**, 3–8
200. Brand, M. D., Brindle, K. M., Buckingham, J. A., Harper, J. A., Rolfe, D. F., and Stuart, J. A. (1999) The significance and mechanism of mitochondrial proton conductance. *Int. J. Obes. Relat. Metab. Disord.* **23 Suppl 6**, S4-11
201. Echtay, K. S., Liu, Q., Caskey, T., Winkler, E., Frischmuth, K., Bienengräber, M., and Klingenberg, M. (1999) Regulation of UCP3 by nucleotides is different from regulation of UCP1. *FEBS Lett.* **450**, 8–12
202. GOGLIA, F., and SKULACHEV, V. P. (2003) A function for novel uncoupling proteins: antioxidant defense of mitochondrial matrix by translocating fatty acid peroxides from the inner to the outer membrane leaflet. *FASEB J.* **17**, 1585–1591
203. GRAIER, W., TRENKER, M., and MALLI, R. (2008) Mitochondrial Ca_2^+, the secret behind the function of uncoupling proteins 2 and 3? *Cell Calcium*. **44**, 36–50
204. Busiello, R. A., Savarese, S., and Lombardi, A. (2015) Mitochondrial uncoupling proteins and energy metabolism. *Front. Physiol.* **6**, 36
205. Anedda, A., López-Bernardo, E., Acosta-Iborra, B., Saadeh Suleiman, M., Landázuri, M. O., and Cadenas, S. (2013) The transcription factor Nrf2 promotes survival by enhancing the expression of uncoupling protein 3 under conditions of oxidative stress. *Free Radic. Biol. Med.* **61**, 395–407
206. Samec, S., Seydoux, J., and Dulloo, A. G. (1998) Interorgan signaling between adipose tissue metabolism and skeletal muscle uncoupling protein homologs: is there a role for circulating free fatty acids? *Diabetes*. **47**, 1693–8
207. Berardi, M. J., Shih, W. M., Harrison, S. C., and Chou, J. J. (2011) Mitochondrial uncoupling protein 2 structure determined by NMR molecular fragment searching. *Nature*. **476**, 109–13
208. Aguirre, E., and Cadenas, S. (2010) GDP and carboxyatractylate inhibit 4-hydroxynonenal-activated proton conductance to differing degrees in mitochondria from skeletal muscle and heart. *Biochim. Biophys. Acta - Bioenerg.* **1797**, 1716–1726
209. Woyda-Ploszczyca, A. M., and Jarmuszkiewicz, W. (2014) Different effects of guanine nucleotides (GDP and GTP) on protein-mediated mitochondrial proton leak. *PLoS One*. **9**,

e98969
210. Zhang, C.-Y., Parton, L. E., Ye, C. P., Krauss, S., Shen, R., Lin, C.-T., Porco, J. A., and Lowell, B. B. (2006) Genipin inhibits UCP2-mediated proton leak and acutely reverses obesity- and high glucose-induced β cell dysfunction in isolated pancreatic islets. *Cell Metab.* **3**, 417–427
211. Vidal-Puig, A. J., Grujic, D., Zhang, C.-Y., Hagen, T., Boss, O., Ido, Y., Szczepanik, A., Wade, J., Mootha, V., Cortright, R., Muoio, D. M., and Lowell, B. B. (2000) Energy metabolism in uncoupling protein 3 gene knockout mice. *J. Biol. Chem.* **275**, 16258–16266
212. Muoio, D. M. (2014) Metabolic inflexibility: when mitochondrial indecision leads to metabolic gridlock. *Cell*. **159**, 1253–1262
213. Pastore, A., and Piemonte, F. (2013) Protein glutathionylation in cardiovascular diseases. *Int. J. Mol. Sci.* **14**, 20845
214. Applegate, M. A. B., Humphries, K. M., and Szweda, L. I. (2008) Reversible inhibition of α-ketoglutarate dehydrogenase by hydrogen peroxide: glutathionylation and protection of lipoic acid †. *Biochemistry*. **47**, 473–478
215. Lark, D. S., Fisher-Wellman, K. H., and Neufer, P. D. (2012) High-fat load: mechanism(s) of insulin resistance in skeletal muscle. *Int. J. Obes. Suppl.* **2**, S31–S36
216. Kramer, P. A., Duan, J., Qian, W.-J., and Marcinek, D. J. (2015) The measurement of reversible redox dependent post-translational modifications and their regulation of mitochondrial and skeletal muscle function. *Front. Physiol.* **6**, 347
217. Humphries, K. M., Juliano, C., and Taylor, S. S. (2002) Regulation of cAMP-dependent Protein Kinase Activity by Glutathionylation. *J. Biol. Chem.* **277**, 43505–43511
218. Zmijewski, J. W., Banerjee, S., Bae, H., Friggeri, A., Lazarowski, E. R., and Abraham, E. (2010) Exposure to hydrogen peroxide induces oxidation and activation of AMP-activated protein kinase. *J. Biol. Chem.* **285**, 33154–33164
219. Campbell, M. D., Duan, J., Samuelson, A. T., Gaffrey, M. J., Merrihew, G. E., Egertson, J. D., Wang, L., Bammler, T. K., Moore, R. J., White, C. C., Kavanagh, T. J., Voss, J. G., Szeto, H. H., Rabinovitch, P. S., MacCoss, M. J., Qian, W.-J., and Marcinek, D. J. (2019) Improving mitochondrial function with SS-31 reverses age-related redox stress and improves exercise tolerance in aged mice. *Free Radic. Biol. Med.* **134**, 268–281
220. Kalyanaraman, B., Darley-Usmar, V., Davies, K. J. A., Dennery, P. A., Forman, H. J., Grisham, M. B., Mann, G. E., Moore, K., Roberts, L. J., and Ischiropoulos, H. (2012) Measuring reactive oxygen and nitrogen species with fluorescent probes: challenges and limitations. *Free Radic. Biol. Med.* **52**, 1–6
221. Wong, H.-S., Benoit, B., and Brand, M. D. (2019) Mitochondrial and cytosolic sources of hydrogen peroxide in resting C2C12 myoblasts. *Free Radic. Biol. Med.* **130**, 140–150
222. Horn, A., Van der Meulen, J. H., Defour, A., Hogarth, M., Sreetama, S. C., Reed, A., Scheffer, L., Chandel, N. S., and Jaiswal, J. K. (2017) Mitochondrial redox signaling enables repair of injured skeletal muscle cells. *Sci. Signal.* 10.1126/scisignal.aaj1978
223. Shih, A. Y., Li, P., and Murphy, T. H. (2005) A small-molecule-inducible Nrf2-mediated antioxidant response provides effective prophylaxis against cerebral ischemia in vivo. *J. Neurosci.* **25**, 10321–10335
224. Picklo, M. J., Long, E. K., and Vomhof-DeKrey, E. E. (2015) Glutathionyl systems and metabolic dysfunction in obesity. *Nutr. Rev.* **73**, 858–868
225. Mailloux, R. J., and Harper, M.-E. (2012) Mitochondrial proticity and ROS signaling:

lessons from the uncoupling proteins. *Trends Endocrinol. Metab.* **23**, 451–458
226. Affourtit, C., Jastroch, M., and Brand, M. D. (2011) Uncoupling protein-2 attenuates glucose-stimulated insulin secretion in INS-1E insulinoma cells by lowering mitochondrial reactive oxygen species. *Free Radic. Biol. Med.* **50**, 609–616
227. Goncalves, R. L. S., Bunik, V. I., and Brand, M. D. (2016) Production of superoxide/hydrogen peroxide by the mitochondrial 2-oxoadipate dehydrogenase complex. *Free Radic. Biol. Med.* **91**, 247–255
228. Dröse, S., Brandt, U., and Wittig, I. (2014) Mitochondrial respiratory chain complexes as sources and targets of thiol-based redox-regulation. *Biochim. Biophys. Acta - Proteins Proteomics*. **1844**, 1344–1354
229. Wong, H.-S., Dighe, P. A., Mezera, V., Monternier, P.-A., and Brand, M. D. (2017) Production of superoxide and hydrogen peroxide from specific mitochondrial sites under different bioenergetic conditions. *J. Biol. Chem.* **292**, 16804–16809
230. Lefort, N., Glancy, B., Bowen, B., Willis, W. T., Bailowitz, Z., De Filippis, E. A., Brophy, C., Meyer, C., Højlund, K., Yi, Z., and Mandarino, L. J. (2010) Increased reactive oxygen species production and lower abundance of complex I subunits and carnitine palmitoyltransferase 1B protein despite normal mitochondrial respiration in insulin-resistant human skeletal muscle. *Diabetes*. **59**, 2444–52
231. Chouchani, E. T., Kazak, L., Jedrychowski, M. P., Lu, G. Z., Erickson, B. K., Szpyt, J., Pierce, K. A., Laznik-Bogoslavski, D., Vetrivelan, R., Clish, C. B., Robinson, A. J., Gygi, S. P., and Spiegelman, B. M. (2016) Mitochondrial ROS regulate thermogenic energy expenditure and sulfenylation of UCP1. *Nature*. **532**, 112–6
232. Fisher-Wellman, K. H., Gilliam, L. A. A., Lin, C.-T., Cathey, B. L., Lark, D. S., and Darrell Neufer, P. (2013) Mitochondrial glutathione depletion reveals a novel role for the pyruvate dehydrogenase complex as a key H2O2-emitting source under conditions of nutrient overload. *Free Radic. Biol. Med.* **65**, 1201–1208
233. Perevoshchikova, I. V., Quinlan, C. L., Orr, A. L., Gerencser, A. A., and Brand, M. D. (2013) Sites of superoxide and hydrogen peroxide production during fatty acid oxidation in rat skeletal muscle mitochondria. *Free Radic. Biol. Med.* **61**, 298–309
234. Oldford, C., Kuksal, N., Gill, R., Young, A., and Mailloux, R. J. R. J. (2019) Estimation of the hydrogen peroxide producing capacities of liver and cardiac mitochondria isolated from C57BL/6N and C57BL/6J mice. *Free Radic. Biol. Med.* **135**, 15–27